THE TRAPPING OF A GUN-INJECTED PLASMA BY A TOKAMAK

by

ANTHONY WILLIAM LEONARD

A thesis submitted in partial fulfillment of the requirements for the degree of

DOCTOR OF PHILOSOPHY

(Physics)

at the

UNIVERSITY OF WISCONSIN-MADISON

1986

THE TRAPPING OF A GUN INJECTED PLASMA

BY A TOKAMAK

Anthony William Leonard

Under the supervision of Professor J. C. Sprott

A Marshall gun was used to refuel a tokamak discharge on the Tokapole II device. Gun injection was able to increase the line-averaged density of the discharge by 50%. The density profile became more peaked due to gun injection.

A model is discussed which describes the trapping of a gun injected plasma in a pure octupole field, due to a depolarization current. This model is expanded to include arbitrary toroidal fields added to the poloidal field. A slowing time, τ_s, is derived for the trapping of an injected plasma of density n_b, and temperature, T_e, into poloidal field, B_p and toroidal field, B_t.

Experimental observation of plasma injected into an octupole field fits the derived slowing relation, with an exception in the beam density dependence. An anomalous resistivity at low field

strengths could account for the conflict, though the nature of this resistivity is not understood.

The more tokamak-like case of injection into poloidal and toroidal fields fits the data. Trapping is seen to be most strongly controlled by the poloidal to toroidal field ratio, B_p/B_t. The slowing time is also inversely proportional to the beam density, n_b.

The experiment is extended to the tokamak discharge by the addition of plasma density and current to the vacuum fields, B_p and B_t. Plasma density is seen to not significantly affect trapping. The increase in trapping with plasma current is explained in terms of additional poloidal field added to the central current channel.

An extrapolation is made of the refueling system to the reactor-size tokamak TFTR. An effective system seems easily obtainable.

ACKNOWLEDGMENTS

I would like to thank my major professor, J. C. Sprott for his continued help in this project. His suggestions and criticisms were invaluable in bringing this work to a conclusion.

I thank professor Richard Dexter for discussions and suggestiors in my research.

Tom Lovell and his technical staff have been of great service when dealing with technical and engineering issues. I wish to thank Jeremy Wight who helped considerably in construction of hardware used for this experiment.

I am grateful to all of my fellow graduate students in plasma physics. They helped with advice and encouragement throughout this work. They were very reasonable in accommodating schedules for use of the experimental devices. I thank all my fellow graduate students not in plasma physics who have provided encouragement and support throughout my stay in Madison.

Finally I wish to most graciously thank my parents, Jack and Irene, who have unfailingly encouraged my education from its beginning.

Financial support has been provided by the United States Department of Energy.

TABLE OF CONTENTS

PLP REPORTS

In this thesis, a number of references are made to the internal reports of the University of Wisconsin Plasma Physics Group. These reports, which are identified by PLP numbers, are available upon request from:

Plasma Physics Office

University of Wisconsin

1150 University Avenue

Madison, Wisconsin 53706

CHAPTER I

INTRODUCTION

As fusion devices have grown larger, plasma refueling has become an issue which has taken on increased significance. This is especially true for the largest machines and those which incorporate divertors. The issue of refueling will have to be investigated and understood before an efficient reactor can be designed and built.

Typically in a plasma device, such as a tokamak, the working gas is puffed in from the outside of the discharge. The gas then penetrates into the discharge before being ionized by the plasma. This provides fuel to the bulk of the plasma. If too much of the gas is ionized near the edge of the discharge, plasma will be trapped by the magnetic field and not reach the hot, central core. In large devices, and those with divertors, there is a large, cool, edge region, which can ionize gas puffed from the outside. In these devices gas puffing would cause the density profile to become very flat. A peaked density profile is much more desirable.

A peaked density profile has several advantages varying from enhanced fusion power production to being important in some schemes of steady state current generation in tokamaks.[1,2] Also the highest energy confinement achieved in tokamaks have a peaked density profile.[3]

A recently developed technique for refueling the center of a tokamak with plasma is the injection of pellets of deuterium ice into the discharge. These fast moving pellets penetrate far into the plasma before being vaporized and ionized. The highest density and energy confinement times in tokamaks have been produced using this method of refueling.[4,5]

An alternative to pellet fueling is gun injection[6]. A Marshall gun, by means of an arc discharge, produces a very dense plasma which travels from the gun at a high rate of speed.[7] If this moving plasma can penetrate into a tokamak discharge and then be stopped in the center, gun injection may provide a new efficient method of refueling a plasma. Marshall guns have the advantage of being a much simpler technology than pellet injectors and could easily be scaled up in size for a reactor. This report details the use of a Marshall gun to refuel the Tokapole II tokamak.

It has been known for some time that a moving plasma can cross magnetic field lines provided the extent of the plasma is smaller than the extent of the field, and it meets the condition[8]

$$1+\omega_{pi}^2/\omega_{ci}^2 \gg 1$$

where ω_{pi} is the plasma frequency of the moving plasma and ω_{ci} is the ion cyclotron frequency in the magnetic field the plasma is crossing.

As a stream of plasma, moving with a velocity $\vec{V}$, encounters a transverse magnetic field, electrons are deflected in one direction and ions in the other direction, due to the Lorentz force. This charge separation builds up an electric field $\vec{E}$ perpendicular to the magnetic field $\vec{B}$. The electric field increases in magnitude until

$$\vec{E} = -\vec{V}\times\vec{B}$$

The bulk of the moving plasma then sees this field and can continue to move with it's original velocity, or

$$\vec{V} = \vec{E}\times\vec{B}/B^2$$

The plasma can do this provided its density is great enough in comparison to the magnetic field strength.

Baker and Hammel showed how a plasma stream moving across magnetic field lines could be stopped if the polarization electric field could be eliminated[9]. An external conductor that connects magnetic field lines of different potential due to the polarization electric field would allow current to flow to short out the electric field. If the inductance of the current path is low enough, the current would build up quickly to stop the plasma in time t if

$$\Delta\rho\vec{V} = -\int_0^t \vec{J}\times\vec{B}dt$$

where ρ is the mass density of a fluid element in the plasma stream and $\vec{J}$ is the current density through that element. The experiments of Baker and Hammel agreed quite well with this model.

Since then plasma guns have been used to fill toroidal octupoles with plasma[10]. These machines have only a poloidal field in contrast to a tokamak which has poloidal and toroidal magnetic fields. For fueling an octupole the moving plasma stream is launched perpendicular to the magnetic field lines. The plasma easily crosses the magnetic field lines until it reaches the center of the machine. Once past the center the plasma encounters field lines in the opposite direction, and thus the polarization electric field switches sign. In this way the magnetic field lines themselves can act as the external conductor to stop the moving plasma.

Finally work by Sprott and Strait showed that an octupole field with an applied toroidal field and with an existing plasma could still trap an injected plasma.[11] This was as close an experiment to refueling a tokamak as has been done using a gun. All of these past encouraging results have led us to test refueling a tokamak with plasma gun injection.

This thesis consists of two parts. The first is concerned with showing the feasibility of using a Marshall gun as a means of refueling a tokamak. Important topics such as an immediate increase in density and peaking of the density profile are documented. Other issues such as confinement time improvement and impurity generation

are also briefly discussed. These are issues that are of concern to the fusion community and need to be addressed when comparing various refueling schemes.

The second part of this thesis deals with understanding the injection process itself. The trapping of injected plasma is seen within the framework of a depolarization current mechanism. The theoretical considerations of this mechanism are explored for the case of plasma injected into a combination of poloidal and toroidal fields. The theoretical model is then compared to the experimental observations of injection into Tokapole II. The previous work in this area is extended by injection into poloidal fields with an added strong toroidal field, and finally the injection of plasma into a tokamak discharge is studied. The experiments are seen to agree reasonably with the mechanism described.

B. Outline of Thesis

Chapter 2 contains a brief description of the experimental apparatus. The properties of Tokapole II along with the Marshall gun are described. Also the experimental diagnostics are briefly explained.

Chapter 3 contains a description of the refueling process. This includes issues relevant to the fusion community such as profile peaking, confinement times and impurity production.

In chapter 4 a theoretical model of the trapping process is derived. This model, based on a depolarization current mechanism, describes the injection of plasma into a combination of poloidal and toroidal fields.

Chapter 5 consists of trapping experiments that were carried out in vacuum fields with no plasma present as an extension of previous work of injection into octupoles. This is a bridge to the tokamak refueling case.

Chapter 6 describes experiments done with trapping of injected plasma in a tokamak discharge. This is compared with the earlier theoretical description. Other possible trapping mechanisms are discussed, with a final discussion of the trapping model and its accuracy and limitations in describing gun refueling of a tokamak. This chapter also contains an extrapolation of the model to a reactor size experiment with the considerations involved in using a gun to refuel a reactor. Suggestions for further work are also made.

Chapter 8 is a final summary of the conclusions reached in this work.

References for Chapter I

[1]J. Kesner and R. W. Conn, Nucl. Fusion 16, 397 (1976)

[2]N. J. Fisch and C. F. F. Karney, Phys. Fluids 24, 27 (1981)

[3]R. J. Fonck, et al., Proceedings of the sixth International Conference on Plasma Surface Interactions in Controlled Fusion Devices, Nagoya, Japan, May 1984 J. Nucl. Mater.(Netherlands) 128, 330 (1984)

[4]ibid.

[5]M. Greenwald, D. Gwinn, S. Milora, J. Parker, R. Parker, S. Wolfe, et al., Phys. Rev. Lett. 53, 352 (1984)

[6]E. Ott and W. M. Manheimer, Nuclear Fusion 17, 1057 (1977)

[7]J. Marshall, Phys. Fluids 3, 134 (1966)

[8]G. Schmidt, Phys. Fluids 3, 961 (1960)

[9]D. A. Baker and J. Hammel, Phys. Fluids 8, 713 (1965)

[10]R. A. Dory, D. W. Kerst, D. M. Meade, W. E. Wilson, and C. W. Erickson, Phys. Fluids 9, 997 (1966)

[11]E. J. Strait and J. C. Sprott, Nuclear Fusion 18, 1595 (1978)

CHAPTER II

APPARATUS AND DIAGNOSTICS

A. Tokapole II

The experiments for this thesis were carried out in Tokapole II,[1] (Figure 2-1), a 4-node poloidal divertor tokamak which has been in operation at the University of Wisconsin-Madison Physics Department since 1978. A complete description of the engineering and physics considerations involved in the design of the device can be found in references 2 and 3.

The vacuum vessel consists of a 44 cm square cross section torus with a major radius of 50 cm (figure 2-2). The vessel wall is constructed of 3-cm-thick aluminum with insulated breaks both toroidally and poloidally to allow magnetic fields to enter. The poloidal divertor configuration is generated by four, high conductivity, chromium-copper-alloy hoops which are electrically insulated from the tank. Each of these 5 cm diameter hoops is supported inside the vessel by three rods made of a high tensile strength beryllium copper alloy. The vertical position of these hoops may be varied by ±5.0 mm and has been adjusted to create an optimal tokamak discharge.

Figure 2-1. Tokapole II.

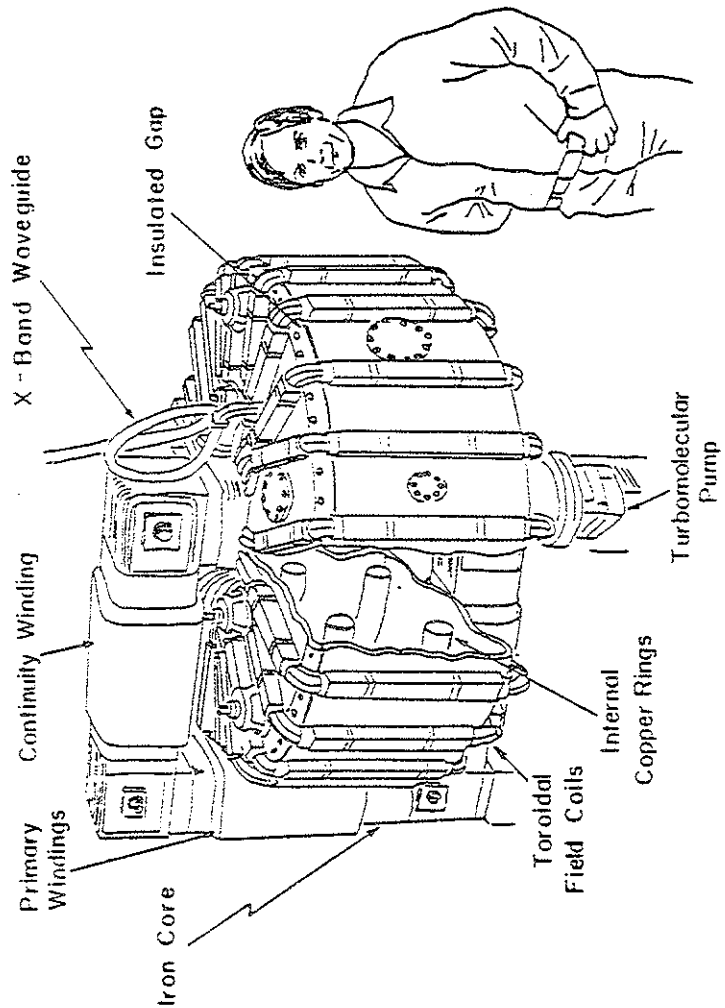

Figure 2-1

Figure 2-2. Cross section of vacuum vessel showing the internal hoops.

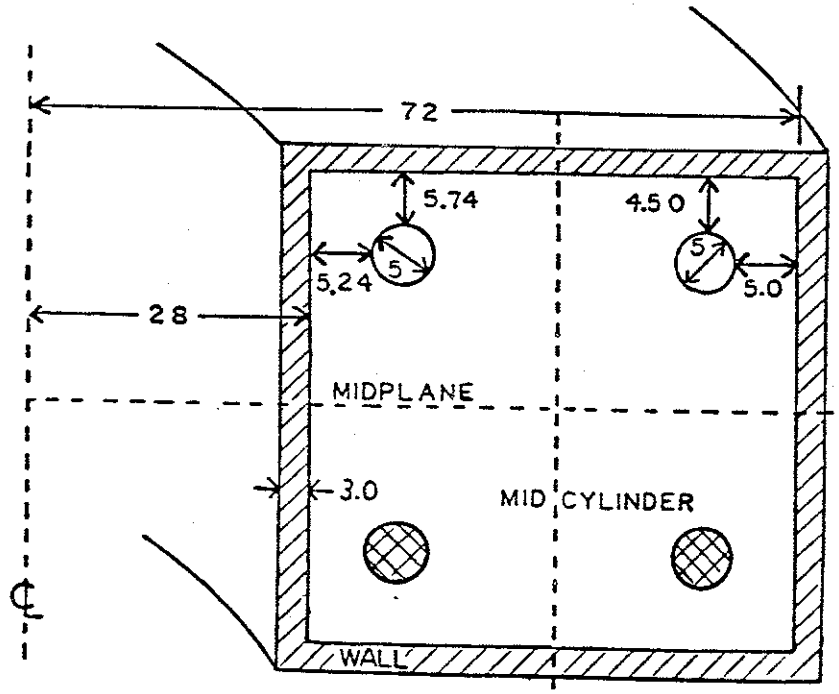

Figure 2-2

Current in the internal hoops and plasma is driven inductively by a 7.2 mF, 5 kV (90 kJ) capacitor bank through an iron core transformer. The 40:1 turns ratio on the transformer gives a sinusoidal field shape in time which has a half period of 5.6 msec. The poloidal field can be crowbarred actively by adding a 450 V, 0.96 F (97 kJ) capacitor bank. A damping resistor can also be added to the circuit to shorten the initial voltage spike. The damped and undamped poloidal circuit voltage waveforms are shown in figure 2-3.

The toroidal field, shown in figure 2-3, is created by external windings driven by a 52 mF, 5 kV (650 kJ) capacitor bank, which is passively crowbarred with a half period of 10 msec. The toroidal field is typically fired 6 msec before the poloidal field, leading to a relatively constant toroidal field for the duration of the discharge. A typical value for the toroidal field on axis for a tokamak discharge is 5 kG.

For these experiments Tokapole II was run in one of two modes. The first was an octupole mode. In this case the poloidal field was created by the inductively driven internal hoops alone, i.e. no plasma current. This was done by applying the undamped voltage waveform to the primary of the transformer, without puffing gas into the vacuum vessel. This configuration, with a total hoop current of 200 kA, produced a flux plot similar to that shown in figure 2-4. This mode was very similar to previous octupole experiments in which gun injection was done. Also an arbitrary toroidal field could be superimposed on to this existing field.

Figure 2-3. The wave form for a) the poloidal gap voltage both damped and undamped. b)the hoop current resulting from the gap voltage, and c) a typical toroidal field waveform.

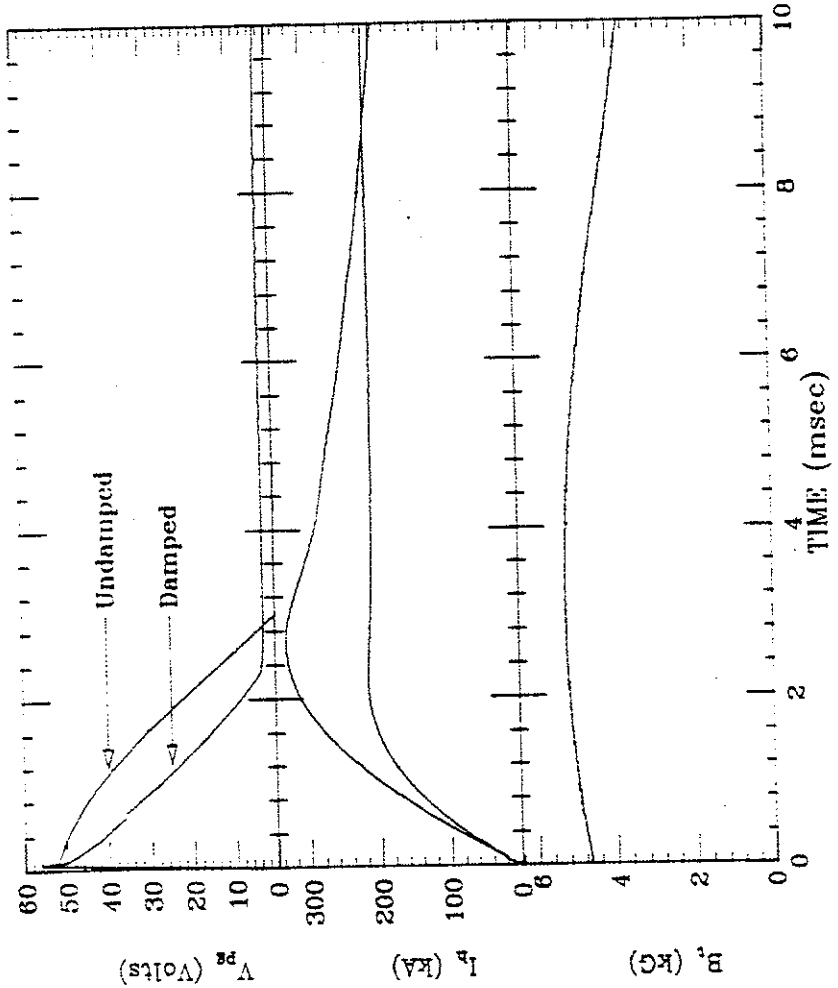

Figure 2-3

Figure 2-4. Vacuum poloidal field flux plot. Contours of poloidal field due to internal hoop current.

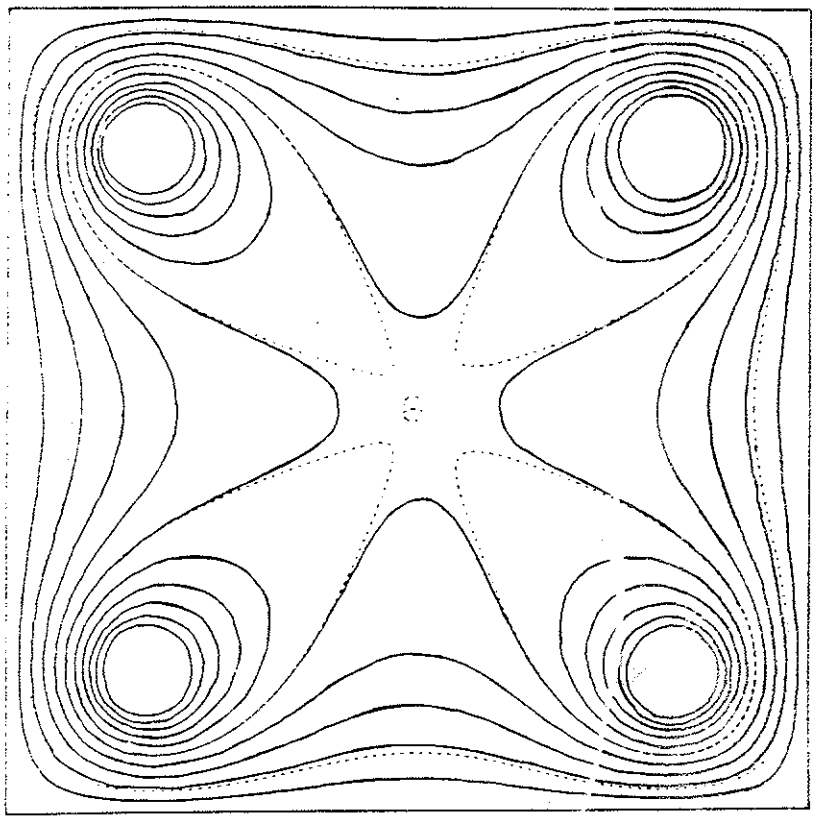

Figure 2-4

The other mode of operation was the divertor tokamak mode. In this case the vacuum vessel was filled to approximately 3×10^{-4} torr with hydrogen by use of a fast piezoelectric puff valve, just prior to the firing of the toroidal field. Microwave preionization (10 kW of 16 GHz) which was resonant with the electron cyclotron frequency of the toroidal field (5 kG) created a weak plasma just before the damped poloidal voltages were fired. A plasma current was then driven down the center of the device in addition to the hoop current. This addition of the plasma current produced a flux plot such as that shown in figure 2-5. This flux plot was calculated with an MHD equilibrium code for parameters that were characteristic of those used in these experiments.

B. Marshall Gun Characteristics

A coaxial Marshall gun was used as the external plasma source for these refueling experiments. The Marshall gun consisted of two concentric barrels, or electrodes. A working gas, hydrogen in this case, was puffed into the region between the barrels. High voltage was then applied between the electrodes, ionizing the hydrogen gas and allowing current to flow between the two barrels. The magnetic field created by this current resulted in a $\vec{J}\times\vec{B}$ force on the plasma which propelled it down the gun barrel, as illustrated in figure 2-6. As the plasma moved down the barrel, the current through it ionized gas as it traveled until ejected from the gun. Typically a

Figure 2-5. Poloidal magnetic flux plot calculated with a MHD equilibrium code for a typical tokamak discharge in Tokapole II.

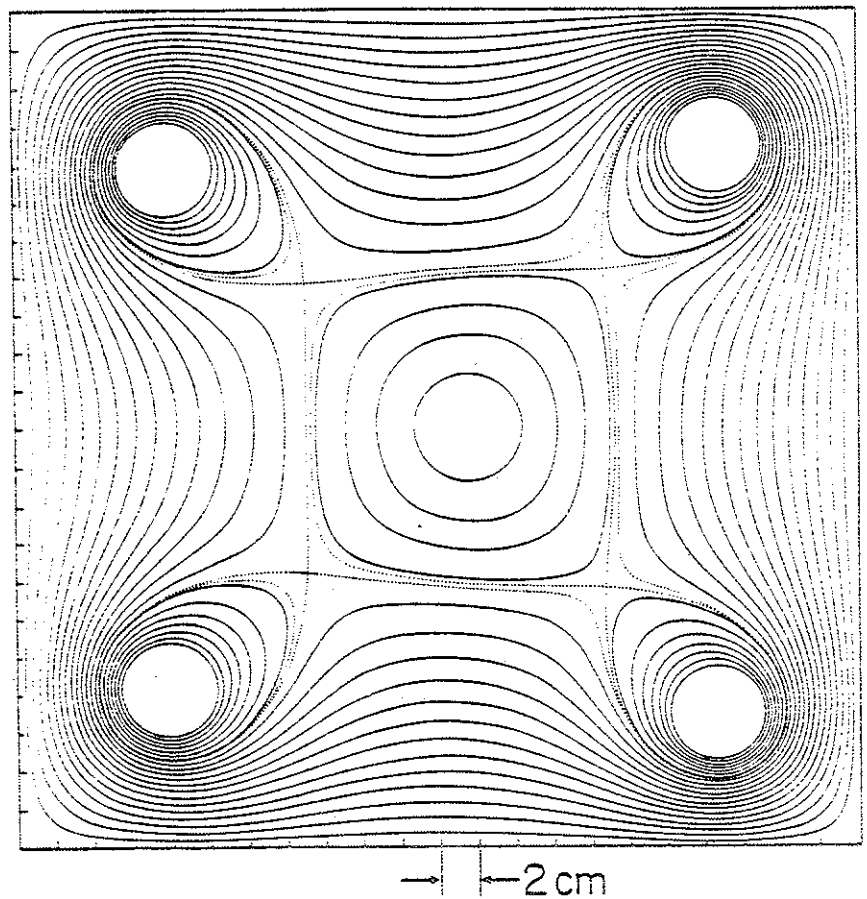

Figure 2-5

Figure 2-6. A Marshall gun discharge is illustrated. High voltage ionizes the gas, and the resultant current creates a $\vec{J}\times\vec{B}$ force which propels the plasma down the barrel.

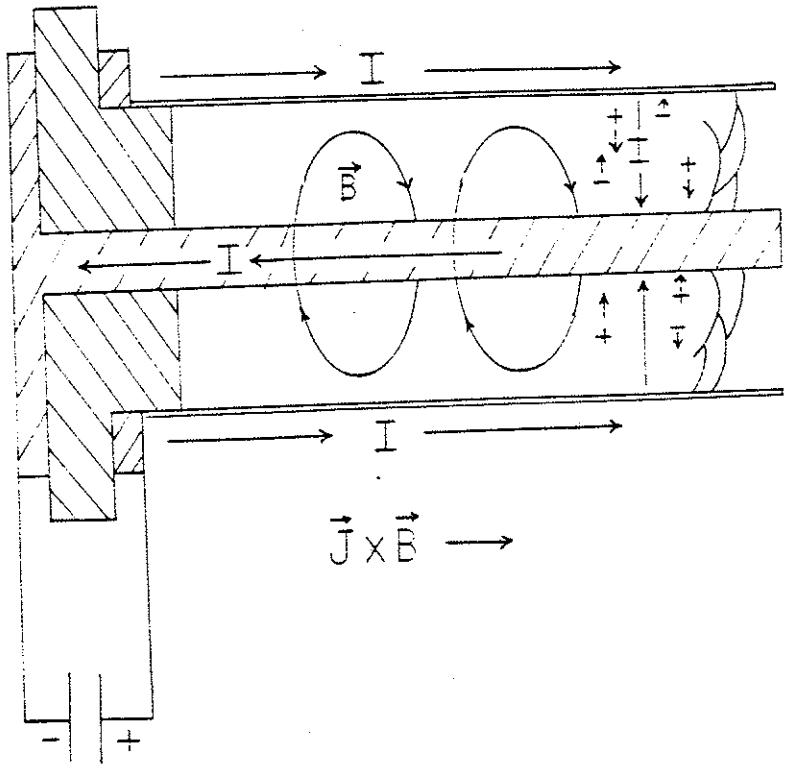

Figure 2-6

gun of this type has a slow component of plasma moving with a directed energy of ~100 eV and a smaller (~%1) component moving near 1 keV. The electrons are moving along with the ions and are usually much colder (<10eV). This is a simple view of what is actually a very complicated process, as evidenced by the lack of homogeneity of the created plasma. This description will be adequate for understanding the experiments that follow, however. A more complete description of the physics of plasma guns can be found in references 4-6 at the end of this chapter.

A schematic drawing of the Marshall gun that was used in these experiments can be found in figure 2-7, with an electrical circuit drawing in figure 2-8. This gun is 55 cm from muzzle to breach with a 5 cm diameter stainless steel outer barrel and a 1.5 cm diameter copper inner barrel. Between the inner and outer barrel there is a 1.25 cm thick Plexiglas insulator which electrically insulates one barrel from the other. This insulator also serves as a vacuum seal.

Gas is puffed into this gun by means of a magnetic valve. This valve is located in the inner barrel 3.5 cm from the breach of the gun. A 60 μF, 5 kV capacitor activates the valve 400 to 600 μsec before the gun is fired. Hydrogen gas is puffed into the gun, and the fill pressure can be varied over a wide range. For most of these experiments the gun was filled to a pressure between 50 mtorr and 200 mtorr. The timing of the gas puff was arrived at by maximizing the amount of plasma trapped by octupole fields upon firing of the gun.

Figure 2-7. Schematic of Marshall gun.

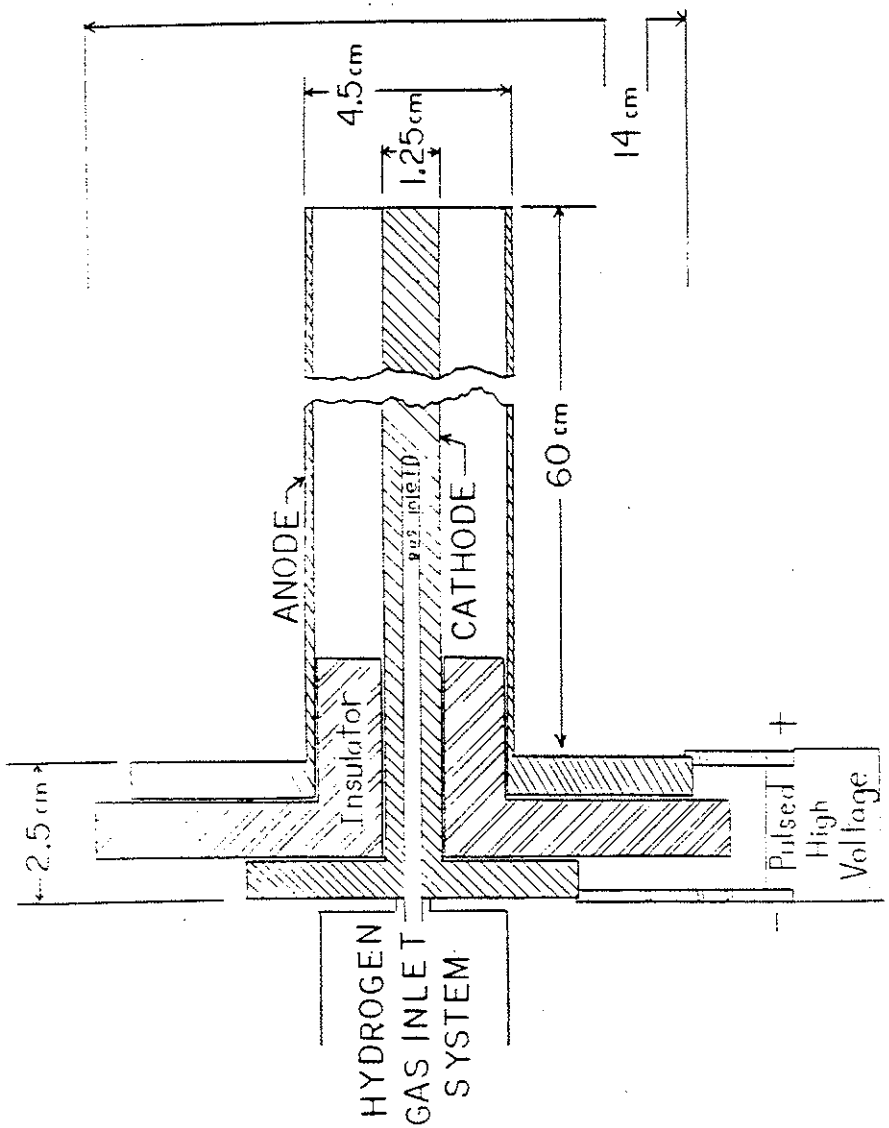

Figure 2-7

Figure 2-8. Electrical circuit diagram for firing Marshall gun.

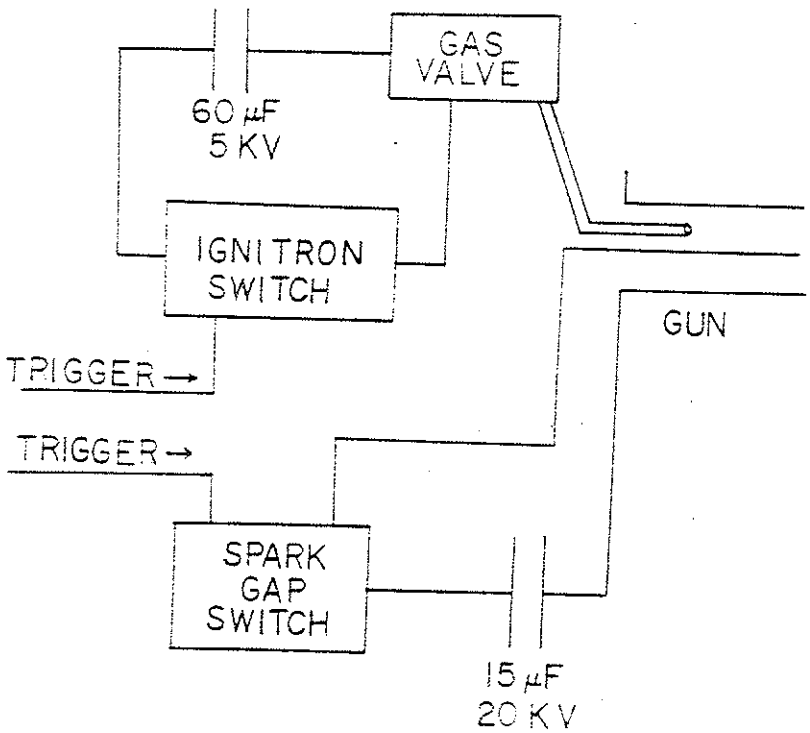

Figure 2-8

The main gun bank consists of a single 15 uF, 20 kV (3 kJ) capacitor. This circuit is triggered by means of a low inductance spark gap which allows the current to rise quickly. This produces a sinusoidal current waveform with a period of about 10 μsec and a maximum current of 200 kA. This current produces the plasma ejected by the gun. A more complete description of the plasma ejected from the gun that was used in this experiment will be given in chapter 2.

C. Interferometer

Plasma density was measured by means of a 70 GHz microwave interferometer (figure 2-9), which has a line of sight down the mid-cylinder of Tokapole II. For the case of a cold, collisionless, unmagnetized plasma the microwave radiation propagates with its wavelength increased from the vacuum value by the factor[7]

$$\mu = \left[1 - \frac{\omega_p^2}{\omega^2}\right]^{1/2}$$

where ω is the microwave frequency and $\omega_p = [ne^2/m\epsilon_o]^{1/2}$, the plasma frequency. If the approximation $\omega^2 >> \omega_p^2$ is used the phase change due to plasma along the path ℓ becomes

$$\Delta\Phi = \frac{e^2}{2m\epsilon_o\lambda_o}\int n_e(\ell)d\ell$$

Figure 2-9. Schematic of interferometer showing reference arm and arm through plasma in Tokapole II which are later mixed for measurement of phase difference.

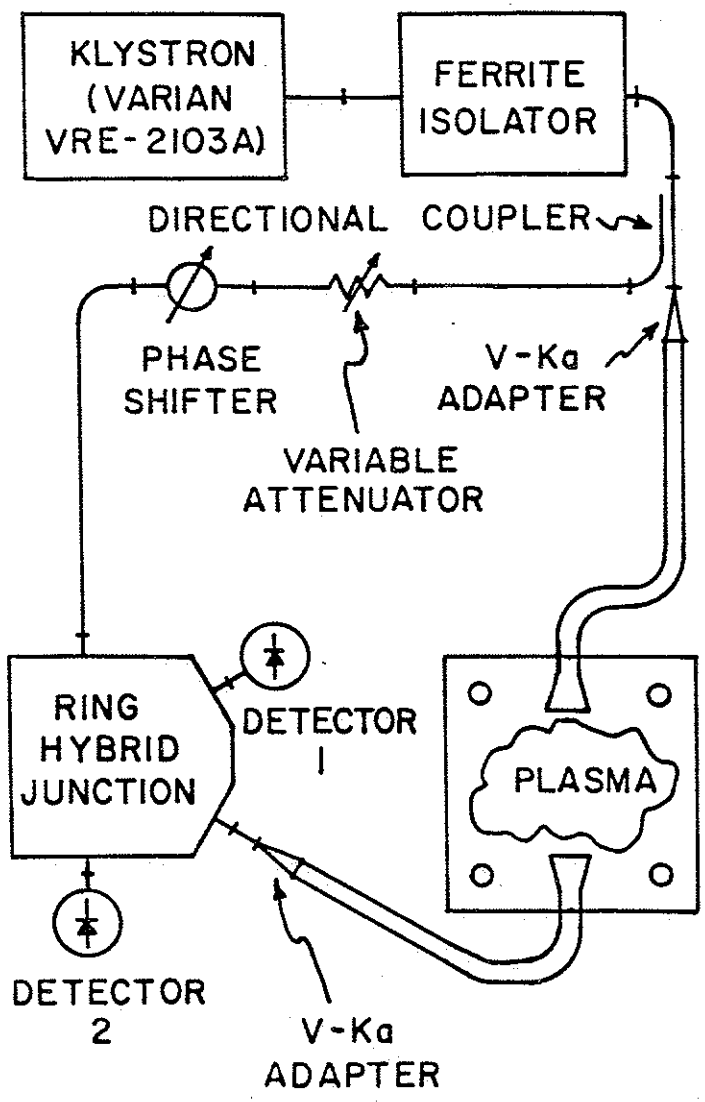

Figure 2-9

where m is the electron mass and λ_o is the wavelength of the microwave radiation in free space. When the density is varied, the phase of the radiation will be seen to change with respect to the reference arm of the microwave system. This measured phase change is then proportional to the line integrated density along the path length, and thus it is a global measurement instead of a local one.

The microwave horns are mounted such that the $\vec{E}$ field of the microwave radiation is parallel to the toroidal magnetic field, since $B_t >> B_p$. This allows the ordinary mode to propagate across the device. The ordinary mode has the same dispersion relation as radiation in an unmagnetized plasma. This makes the equation for phase change as a function of density still valid, even in the presence of a strong toroidal field.

In order to get a density measurement from the phase shift, a Princeton digital interferometer circuit was used[8]. The klystron frequency is modulated by a 1 MHz sawtooth wave. As the klystron frequency varies, a zero-crossing detector senses interference minima due to difference in electrical path length between the plasma arm and the reference arm of the interferometer. The digital circuit, with use of a phase lock loop, detects changes in phase during the 1 usec ramp where the minima occur. A complete 2π phase change of this minimum with respect to the ramp signal represents one microwave wavelength change in optical path length. The digital circuit counts these fringes and then converts the total phase change to an analog density signal.

D. Langmuir Probes

For local measurements of density, Langmuir probes were used. For a complete description of probe theory, see Chen[10], and for a description of the electronic considerations of probe use see Sprott[11].

An ungrounded metal probe inserted into a plasma will reach a steady state floating potential, V_f, such that there is no net current to the probe. If the probe is biased positive or negative with respect to V_f, it will attract or repel electrons, and in the opposite sense ions. This will cause a net current to flow. If the probe is biased negatively enough, all electrons in the area will be repelled and all ions traversing the effective probe area, A (equal to the probe area if the plasma sheath is small), will be collected. This ion saturation current is given by,

$$I_{sat} = \frac{1}{4} n e A v^* \quad \text{where } v^* = \left[\frac{8KT_e}{\pi m_i}\right]^{1/2} \quad \text{for} \quad T_i \ll T_e$$

and where n, m_i, T_i, and T_e are the ion density, ion mass, ion temperature and electron temperature respectively. Thus the density can be determined if the area of the probe tip and the electron temperature are known.

A method of determining the electron temperature,[11] based on measuring the slope of the I-V curve at V_f, was used in conjunction with saturation current measurements to obtain densities. The admittance, Y, is defined as

$$Y = \frac{1}{R} = \frac{dI_i}{dV}\Big|_{Vf} = \frac{eI_{sat}}{kT_e}$$

The admittance can be measured by use of a capacitance bridge that is balanced for zero output signal in the absence of plasma. The addition of plasma unbalances the bridge, and if the output of the bridge is calibrated against known resistances, the admittance, or inverse resistance, of the plasma sheath can be determined. In this way a probe, consisting of two probe tips of the same area, where one is measuring the ion saturation current and the other is measuring the plasma admittance, can monitor the time evolution of the plasma density and temperature at a single point in space.

E. SXR and other Impurity Signals

As a general diagnostic of central plasma conditions of a Tokapole II discharge, soft X-ray radiation, or SXR, signals were used. Radiation in the SXR region in plasmas comes primarily from sources with emissivity strongly dependent on the electron temperature, T_e, so that even though a collimated detector averages

over a chord, the detected signal comes primarily from the hottest point along the chord. The central temperature in a Tokapole II discharge is approximately 100 eV[12]. At this temperature SXR radiation comes primarily from line radiation. Groebner and Dexter determined from doping experiments that radiation from light impurities (carbon, oxygen, etc) accounted for <20% of the SXR signal[13]. At 100 eV the intensity of radiation from metals primarily varies as[14]

$$I \sim n_e n_i e^{-E/Te}$$

where n_e is electron density, n_i is the ion density in the i^{th} charge state, T_e is the electron temperature, and E is the photon energy.

Surface barrier diodes with polypropylene filters were used for SXR detectors on Tokapole II. This detector filter combination allows sensitivity down to a photon energy of about 60 eV. The vertical detector array consists of seven detectors spaced 3.2 cm apart along the outside wall at one toroidal azimuth. Each detector views a spot size of ~3 cm at the midcylinder. The central chord SXR signal was then a good diagnostic for viewing changes in the central current channel's temperature and density.

For general measurement and monitoring of impurity signals, filtered photomultipliers were used. This produced impurity signals for O_{III}, C_{III}, N_{III}, and Cu_I, which are a good monitor of the

cleanliness of the discharge and the impurity concentrations being ejected from the gun into Tokapole II.

F. Data Handling

Most of the data taken for this thesis was handled by a PDP 11/23 computer. Early data however were taken on oscilloscopes and stored on Polaroid film. A LeCroy 8210 digitizer was used in conjunction with the computer. The 8210 is a 4-channel, bipolar, 10-bit digitizer that can digitize up to 10^6 samples/sec. Each 8210 has 32k points of memory that can be divided among the channels used. After each run of data was taken, the data were read on to magnetic tape and transferred to a VAX computer. All of the data analysis was performed on the large computer.

References for Chapter II

[1] A. P. Biddle, R. N. Dexter, R. J. Groebner, D. J. Holly, B. Lipshultz, M. W. Phillips, S. C. Prager, and J. C. Sprott, Nucl. Fusion 19, 1509 (1979)

[2] J. C. Sprott, University of Wisconsin-PLP 744 (1978)

[3] R. J. Groebner, PhD Thesis, University of Wisconsin (1979)

[4] J. Marshall, Phys. Fluids 3, 135 (1960)

[5] L. C. Burkhardt and R. H. Lovberg, Phys. Fluids 5, 341 (1962)

[6] J. Marshall, Proc. High Beta Workshop, Los Alamos, New Mexico, July 28-August 1, 1975, ERDA-76/108, p470

[7] F. F. Chen, Introduction to Plasma Physics, (Plenum Press, New York 1974)

[8] H. R. Garner, University of Wisconsin PLP 833 (1981)

[9] F. F. Chen, "Electric Probes" in Plasma Diagnostic Techniques, R. H. Huddlestone and S. L. Leonard Eds., (Academic Press, New York, 1965), Ch. 4

[10] J. C. Sprott, University of Wisconsin PLP 88 (1966)

[11] J. C. Sprott, Rev. of Sci. Inst. 39, 1569 (1968)

[12]R. J. Groebner, PhD Thesis, University of Wisconsin (1979)

[13]R. J. Groebner and R. N. Dexter, University of Wisconsin-PLP 770 (1978)

[14]G. M. McCracken and P. E. Stott, Nucl. Fusion 19, 889 (1979)

CHAPTER III

GUN INJECTION REFUELING IN TOKAPOLE II

In this chapter the refueling process is characterized with a thorough description of a gun refueled tokamak discharge in Tokapole II. This has relevance to understanding the mechanisms involved in the refueling process itself, but also is important to the fusion community where such characteristics may be very crucial to reactor design. First the injected plasma beam will be described, followed by a short description of a typical tokamak discharge in Tokapole II without gun refueling. A complete description of a gun refueled discharge will then be given, with the important characteristics explained.

A. The Injected Plasma

Measurements of the gun plasma were made using a floating double Langmuir probe. A floating probe was necessary because of the high floating potentials associated with this type of discharge. For these measurements the gun was fired into Tokapole II with no fields present. The Langmuir probe was inserted into the plasma path through a swivel port from above. This allowed placement of the probe at different distances from the gun. A typical trace of the ion saturation current in this situation is shown in figure 3-1.

Figure 3-1. Waveform of ion saturation current from plasma beam streaming by probe.

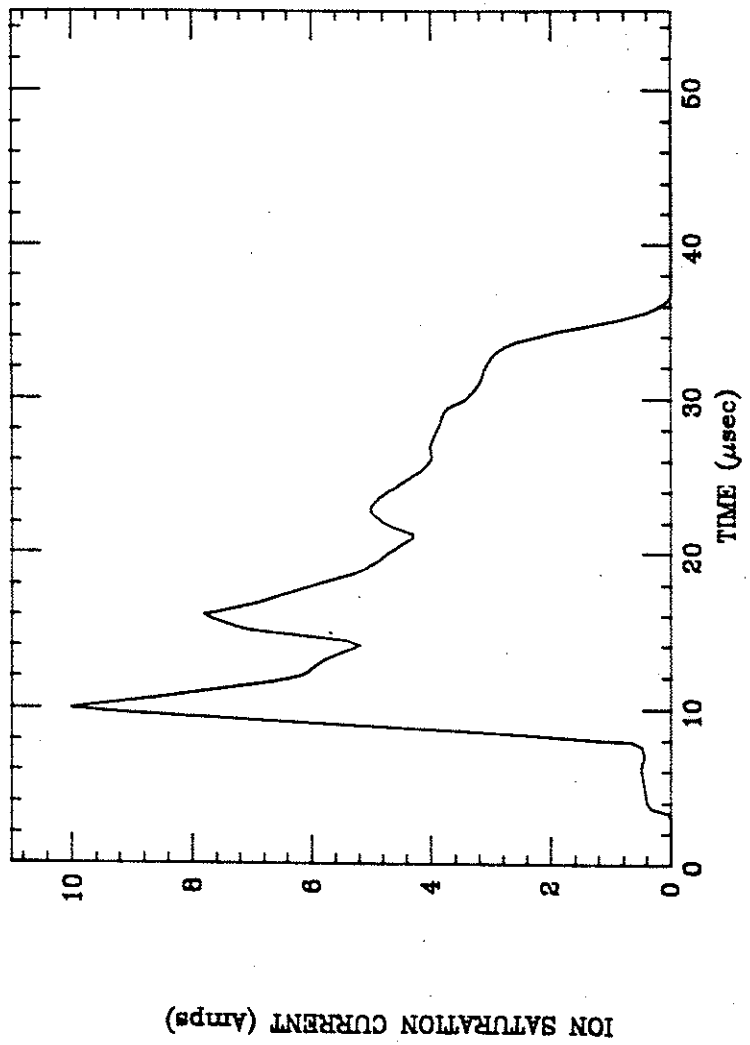

Figure 3-1

The trace was triggered by the rise of current in the gun transmission line. As can be seen, the plasma arrived at the probe several microseconds after current started in the gun. The time of flight of this plasma was measured by placing the probe at different distances from the gun and observing the arrival time of the plasma after the trigger. For gun plasmas used in the refueling experiments, the velocity of the plasma was $\sim 5\times10^6$ cm/sec.

The density of a gun plasma can be derived from the saturation current by using the velocity of the plasma beam. The saturation current is given by

$$j_{sat} = n_b e v_i A$$

where n_b is the beam density, A is the effective probe area, and v_i is the ion directed velocity, which brings new plasma into the probe sheath area. Using this method and the saturation current shown in figure 3-1, the typical gun plasma density was found to be $\sim 1\times10^{15}$ cm^{-3}. There was uncertainty in this measurement because of turbulence, embedded fields and high potentials of the gun plasmas.

In order to confirm this measurement, global measurements of the trapped plasma were also used. First the gun was fired into an octupole field and the average density of the plasma that was trapped was measured by an interferometer. With the known volume of the vacuum chamber at 0.6 m^3 and the dimension of the beam measured by Langmuir probes, a reasonably accurate density can be obtained.

The characteristics of a typical plasma beam that was efficient at refueling are given in the table of figure 3-2. These parameters are not constant however. By changing the voltage on the main gun bank and the gas fill in the gun, the density of the plasma beam and to a lesser extent, its velocity, can be varied over some range. Shown in figure 3-3 is the density trapped by an octupole field as both the gun voltage and gas fill were varied.

A significant amount of neutral gas is also a characteristic of a gun discharge. With a known amount of gas fill, the density trapped in an octupole field implies about a 30% ionization rate, assuming 100% trapping of the plasma. This neutral gas, not ionized by the gun discharge, travels down the gun barrel, at or near the sound speed, after the plasma. The effects of this on the refueling process will be discussed later in this chapter.

B. The Tokamak Plasma

The plasma discharge in Tokapole II is that of a divertor tokamak. Shown in figure 3-4 are the time evolution of several plasma parameters typical of this type of discharge. This is very characteristic of all discharges in which this research was carried out. These three diagnostics were especially important in evaluating the refueling effectiveness.

The first diagnostic is the average density in the discharge as measured by the interferometer. This signal displays the line-averaged density on a chord through the mid-cylinder. Because

Figure 3-2. Characteristics for plasma beam used for refueling.

PLASMA BEAM PARAMETERS

Velocity	5×10^4 m/sec
Pulse Length	20×10^{-6} sec
Length	1.0 meter
Beam Radius	3.0 cm
Total Particles	3.0×10^{18}
Density	1.1×10^{15} cm^{-3}
Electron Temperature	< 5 eV

Figure 3-2

Figure 3-3a. The density trapped in an octupole field as the gun supply voltage is varied.

Figure 3-3b. The density trapped in an octupole field as the gas fill is varied.

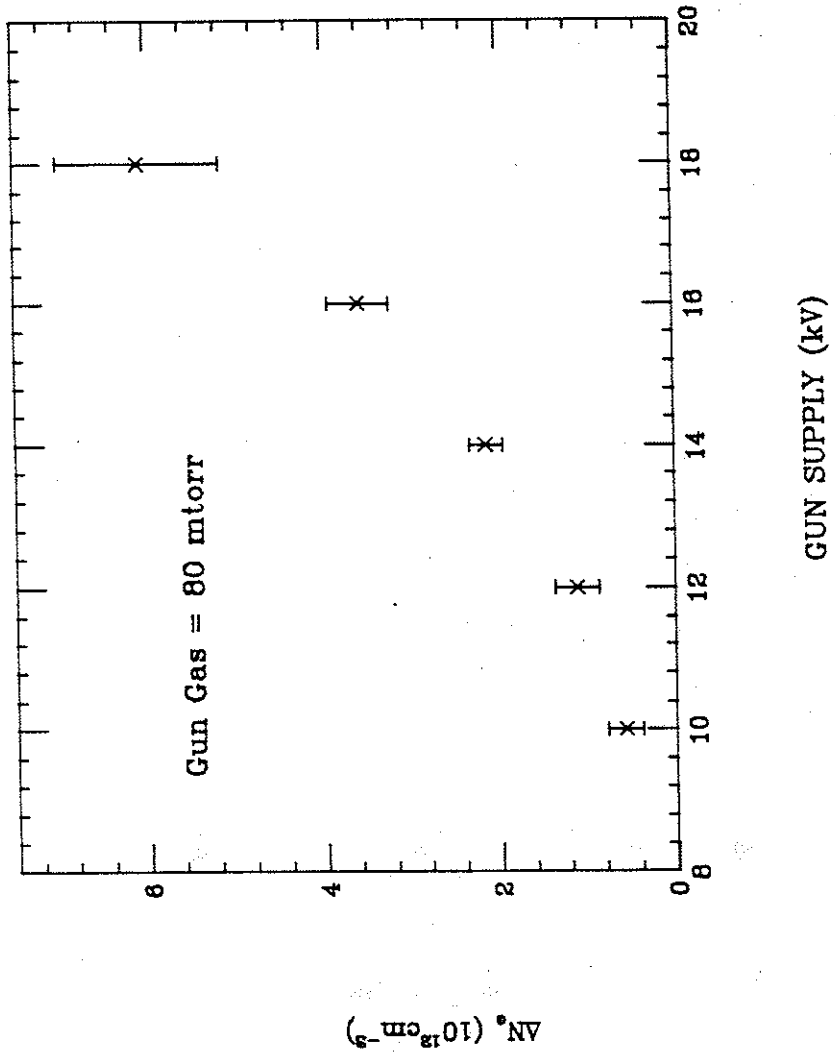

Figure 3-3a

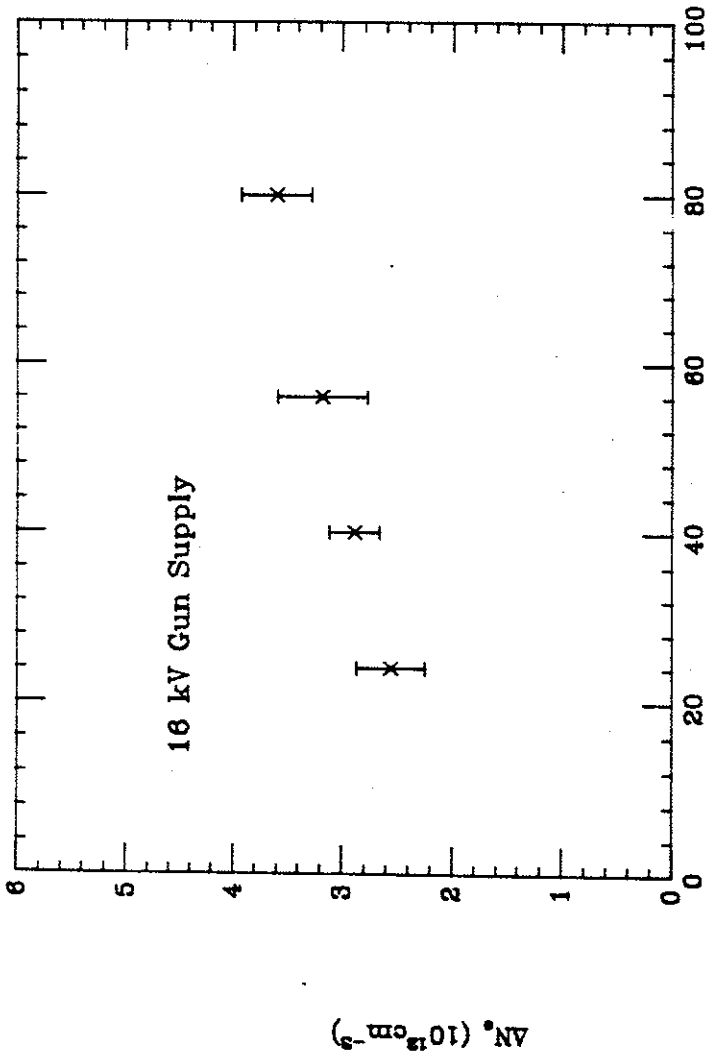

Figure 3-3b

Figure 3-4. Shown are three diagnostic signals for a standard Tokapole II discharge. They are a) line-averaged density from an interferometer, b) central chord SXR signal, and c) plasma current.

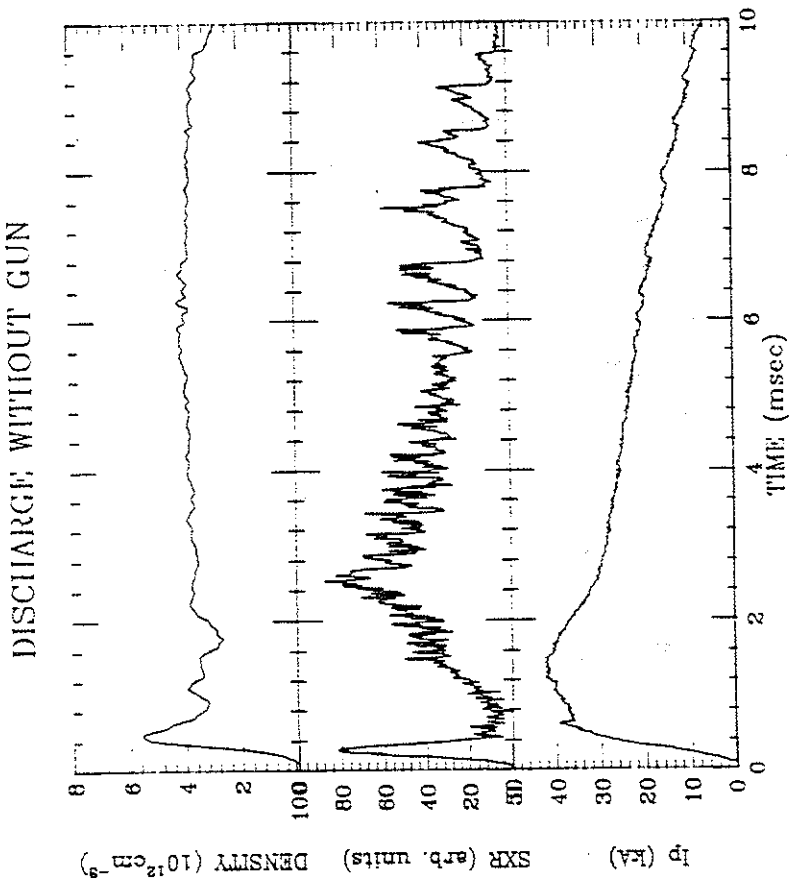

Figure 3-4

the goal of refueling is to add fuel, or density to the discharge, this serves as a basic measure of the effectiveness of the refueling process.

The second diagnostic displayed is the central chord SXR signal. This signal gives a good indication of the relative conditions existing in the central current channel. As explained in chapter 2 the SXR signal depends on both temperature and density. Useful information can be extracted from this diagnostic even though the two parameters are combined together.

The third diagnostic displayed is the plasma current. Plasma current is the mechanism for adding energy as well as providing confinement of the tokamak discharge. This signal characterizes the robustness of the discharge. Also a conductivity temperature of the current channel can be extracted from the plasma current, as will be described next. This also helps to describe the refueling process.

Additional global parameters can be derived if the average density, n_e, the plasma current, I_p, the hoop current, I_h, and the poloidal gap voltage, V_{pg}, are known. This process is documented by Sprott[1] and will be discussed briefly here. Typical values for these parameters are listed in the table in figure 3-5.

If the plasma current is assumed to distribute itself evenly inside the separatrix, then the plasma radius, a, is given by

$$a = 17.4\left|I_p/I_h\right|^{1/4}$$

Figure 3-5. Table of typical derived parameters for a standard Tokapole II discharge.

TOKAPOLE II STANDARD DISCHARGE

Major Radius	50 cm
Minor Radius	10 cm
Toroidal Field	5.2 kG
Hoop Current	200 kA
Plasma Current	25 kA
Average Density	4.0×10^{12} cm^{-3}
Electron Temperature	60 eV
Loop Voltage	4.5 Volts
Safety factor, q	2.2
Energy Confinement Time	0.33×10^{-3} sec

Figure 3-5

This is the radius of a circle with the same cross sectional area as the square-like area inside the separatrix. This area was determined by running computer code calculations with a given I_p and I_h.

After experimental measurements the resistive loop voltage, V_ℓ, seen by the plasma, was fitted to

$$V_\ell = 1/2(1 + t/75)V_{pg} + 0.0045(1 - t/37)I_h - 2.3\dot{I}_p/a^{1/2}$$

where t is time in msec after the start of the discharge and $\dot{I}_p$ is the time rate of change of the plasma current. With this the ohmic input power, P_{oh}, can be calculated from

$$P_{oh} = I_p V_\ell$$

The electron temperature, T_e, can be inferred from I_p, V_ℓ, and plasma radius, a, if we assume Spitzer conductivity with no impurities, $Z_{eff}=1$:

$$T_e = 376(|I_p/V_\ell|/a^2)^{2/3}$$

where the electron temperature, T_e, is measured in eV.

The final parameter to derive is the energy confinement time, τ_E. It is given by

$$\tau_E = \frac{0.144\langle n\rangle_e T_e}{P_{oh}}$$

In this case the entire volume of stable confinement is used and thus this represents a total machine confinement time.

There are numerous approximations in the derivation of these parameters as discussed in reference 1. These parameters, some of which are measured directly while others are inferred, allow observation of gross changes in the plasma behavior due to gun refueling. We can then evaluate the effectiveness of this refueling scheme.

C. The Refueling Process

The effects of gun refueling upon a Tokapole II discharge can be seen in the data of figure 3-6. The most pronounced change in the discharge was an increase in the average density immediately after injection. This is the first requirement for an effective refueling scheme. The interferometer showed this increase to take place in less than 50 μsec after the gun fired. The density rose by ~50% and more or less maintained that to the end of the discharge. If plasma from the gun was deposited into the discharge all at one time, with no other source of fuel, the density should decay after injection with a characteristic particle confinement time. The other source of fuel must be the un-ionized hydrogen gas from the

Figure 3-6. Time evolution of three diagnostics in a gun refueled discharge. They are a) line-averaged density from an interferometer, b) central chord SXR detector and c) plasma current.

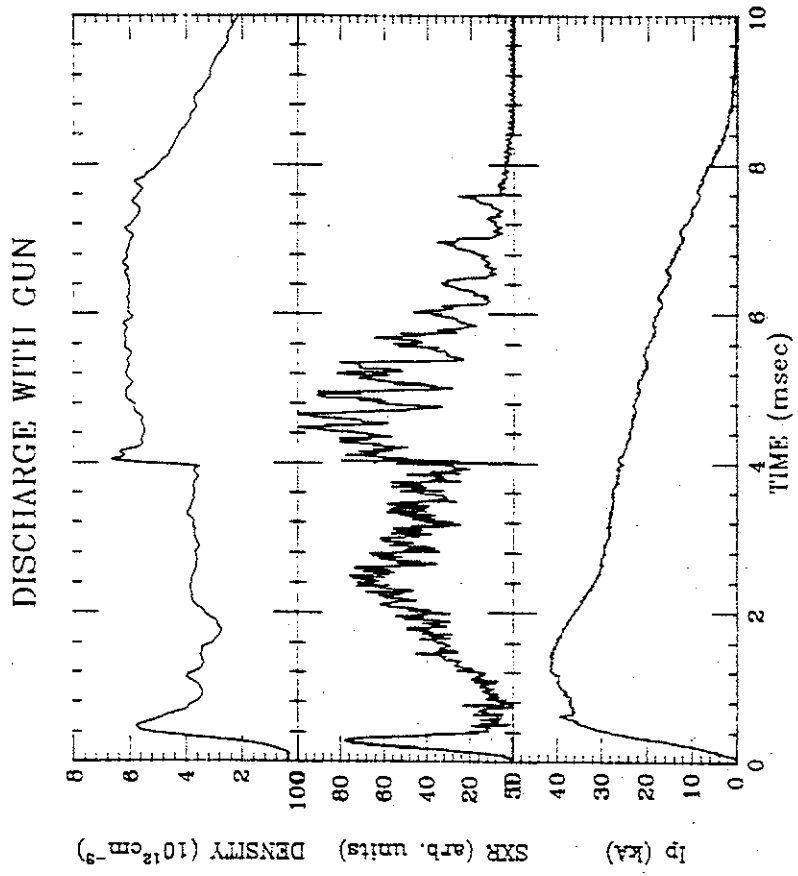

Figure 3-6

gun. As stated earlier only about 30% of the gas that fills the gun is ionized.

If gas from the gun were trapped quickly in the discharge and were responsible for the rapid rise in density, then the gun would be no better than an efficient gas puffer. If this were true the gun would not scale up well to larger tokamaks. In order to determine if the rise in density was just a gas fueling effect, the gun was filled with gas but not fired. Shown in figure 3-7 is the density for two different discharges. The first is a standard gun refueled case, and the second is the case of filling the gun with gas and not firing it. For the gas case the average density did not start to rise until 2-3 msec after the gun would have fired. Apparently the gun firing was responsible for the rapid increase in density. To better illustrate this, the signal from case II was subtracted from case I and is shown in figure 3-8. This signal should contain the effect of just the gun discharge and not the gas that later leaves the gun. As can be seen the density due to the gun discharge rises immediately and then decays with a time consistent with the expected particle confinement time. The fact that this signal goes negative late in time is due to the gun refueled discharge having ended slightly before the gas refueled case. This problem of late gas could be cured on this or other gun refueling systems by several techniques such as a fast shutter.[2]

Figure 3-7. Line-averaged density for two discharges. They are a) a gun refueled discharge, and for b) gun filled with gas but not fired.

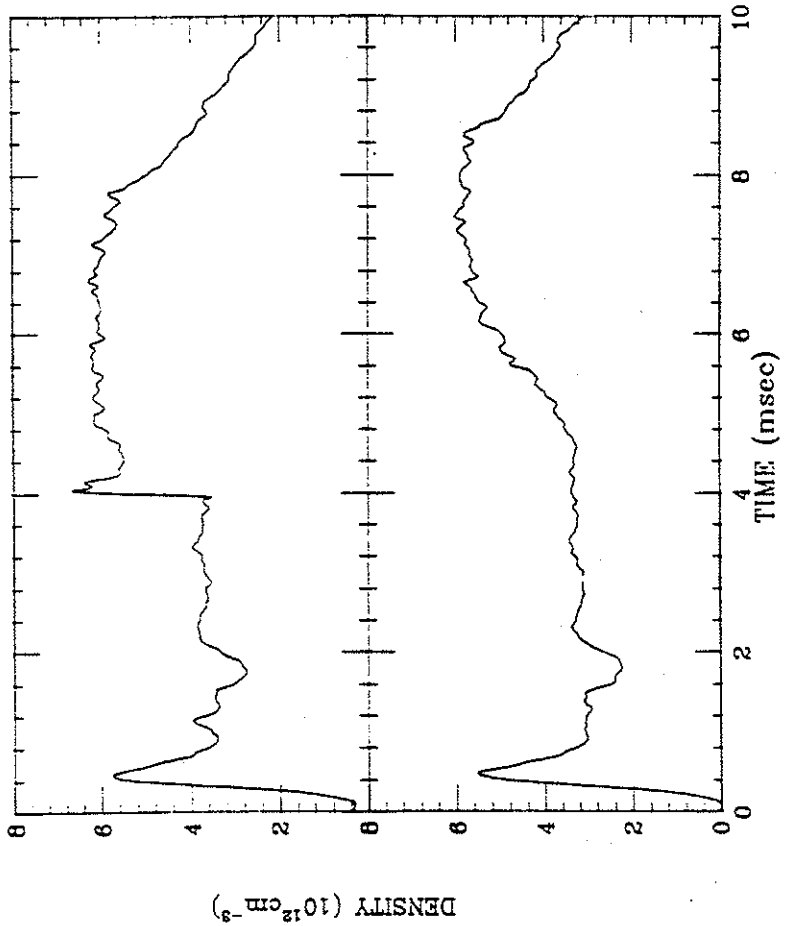

Figure 3-7

Figure 3-8. Line-averaged density from an interferometer for a discharge with gun filled with gas but not fired, subtracted from a gun refueled discharge.

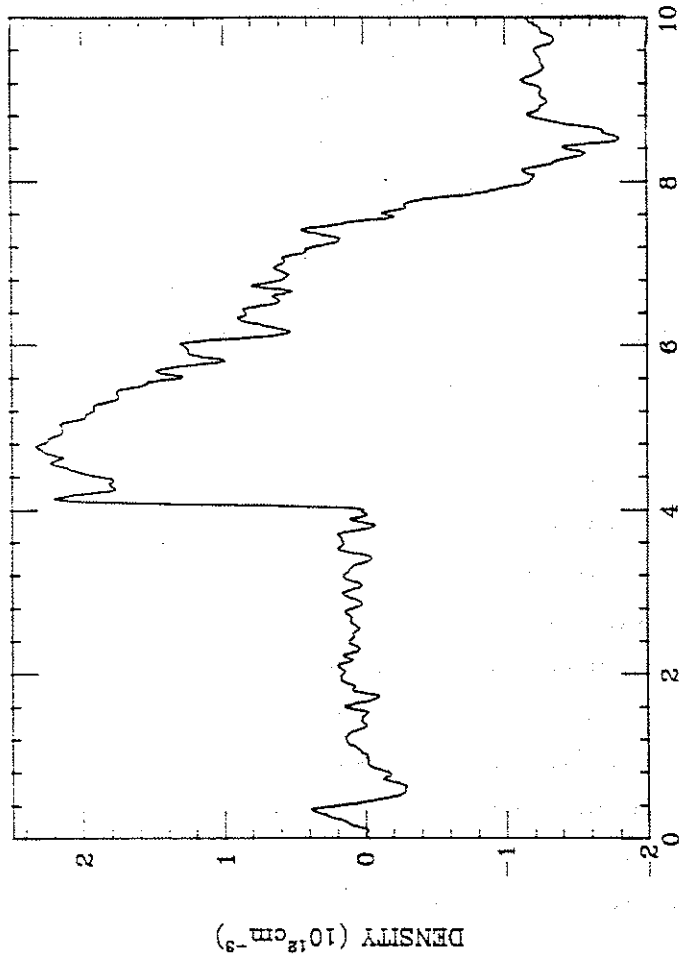

Figure 3-8

The rapid rise in density might also have been caused by energetic neutrals. Neutral hydrogen atoms that were energized by the gun discharge could have traveled at very nearly the speed of the plasma beam and then been ionized by the plasma discharge. In chapter VI it will be shown that the trapping mechanism is not a collisional process. The neutrals need collisions to become plasma and thus are not responsible for this density rise.

The central chord SXR signal also shows changes due to the gun. This signal which is proportional to density in the center and exponentially dependent on temperature does not rise immediately. But 1/2 to 1 msec after the gun fired, the signal rose to a value 2 to 3 times what it would have been without gun refueling. Apparently the gun deposited significant amounts of cold plasma in the center of the discharge. The plasma current then ohmically heated this plasma until an equilibrium was reached. This should have taken an energy confinement time, which was approximately 0.33 msec. The added cold plasma required more input power to heat it up. This additional input power is evidenced by the small decrease in the plasma current for the gun refueled case. The increase in input power, P_{oh}, was supplied by the $-L\frac{dI_p}{dt}$ term in the expression for the resistive loop voltage, V_ℓ. This decrease in I_p means that the equilibrium temperature was slightly lower. The increase in the SXR signal signifies that the central density must be increasing if there is no increase in temperature. Another possibility is an increase in impurities responsible for radiation

in the SXR region. Later in this chapter that will be shown not to be the case.

For efficient refueling it is desirable to deposit as much of the plasma as possible in the center of the discharge. In order to determine where gun refueling was depositing plasma, profiles before and after injection were taken with two different diagnostics. The first profile was taken using the SXR vertical array that exists on the outer wall. These detectors which are separated by 3.2 cm look perpendicularly inward towards the mid-cylinder. The signal from each detector is associated with the hottest part of the discharge along its line of sight. In this way the array represents a radial profile of the SXR emissivity. Figure 3-9 shows a radial profile of the SXR emissivity with and without injection.

It can be seen in figures 3-4 and 3-6 that the central chord SXR signal is modulated very strongly by sawtooth oscillations. To avoid error caused by measuring the SXR signal at different phases of a sawtooth oscillation for discharges with and without gun injection, each point of the profile was taken very near the peak of a sawtooth oscillation just after the gun injection.

The data shows clearly that gun injection has caused the profile to become more peaked. This profile does not necessarily represent the density, but whatever gun injection is doing to the discharge it is affecting the center most strongly.

Figure 3-9. Chordal profile of SXR emissivity with and without gun injection.

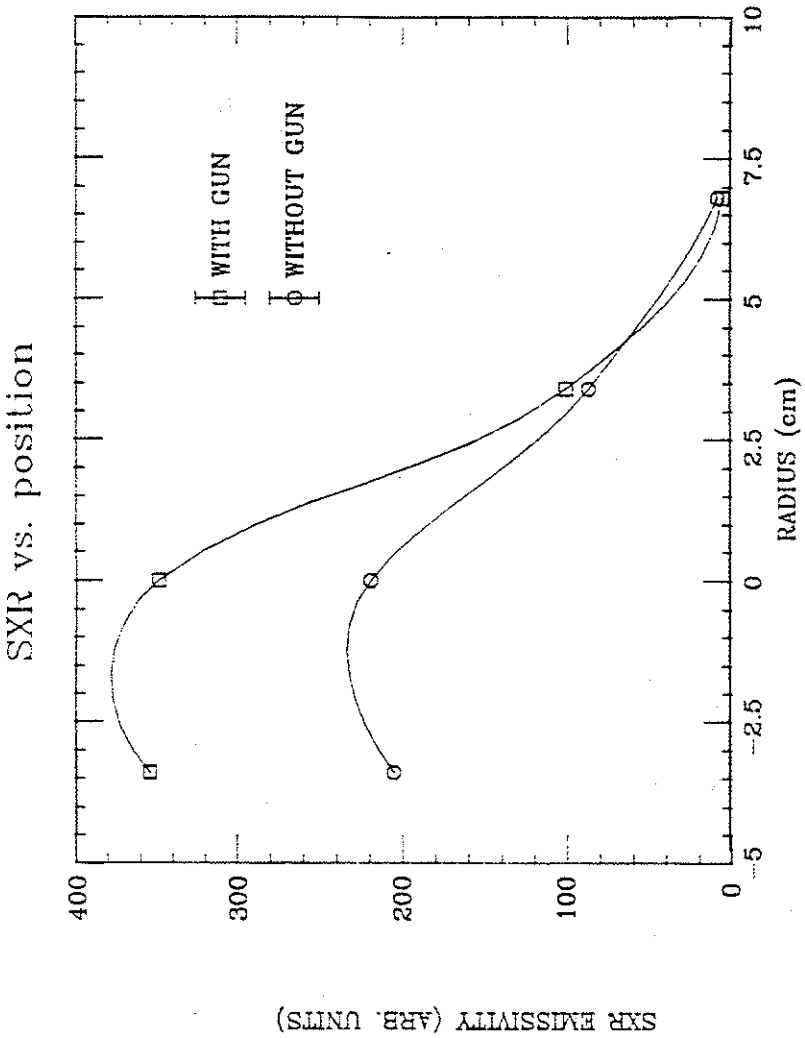

Figure 3-9

To better understand how the density profile was affected by gun-injection, Langmuir probes were used in conjunction with the interferometer. Langmuir probes could be inserted into the edge of the discharge up to the separatrix, or the edge of the current channel, before they were destroyed by the plasma current. This was about 12 cm from the wall, or 10 cm from the center of the discharge. A probe stalk which contained a Langmuir probe and an admittance probe was used over this range to get an edge density profile. This edge profile was taken for a gun-refueled case at a time of ~150 μsec after injection and for a nonrefueled case at the same time during the discharge. Each of these cases also has associated with it a line-integrated density value obtained from the interferometer. With these two different diagnostics, information about the density in the center of the discharge can be inferred.

To obtain a profile using probes and the interferometer, the edge density profile was line-integrated, and then subtracted from the interferometer signal. The remaining value represented a line-integrated density over the central plasma, inside a radius of 10 cm. This signal was then smoothed into a central density profile as a continuation of the edge density profile. This was done making sure the final density profile had a line-integrated value that corresponded to the interferometer value. The result of this process is the inferred density profiles of figure 3-10. This figure contains profiles of the refueled and non-refueled case. The gun refueled discharge had a much higher value for the central

Figure 3-10. Density profile inferred from interferometer in conjunction with edge Langmuir probes for discharge with and without gun refueling.

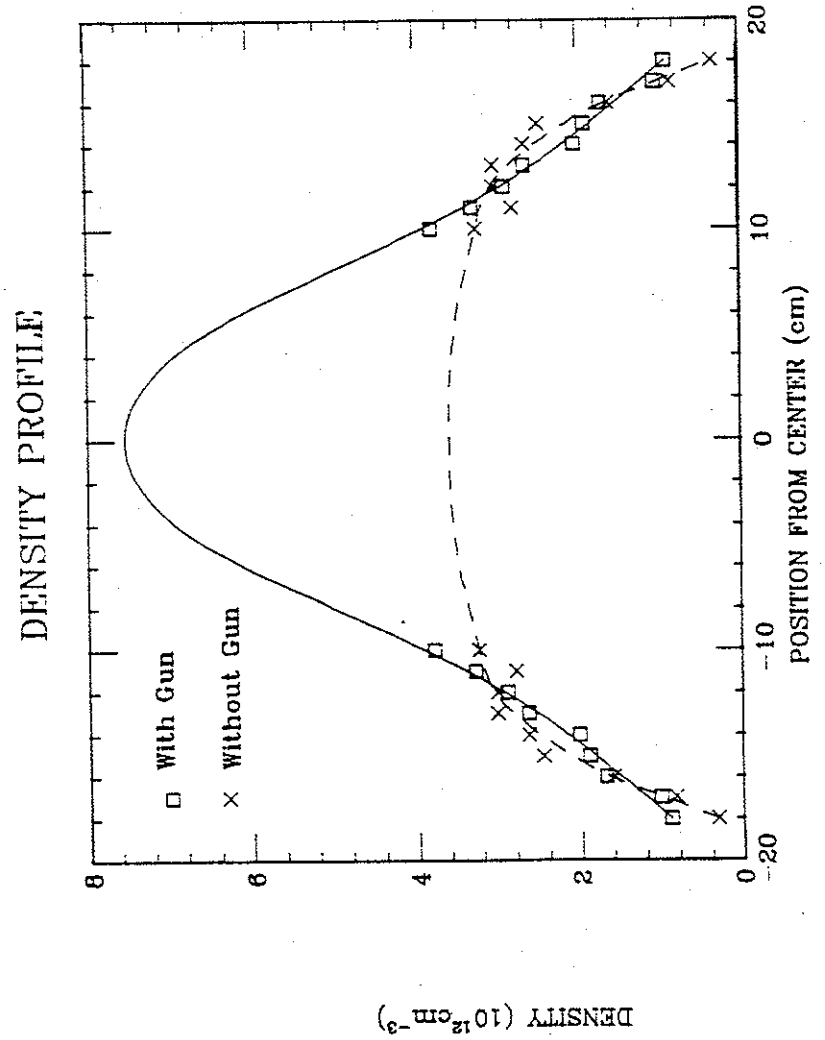

Figure 3-10

density, while the edge densities for the two cases were very similar. The gun was depositing most of its plasma in the center of the discharge.

There were a few assumptions and approximations made in inferring this density profile. First, there was some liberty in choosing the exact shape of the density profile over the center. There was also uncertainty in the absolute magnitude of the probe data, due to such factors as magnetic field and sheath size[2]. This could possibly have led to the non-refueled case having a more peaked central profile than is shown. If this were the case, then the gun-refueled case would also have been affected the same way. The important point is that the line-averaged density was increased 30% to 50% by gun-injection with little or no discernible change in the edge density. All of the plasma was deposited in the center of the discharge.

D. Energy Confinement

Energy confinement in tokamaks has been fit, in the past, to the Alcator scaling law[3]. This empirical scaling law states that the energy confinement time, τ_E, is proportional to the plasma density. At the highest densities in tokamaks, τ_E is seen to fall below this equation[3]. Pellet refueling has restored Alcator scaling at the highest densities, presumably due to peaking of the density profile[5].

On Tokapole II the confinement time was measured to see if gun refueling would increase the energy confinement above that observed with gas puffing. The results proved to be inconclusive. By measuring the energy confinement time as described earlier in this chapter, the table in figure 3-11 was obtained.

Three cases were examined. The first was a standard non-refueled tokamak discharge as shown in figure 3-4, and the second was the gun-refueled case of figure 3-6. The final case was obtained by additional gas puffing to raise the density to that of the gun-refueled case. The confinement time was calculated at intervals of 0.5 msec after the gun fired.

The confinement time τ_E is increased slightly in the gun-refueled case above the standard discharge and extra gas case. The changes in τ_E were small, however, and may fit within the uncertainty of the measurement. Gun-refueling was apparently not a better scheme for refueling than gas puffing on Tokapole II, from an energy confinement point of view. This was probably due to the small size and low densities of Tokapole II. Gun-refueling is more important for large tokamaks where gas puffing may be inefficient. When gun-refueling is carried out on large tokamaks the results of pellet injection might be reproduced.

Figure 3-11. The energy confinement time, τ_s, in 0.5 msec intervals for three separate cases. They are for a) a standard discharge, b) a gun refueled discharge, and c) a standard discharge with extra gas puffing.

ENERGY CONFINEMENT FOR 3 CASES

	τ_E (msec)		
Time (msec)	Std. discharge	Gun Refueling	Extra Gas
0.5	.00	.00	.00
1.0	.04	.04	.03
1.5	.03	.03	.03
2.0	.03	.03	.03
2.5	.08	.08	.07
3.0	.19	.19	.19
3.5	.23	.22	.24
4.0 (Gun Fires)	.29	.20	.24
4.5	.28	.29	.28
5.0	.28	.35	.30
5.5	.34	.51	.29
6.0	.37	.28	.31
6.5	.34	.31	.34
7.0	.29	.25	.19

Figure 3-11

E. Impurity Generation

An issue of concern for tokamaks is impurity contamination. Heavy impurities will radiate energy and cool the plasma. It is desirable to keep them to a minimum. Gun injection has the potential to generate many impurities, especially from sputtering of the electrodes during the arc discharge. On Tokapole II several impurity signals were routinely monitored to observe machine cleanliness. These impurity lines are C_{III}, O_{III}, N_{III}, and Cu_I.

The impurity signals for a gun refueled discharge are shown in figures 3-12 and 3-13. Early in time during start-up the signal is large. This is due to the strong interaction of the plasma and the machine wall before a stable equilibrium is established[6]. After start up the impurity radiation level receded to some equilibrium level. When the gun fired, there was a small increase in the impurity levels that quickly died away. Gun refueling did not increase impurity radiation significantly.

Optimizing the gun to produce fewer impurities was not one of the goals of this work. Yet, the impurity production remained at an acceptably low level. This is encouraging for the possibility of using gun-refueling for a reactor. With some work it seems likely that a Marshall gun could be clean enough for use in a reactor.

Figure 3-12. Impurity radiation for N_{III} and O_{III}. Gun fires at 4.5 msec.

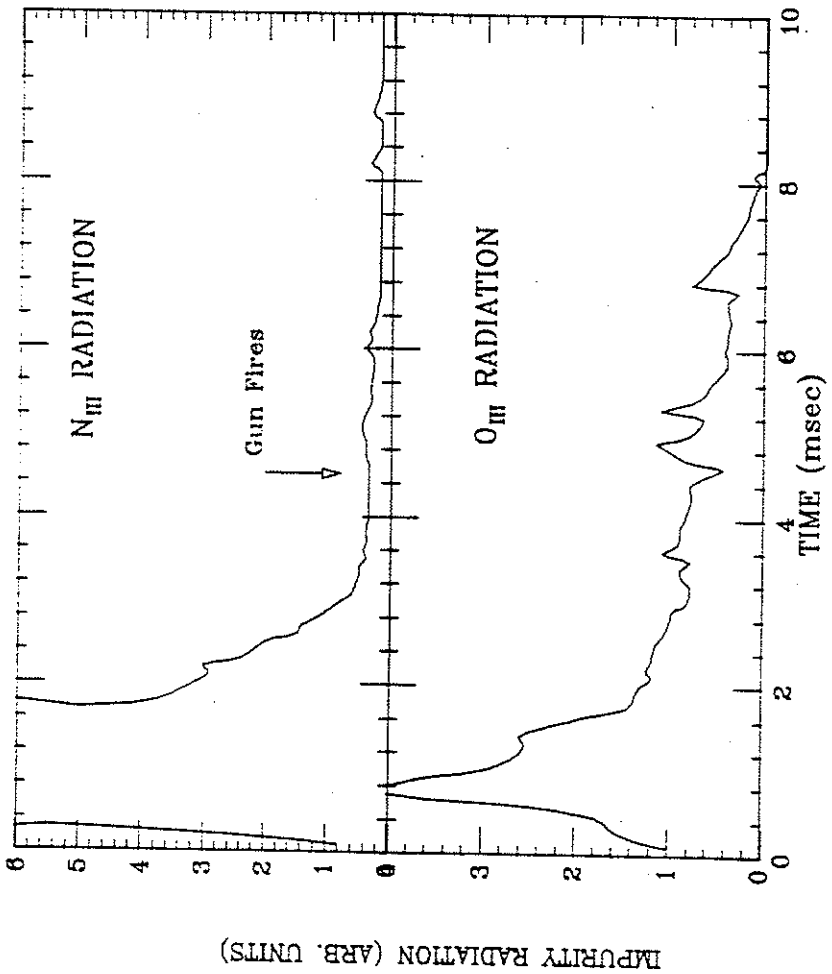

Figure 3-12

Figure 3-13. Impurity radiation for C_{III} and Cu_I. Gun fires at 4.5 msec.

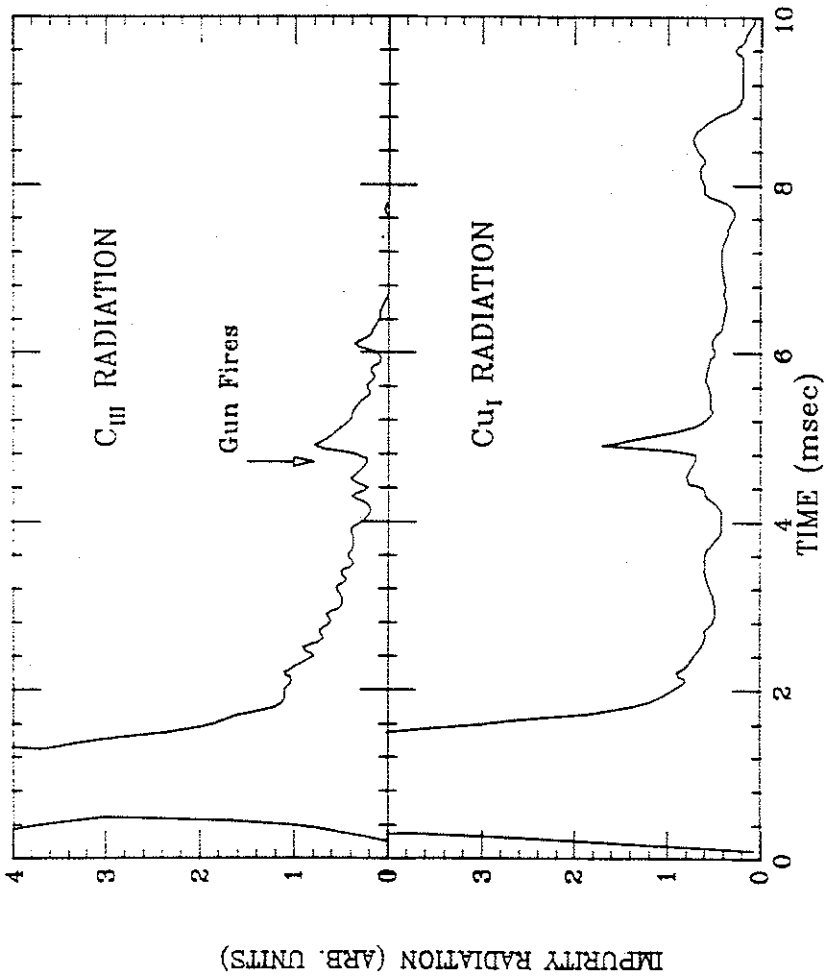

Figure 3-13

References for Chapter III

[1] J. C. Sprott, University of Wisconsin-PLP 889

[2] G. Kuswa, Rev. of Sci. Instr. 37, 189 (1966)

[3] F. F. Chen, "Electric Probes" in Plasma Diagnostic Techniques, R. H. Huddlestone and S. L. Leonard Eds., (Academic Press, New York, 1965), Ch. 4

[4] M. Murakami, Phys. Rev. Lett. 42, 655 (1979)

[5] S. Fairfax et al., Proceedings of the Eighth International Conference on Plasma Physics and Controlled Nuclear Fusion Research, (International Atomic Energy Agency, Brussels, 1980), Vol. 1, p. 439

[6] M. Greenwald, D. Gwinn, S. Milora, J. Parker, R. Parker, S. Wolfe, et al., Phys. Rev Lett. 53, 352 (1984)

[7] N. S. Brickhouse, University of Wisconsin PhD Thesis (1984)

CHAPTER IV

A MODEL FOR THE TRAPPING OF GUN-INJECTED PLASMA

A. Introduction

A moving beam of plasma has the ability to cross magnetic field lines by setting up a polarization electric field[1]. As the beam encounters the magnetic field, electrons are deflected in one direction and ions the other. This continues until an electric field builds up to allow the interior of the plasma beam to $\vec{E}\times\vec{B}$ drift its way across field lines. This moving plasma can be stopped if an external conductor shorts out the polarization field. As the moving plasma tries to reestablish the polarization field, the resulting current will create a $\vec{J}\times\vec{B}$ force to slow the plasma down. Baker and Hammel[2] showed that this model could accurately represent a physical experiment.

Experiments, in which a gun plasma was injected into an octupole field, extended this model to different magnetic configurations with interesting results[3]. The toroidal octupole has only poloidal field, with none in the toroidal direction. In this case the magnetic field lines provide the mechanism for shorting out the polarization field.

In figure 4-1 a plasma beam is shown encountering a purely circular poloidal field, which is an idealization of the octupole field. As the beam encounters the magnetic field a polarization field is set up to allow the plasma to keep moving. As the plasma crosses to the center and then to the other side of the device, the magnetic field lines change direction with respect to the moving plasma. The polarization field must also change in response to this. This shifting will cause an electric field in the direction of travel to be set up along the outer edges of the plasma beam.

The electric field in the direction of $\vec{v}$ causes a current to flow perpendicular to $\vec{B}$ and in the direction of travel. This current is shown as $\vec{J}_D$ in the figure. The conductivity across field lines is smaller than along field lines, but enough current can flow to deplete the polarization charge and field. The plasma beam then attempts to reestablish the polarization field with a polarization current, $\vec{J}_P$. A current loop is thus set up in the plasma with polarization and depolarization currents, $\vec{J}_P$ and $\vec{J}_D$ respectively. This current loop will slow down the plasma. Both legs of $\vec{J}_P$ produce a $\vec{J}_P\times\vec{B}$ force in the $-\vec{v}$ direction while the $\vec{J}_D$ leg of the current loop produces no net force on the plasma.

These polarization and depolarization currents were measured for a plasma injected into a toroidal octupole.[3] The observed currents were large enough to stop the plasma in the device. The result of the experiment was consistent with this model.

Figure 4-1. The mechanism for trapping a plasma beam in poloidal fields. Reversal of the magnetic field allows depolarization current, J_p to flow. The resultant current to support it, J_p, produces a $\vec{J} \times \vec{B}$ force to slow the plasma.

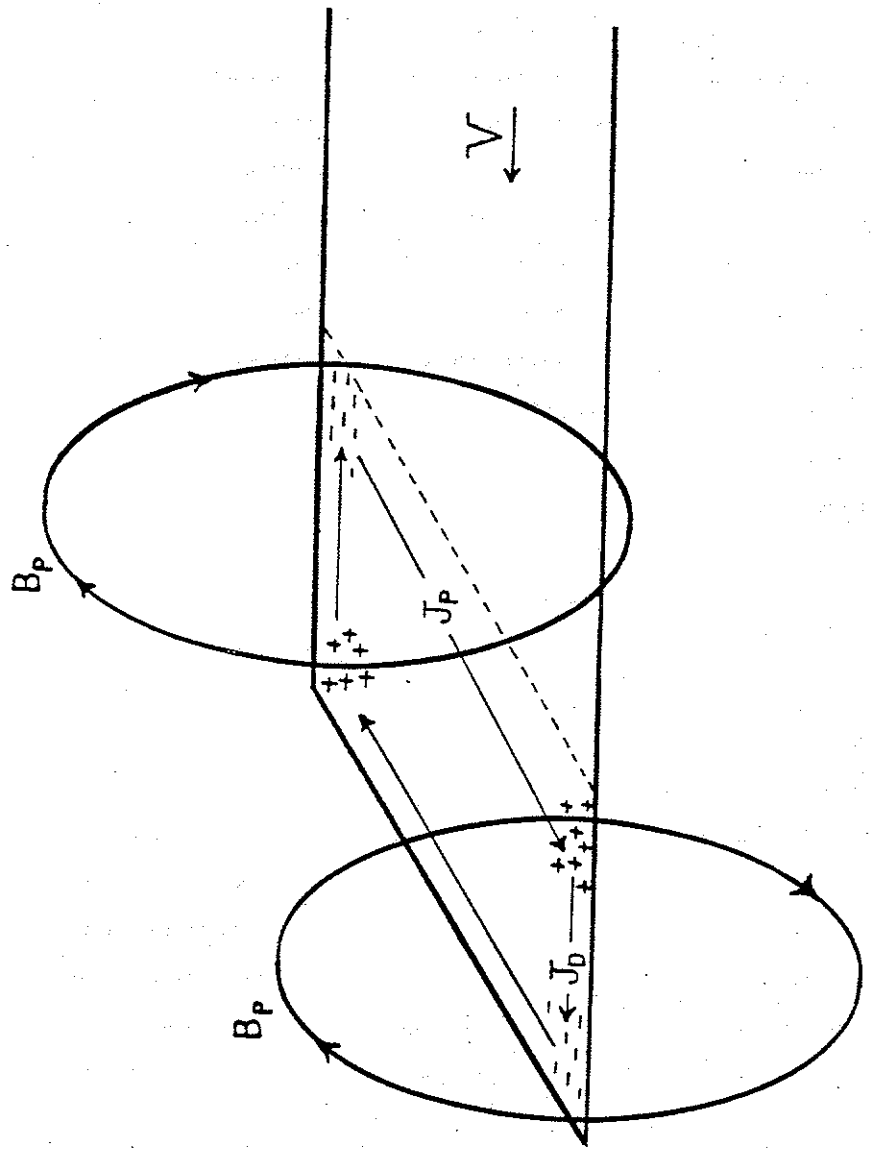

Figure 4-1

A complete and thorough description of this process can now be illustrated, but first a few comments about the current paths are necessary. There are two possible paths the current $\vec{J}_D$ could travel in figure 4-1. Besides the path shown, the current could also flow along field lines, instead of across them, to reach the other side of the device. This current path would also short out the polarization field. A quick calculation shows that conductivity along field lines, for a typical magnetic field strength, should be, at a minimum, an order of magnitude greater than across field lines. Measurements showed that the current flowed parallel to the direction of travel, $\vec{v}$, perpendicular to field lines.[3] Current flow along field lines was not observed and thus will not be considered. In fact, this current parallel to $\vec{B}$, would be ineffective if a weak toroidal field, 1/10 the strength of the poloidal field, were added. This would cause the poloidal field lines to not line up, and an effective depolarization current would not flow. In reality such an added toroidal field barely affects trapping.

Another possible current path to short out the polarization field is perpendicular to both $\vec{B}$ and $\vec{v}$. This current would flow parallel to a cross section, but along the outer edge of the beam. The $\vec{J}\times\vec{B}$ force of this current flow, however, would just cancel the force of the polarization current that supports it. Thus we will consider only a depolarization current strictly parallel to $\vec{v}$, across the magnetic field.

B. The Trapping of Plasma in a Poloidal Field

An idealized case of plasma being injected into an octupole field will now be considered. This case is less complicated than the more general one of injection into a combination of poloidal and toroidal fields, as is the case for a tokamak. This will serve as an exercise to illustrate the procedure for the more general case to follow.

For a plasma beam traveling along the midplane and perpendicular to the magnetic axis, the magnetic field through the center of the device can be approximated by a function proportional to r^3 as shown in figure 4-2. Refer to figure 2-4 for a diagram of the field that this represents. The origin is in the center of the device and the distance L/2 can be any distance of interest from the center of the machine. The functional form of the magnetic field strength with this approximation is given by

$$|B| = -B_o\left\{\frac{2x}{L}\right\}^3 \qquad (4\text{-}1)$$

The injected plasma beam is modeled as a rigid column of square cross section as shown in figure 4-3. The plasma is modeled as a rigid column to simplify the equations that follow into a solvable form. This approximation should not change the underlying physics of the problem. The plasma column has width 2a on each side, with

Figure 4-2. Idealized poloidal field as a function of x.

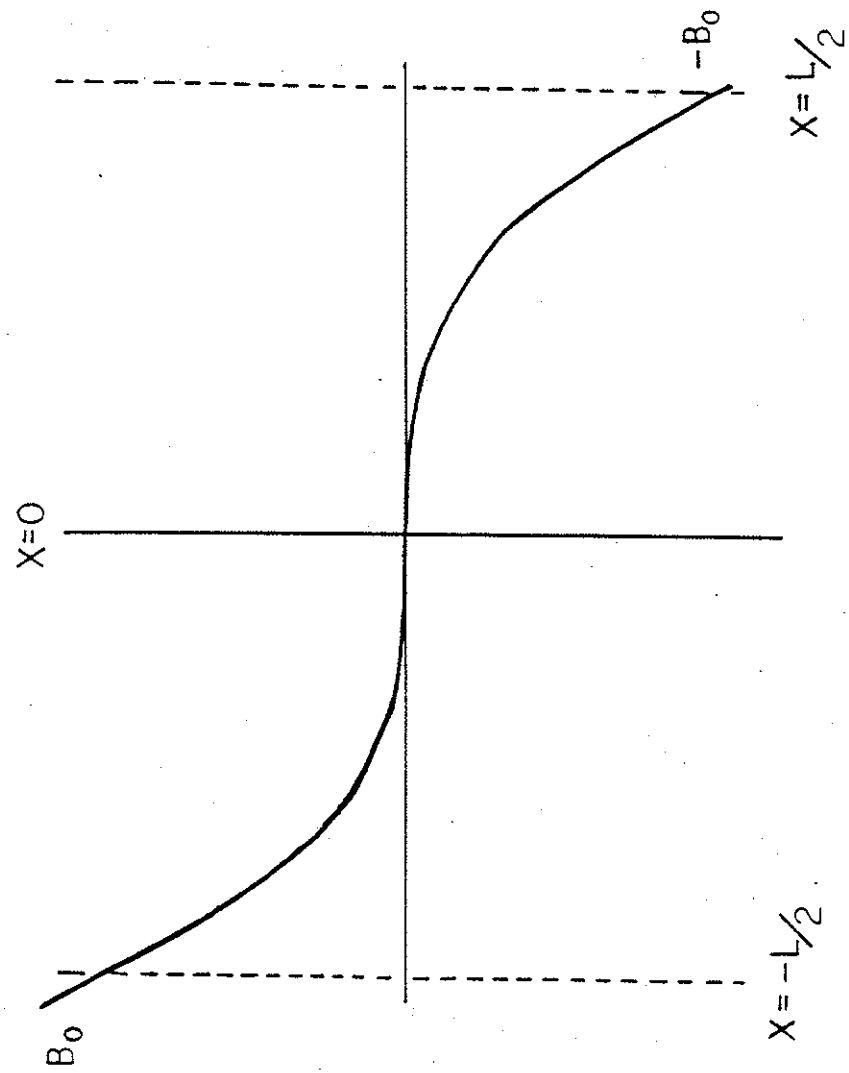

Figure 4-2

Figure 4-3. The injected plasma is modeled as a rigid column crossing the magnetic field structure

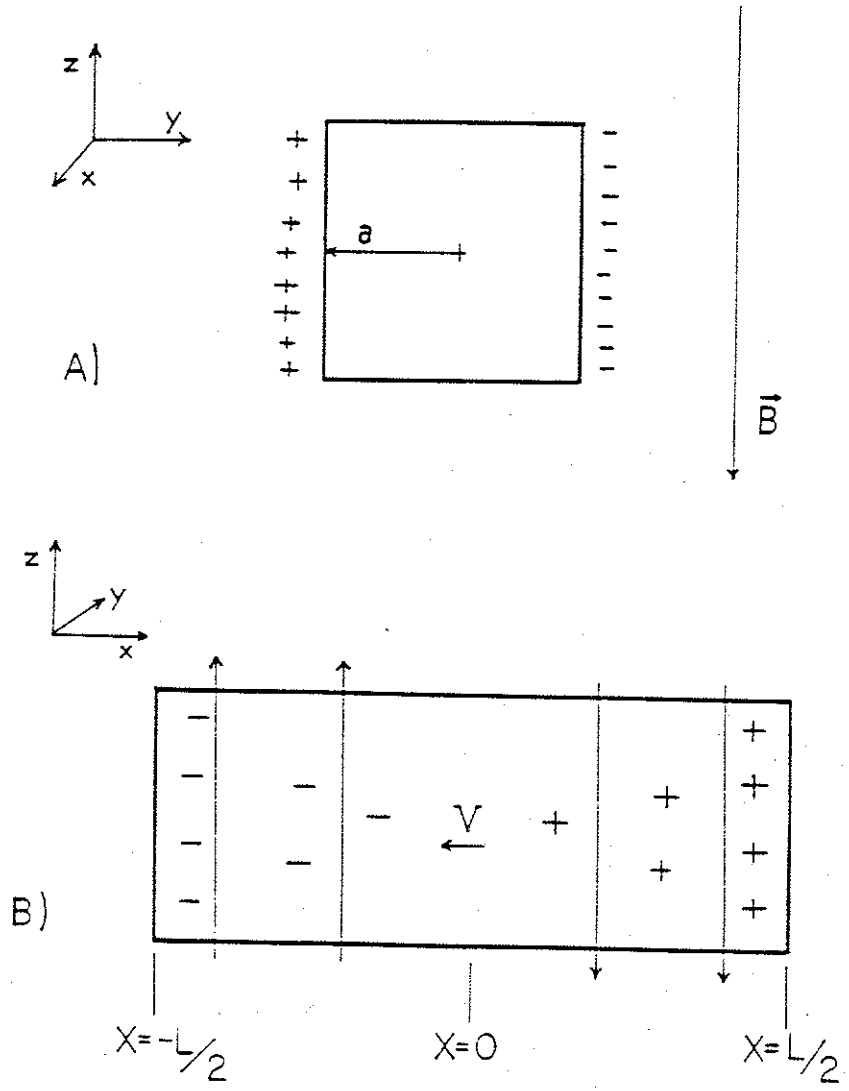

Figure 4-3

length L in the direction of motion. The direction of magnetic field is also shown in the figure to help with orientation.

With the given conditions for plasma to cross a magnetic field, the interior of the plasma sees an electric field,

$$\vec{E} = -\vec{v} \times \vec{B} \tag{4-2}$$

The outer edges of the column with sides parallel to $\vec{B}$ would then be at a potential given by,

$$\phi(x) = B(x)va \tag{4-3}$$

where $\phi(0)$ is taken to be zero. Because $|B|$ varies as a function of x, ϕ does also. This creates an electric field, $\frac{d\phi}{dx}$, in the x direction, which in turn causes a depolarization current, $\vec{J}_D$, to flow. The current density flowing along the edge of the plasma is given by

$$J_x = \sigma \frac{d\phi(x)}{dx} \tag{4-4}$$

where σ is the conductivity of the plasma along the outer edge of the plasma column subject to this electric field. The total current flowing on one side is then

$$I(x) = A\sigma \frac{d\phi(x)}{dx} \tag{4-5}$$

where A is the effective conducting area along the outer edge of the column. The conducting medium is the plasma along the edge of the column that has been stopped by the magnetic field and does not see all of the polarization electric field.

The current in the x direction is the depolarization current that depletes the polarization charge. The plasma column will then support a current through it to maintain the polarization field. The current density through the column would then be given by

$$J(x) = \frac{1}{2a} \frac{dI(x)}{dx} \tag{4-6}$$

as shown in figure 4-4. This results in a current density inside the plasma column of

$$J(x) = \frac{A\sigma v}{2} \frac{d^2B}{dx^2} \tag{4-7}$$

A slowing force is acting on the plasma column due to this current flowing perpendicular to $\vec{B}$ through it. An element in the plasma sees a force

$$mn_b \frac{d\vec{v}}{dt} = \vec{J} \times \vec{B} \tag{4-8}$$

Figure 4-4. Polarization current flowing through the plasma column.

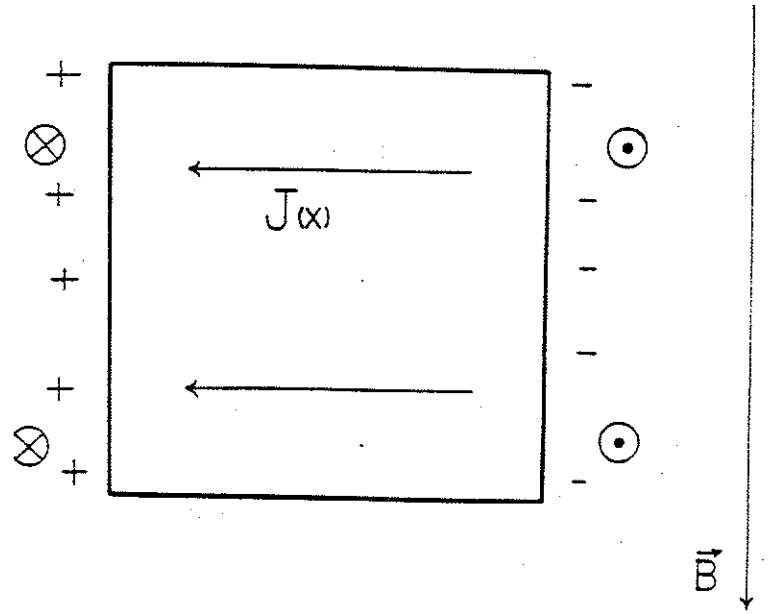

Figure 4-4

with the total force on the plasma column.

$$\int mn_b \frac{d\vec{v}}{dt}\, dV = \int \vec{J} \times \vec{B}\, d\ell dA \qquad (4\text{-}9)$$

Assuming a rigid plasma column, the left side of equation 4-9 becomes

$$\int mn_b \frac{d\vec{v}}{dt}\, dV = 4a^2 Lmn_b \frac{dv}{dt} \qquad (4\text{-}10)$$

or

$$4a^2 Lmn_b \frac{d\vec{v}}{dt} = -\int \vec{J} \times \vec{B}\, d\ell dA \qquad (4\text{-}11)$$

For this case $\vec{J}$ is always perpendicular to $\vec{B}$, with the resultant force in the $-\hat{x}$ direction. The integration over $\hat{y}$ and $\hat{z}$ can be carried out easily since there is no dependence on these variables in J and B. We can then substitute for $\vec{J}$ from equation 4-7 with the result that

$$\frac{dv}{dt} = -\frac{\sigma A v}{2Lmn_b} \int_{-L/2}^{L/2} B \frac{d^2B}{dx^2}\, dx \qquad (4\text{-}12)$$

Using the form of $\vec{B}$ given in equation 4-1, integration of equation 4-12 yields

$$\frac{dv}{dt} = -\frac{12}{5} \frac{\sigma A B_o^2}{n_b m L^2} v \qquad (4\text{-}13)$$

This has a solution for v given by

$$v = v_o e^{-t/\tau_s} \qquad (4\text{-}14)$$

where τ_s is a characteristic slowing down time :

$$\tau_s = \frac{5 n_b m L^2}{12 \sigma A B_o^2} \qquad (4\text{-}15)$$

This result makes intuitive sense. The slowing down time is inversely proportional to the conductivity and effective conducting area of the current-carrying plasma on the edge of the column. The depolarization current which provides the stopping force for the plasma column should be proportional to these two parameters. The factor $(L/B_o)^2$ also appears correct. Since $\vec{J}$ is proportional to $\vec{B}$, $\vec{J} \times \vec{B}$ should be proportional to B^2.

The explicit form of the cross field conductivity, σ, has not yet been specified. The conditions that exist on the outside edge of the moving plasma are not well known. One assumption to be made is that the plasma on the edge is of the same temperature and density as the center of the plasma column. With this approximation there are two possible mechanisms for cross field conductivity. Either a conductivity due to a time-changing electric field or a cross field Spitzer conductivity could be responsible for current flow. Both of these conductivities have a dependence on the density of the conducting medium, n_b, and the magnetic field strength, B.

In the presence of a sinusoidally varying electric field there can be a conductivity across field lines given by,

$$\sigma = \frac{inm\omega}{B^2} \tag{4-16}$$

where ω is the frequency of the time varying field. In our case ω can be approximated by

$$\omega = \frac{2\pi v}{L} \tag{4-17}$$

This mechanism for conductivity was assumed for injection into octupoles and fit fairly well the experimental data.

The gun-injected plasmas used in this work are much more dense than those used previously. For these conditions, cross-field Spitzer conductivity may be more appropriate. This conductivity is given by,

$$\sigma_\perp = \sigma_\parallel \frac{\nu_{ei}^2}{(\nu_{ei}^2+\omega_{ce}^2)} \tag{4-18}$$

where $\sigma_\parallel$ is the traditional Spitzer conductivity. Then

$$\sigma_\perp = \frac{ne^2\nu_{ei}}{m_e(\nu_{ei}^2+\omega_{ce}^2)} \tag{4-19}$$

where n is the plasma density, ν_{ei} is the electron-ion collision frequency and ω_{ce} is the electron cyclotron frequency. If we use this conductivity in equation 4-15 the slowing down time becomes

$$\tau_s = \frac{m_e m_i L^2(\nu_{ei}^2+\omega_{ce}^2)}{2e^2AB_o\nu_{ei}} \tag{4-20}$$

The electron-ion collision frequency is proportional to n and inversely proportional to $T_e^{3/2}$. For scaling purposes τ_s then varies as

$$\tau_s \propto \frac{(n_b^2 + kT_e^3 B^2)}{n_b B^2} \qquad (4\text{-}21)$$

where k is the physical constant 5.4×10^{29} when n_b is cm^{-3}, T_e is eV, and B is kG.

Equation 4-21 describes how the trapping should vary as the magnetic field and injected plasma density change. One interesting feature of 4-21 is that at high magnetic field, or $\nu_{ei} << \omega_{ce}$, the trapping is independent of B. This result arises because at high magnetic field strength the conductivity has an inverse relationship with B. This means the trapping force will saturate at some value of magnetic field.

Another counter intuitive result is that the slowing time is inversely proportional to n_b at large magnetic fields. A stream of plasma with more density and thus more momentum should stop more slowly, assuming a given slowing force. The more dense plasma however, has a higher conductivity, $\propto n_b^2$, which allows more current to flow and apply a greater stopping force. These scaling relations should provide a good means of evaluating data, to see if this trapping mechanism is appropriate for our case. This will be done in the next chapter.

C. The Trapping of Plasma in Poloidal and Toroidal Fields

To understand the trapping of plasma in a tokamak, the model of injection into poloidal fields must be extended to include the effect of toroidal fields. To derive a stopping distance for a plasma beam moving through a tokamak, a procedure will be used which is similar to the one used in the previous section. As the beam travels through magnetic field lines of changing direction, an electric field is set up which is parallel to the direction of travel. This electric field drives a current, along the outside of the beam, which attempts to drain the polarization charge. The plasma column must then support a current to maintain the polarization charge in order to keep moving through the magnetic field. Finally the force on the plasma due to this polarization current is summed up over the whole column to derive a stopping time.

The magnetic field of the tokamak will be modeled as a straight cylinder with a constant plasma current density. As a plasma travels along the midplane, perpendicular to the magnetic axis, it would then see a poloidal field, which varies linearly with the distance from the current axis. If the toroidal magnetic field strength is constant and much larger than the poloidal field, the total field strength is constant with the angle the magnetic field makes with the horizontal midplane being that shown in the graph of figure 4-5. This angle, $\alpha(x)$, is given by

$$\alpha(x) = \frac{2\alpha_o}{L} x \qquad (4\text{-}22)$$

where α_o is a constant angle.

In this model the plasma is once again modeled as a rigid column of plasma with length L. This time the column has a circular cross section of radius a. A diagram of this plasma, traveling on the horizontal midplane, and crossing the previously described magnetic field is shown in figure 4-6. A cross-sectional view of this plasma column is shown in figure 4-7. In this figure, α is the angle between the horizontal midplane and the magnetic field. Theta (θ) is a dummy variable over which to integrate. With θ as the angle between an arbitrary radius and the vertical through the midplane, ψ becomes the angle between this radius and the radius that is perpendicular to $\vec{B}$. Thus,

$$\psi(x) = \theta - \alpha(x) \qquad (4\text{-}23)$$

In order to get a slowing down time, the currents that flow in the plasma cylinder due to a depolarization current are summed up to derive a total slowing force. If the cylindrical plasma column uses a polarization electric field to cross the magnetic field, then in the interior of the plasma,

Figure 4-5. The angle, α, between the magnetic field and the midplane, as a function of x, for constant toroidal field and toroidal plasma current density.

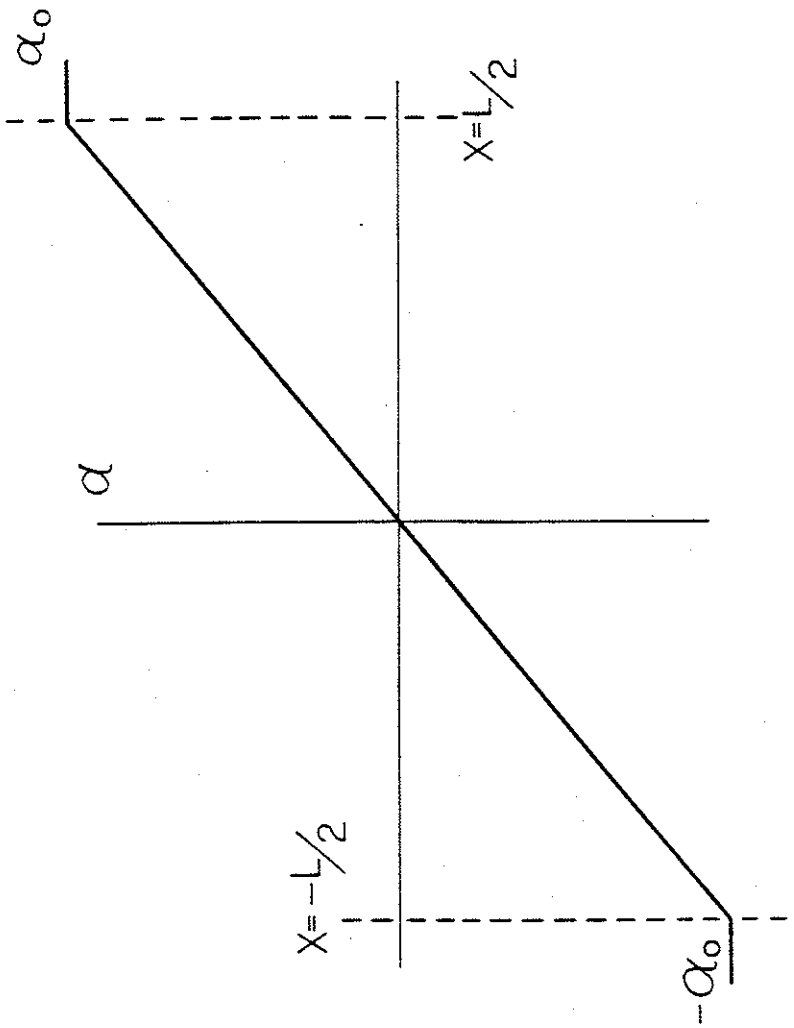

Figure 4-5

Figure 4-6. Cylindrical plasma column crossing tokamak field structure.

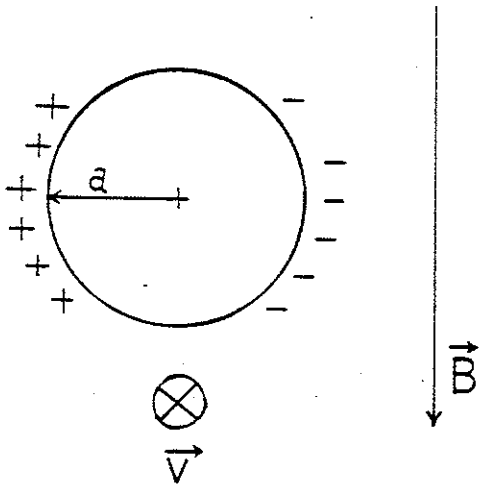

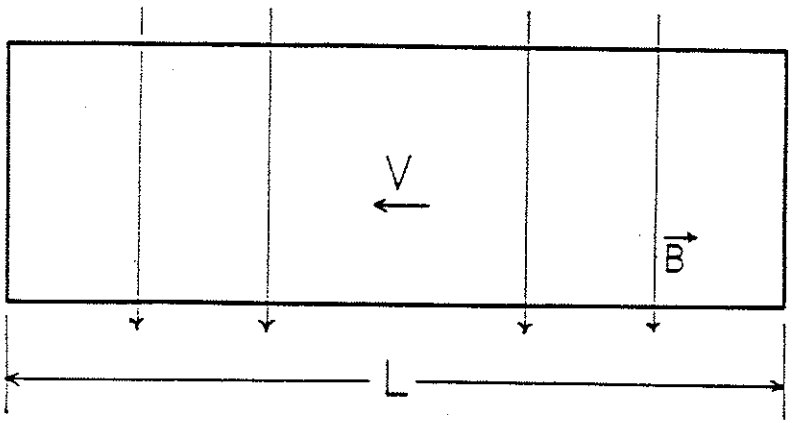

Figure 4-6

Figure 4-7. A cross section of plasma column with definition of coordinates.

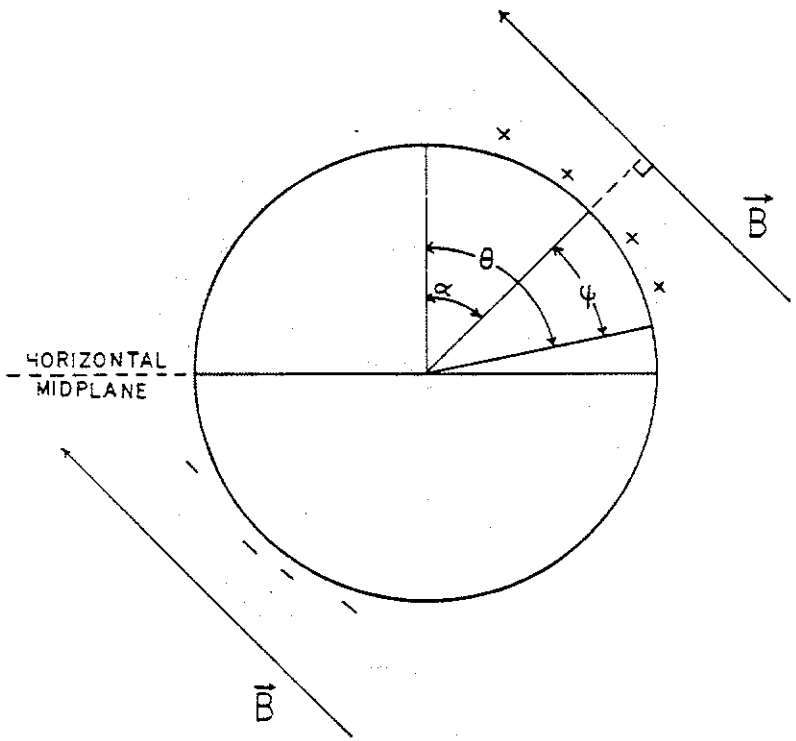

Figure 4-7

$$\vec{E} = -\vec{v} \times \vec{B} \tag{4-24}$$

If the electric potential, ϕ, is taken to be zero on the axis of the cylinder, ϕ on the surface of the cylinder is

$$\phi(x) = vaB\cos(\psi(x)) \tag{4-25}$$

The electric field on the surface of the cylinder which drives a polarization current in the x̂ direction is given by

$$E_x(\theta,x) = \frac{d\phi(\theta,x)}{dx} \tag{4-26}$$

If there is an effective conducting area extending a distance ℓ from the surface of the cylinder, as shown in figure 4-8, the incremental current flowing along the surface, between angles θ and $\theta+d\theta$, is given by

$$dI(\theta,x) = a\sigma\ell E_x(\theta,x)d\theta \tag{4-27}$$

With $|B|$, v, and a not varying with x, the equations 4-23, 4-25, 4-26, and 4-27 combine to yield the depolarization current through a small angle on the surface as a function of θ and x.

$$dI(\theta,x) = a^2\ell\sigma vBd\theta\frac{d}{dx}\left(\cos(\theta-\alpha(x))\right) \tag{4-28}$$

Figure 4-8. Incremental current flowing along surface of cylinder.

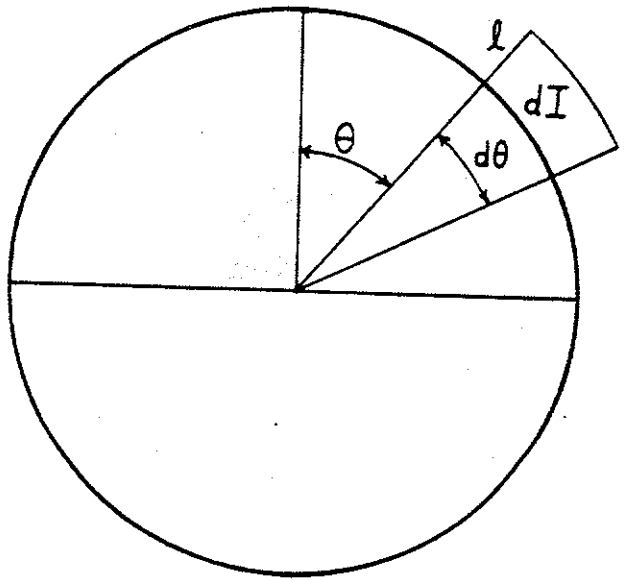

Figure 4-8

In order to support this depolarization current, a polarization current must flow through the plasma column. The current density perpendicular to, or through the surface of the cylinder, is given by

$$J_{\perp}(\theta,x) = \frac{d^2I(\theta,x)}{ad\theta dx} \qquad (4\text{-}29)$$

or with equation 4-28,

$$J_{\perp}(\theta,x) = a\ell\sigma vB\left\{\sin(\phi(x))\frac{d^2\alpha}{dx^2} - \cos(\phi(x))\left(\frac{d\alpha}{dx}\right)^2\right\} \qquad (4\text{-}30)$$

With this current density through the cylinder surface, the force on the cylinder due to the currents can be integrated. The current flowing into the cylinder has two components. One of these components is J_s, current proportional to $\sin\phi$, and the other is J_c, current proportional to $\cos\phi$, as shown in figure 4-9. Because J_s is antisymmetric about $\phi = 0$, it supports a current that is parallel to $\vec{B}$. In a similar way J_c supports a current that is perpendicular to $\vec{B}$. We can model J_c as a current filament perpendicular to $\vec{B}$, and J_s parallel to $\vec{B}$. Because J_s is parallel to $\vec{B}$ it does not contribute to the slowing force. The slowing force expression of equation 4-9 becomes

Figure 4-9. Currents J_s, and J_c, flowing parallel and perpendicular to the magnetic field, through the plasma column.

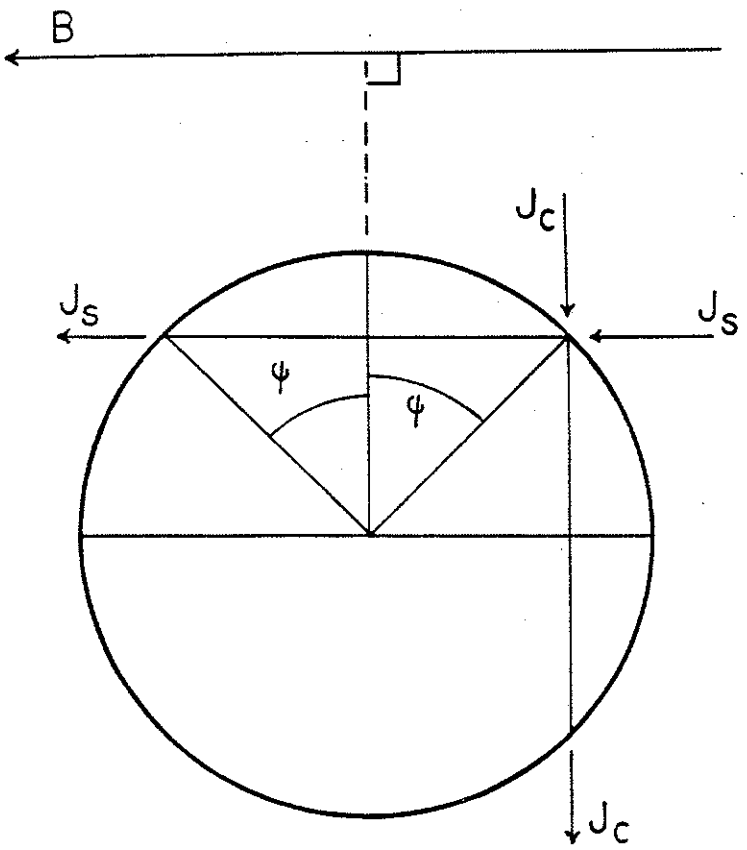

Figure 4-9

$$\int \vec{J}\times\vec{B}\, d\ell dA = -B\int J_c(\theta,x)\, d\ell dA\, \hat{x} \qquad (4\text{-}31)$$

With the current, J_c, constant as shown in figure 4-9, the integral $\int d\ell$ becomes $2a\cos(\theta-\alpha(x))$, with $dA=ad\theta dx$. Equation 4-31 then reduces to

$$\int \vec{J}\times\vec{B}\, d\ell dA = -2a^2B\int \ell_{av}B\left(\frac{d\alpha}{dx}\right)^2\cos^2(\theta-\alpha(x))d\theta dx\, \hat{x} \qquad (4\text{-}32)$$

so the stopping force becomes

$$\int mn_b\frac{dv}{dt}\, dV = -\pi B^2a^3\ell_{av}\int_{-L/2}^{L/2}\left(\frac{d\alpha}{dx}\right)^2 dx \qquad (4\text{-}33)$$

with equation 4-22 for $\alpha(x)$, the equation for the velocity, v, becomes

$$\frac{dv}{dt} = -\frac{4a\ell_{av}\alpha_o^2B^2}{mn_bL^2}\, v \qquad (4\text{-}34)$$

Solving for v we obtain

$$v = v_oe^{-t/\tau_s} \qquad (4\text{-}35)$$

with the characteristic slowing down time τ_s given by

$$\tau_s = \frac{L^2 n_b m}{4\alpha_o^2 B^2 a\ell\sigma} \qquad (4\text{-}36)$$

This slowing down time is very similar to the slowing down time for injection into purely poloidal fields, as in equation 4-16. The quantity τ_s is proportional to m and n_b, and inversely proportional to B^2 and σ. In this case the effective conducting area outside of the cylinder is $4a\ell$, which seems reasonable. Finally τ_s is inversely proportional to $(\alpha_o/L)^2$, which is just the changing pitch of the field lines per scale length. This case will reduce to the pure poloidal case if $\alpha_o = \pi/2$, with the only difference being a geometric factor.

The final consideration is once again the conductivity σ. The conductivity has the form of equation 4-19, with the same considerations. For the present case with toroidal field this conductivity is actually more accurate since $|B|$ does not vary with x.

For scaling purposes τ_s varies as

$$\tau_s \propto \frac{L^2(n_b^2 + kT_e^3 B^2)}{n_b \alpha_o^2 B^2} \qquad (4\text{-}37)$$

where k is the same physical constant as in equation 4-21. This equation has different characteristics, for variations with n and B,

depending on what regime is under consideration. Figures 4-10 and 4-11 show the variation of τ_s with n_b, B and α_o. The value $\omega_{ce} = \nu_{ei}$ is an important transition region, where scaling changes from one form to another. When $\omega_{ce} < \nu_{ei}$ scaling goes as $n_b \alpha_o^{-2} B^{-2}$. At higher magnetic fields, when $\omega_{ce} > \nu_{ei}$, the slowing time goes as $n_b^{-1} \alpha_o^{-2}$. This is a much different form of slowing. These changes in scaling are much the same as the pure poloidal field case.

The scaling laws derived above should present a unique signature in experimental data. By injecting a gun plasma into various magnetic field configurations, including that of a Tokamak, this structure can be tested. In the following chapters, such experiments will be described. An evaluation of the model will then be made to see if it represents the physical mechanisms that control the process.

Figure 4-10. Variation of trapping time with magnetic field, and density.

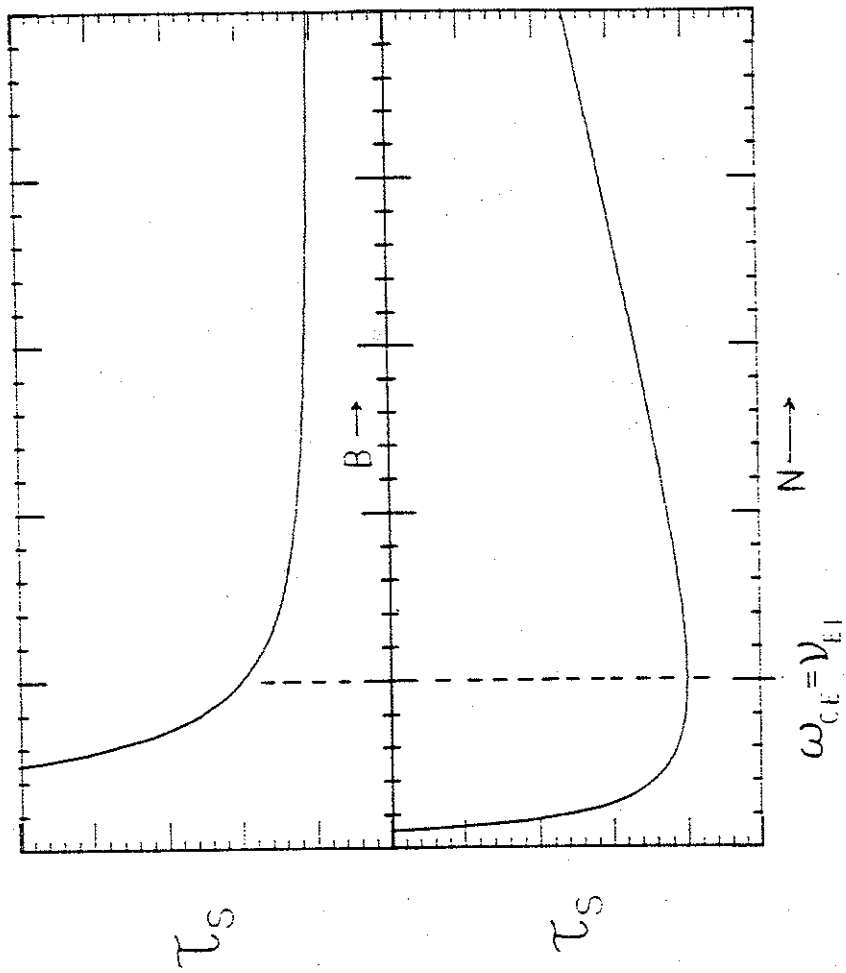

Figure 4-10

Figure 4-11. Variation of slowing time with pitch of field lines, α.

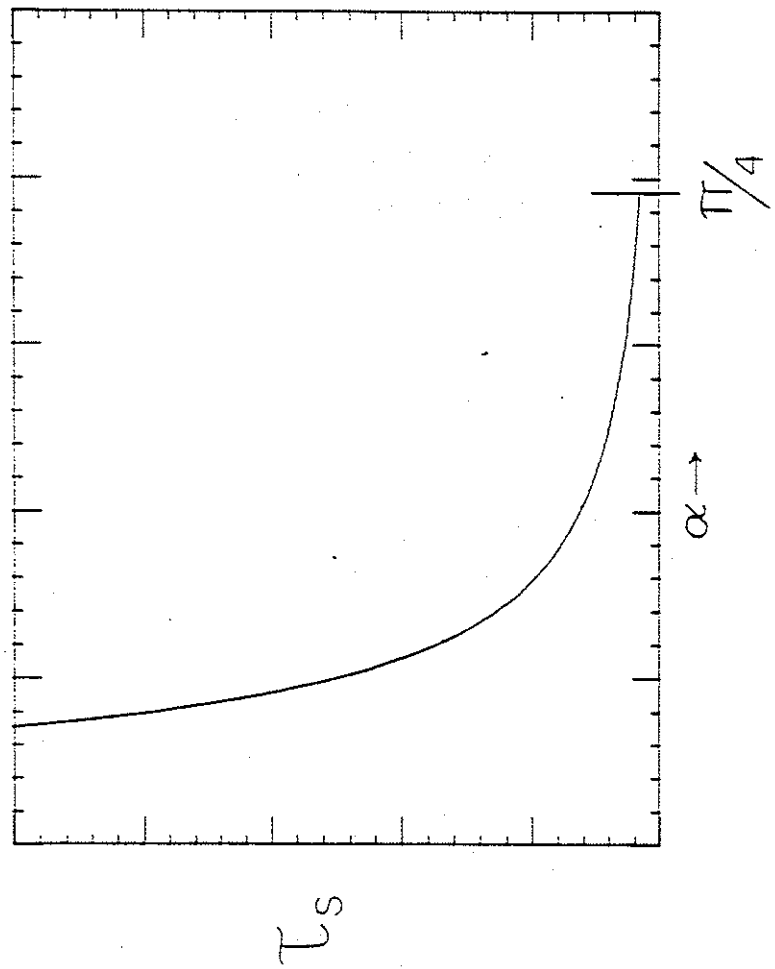

Figure 4-11

References for Chapter IV

[1]G. Schmidt, Phys. Fluids 3, 961 (1960)

[2]D. A. Baker and J. Hammel, Phy. Fluids 8, 713 (1965)

[3]R. A. Dory, D. W. Kerst, D. M. Meade, W. E. Wilson, and C. W. Erickson, Phys. Fluids 9, 997 (1966)

CHAPTER V

EXPERIMENTAL RESULTS FOR VACUUM FIELDS

A. Introduction

In this chapter, experimental data will be examined to determine how well the theoretical model, discussed in the previous chapter, fits the physical reality of gun-injection of plasmas into various magnetic field configurations. The experimental conditions of a tokamak discharge in Tokapole II are a combination of four parameters. The first is a poloidal field, B_p, which results from the divertor hoop current. The second is toroidal field, B_t. The effects of plasma in the discharge result in the injected plasma beam seeing a tokamak density, n_e, and a toroidal plasma current, I_p. Each of these factors has been isolated and investigated separately to evaluate their effect on the trapping process. In this chapter the vacuum magnetic fields will be investigated. The vacuum magnetic fields are B_p and B_t without plasma present. In the idealized model, the plasma beam experienced only poloidal and toroidal fields. The vacuum field case should then be effective in checking the validity of the model.

The additional effects of plasma and plasma current due to a tokamak discharge will be investigated in the next chapter. In this

way the conditions of the tokamak discharge can be separated to see if the trapping observed in Chapter III is described by the model.

This chapter will investigate two vacuum field cases. The first will be a pure poloidal, or octupole field case. The second will be the more general poloidal with added toroidal field case. Octupole fields are a limiting case of the more general one and will be discussed first. The model of Chapter IV Section B describes this case and a comparison will be made. The real test of the model, especially for describing trapping in a tokamak, will be the case of trapping in a combination of poloidal and toroidal fields. This will be the second case investigated in this chapter. A final conclusion will be reached as to the validity of the proposed trapping mechanism.

The predictions of the model can be checked two ways. The first is by evaluating the experimental parameters and substituting them into the slowing equations 4-16 and 4-41. Consistency between the slowing time, τ_s, and the experimental results can then be looked for. There is much uncertainty however, in some of the parameters of the injected plasma. This is especially true for the temperature of the injected plasma, which strongly affects the value of the conductivity, σ. The injected plasma also has significant turbulence with high frequency fluctuations in density and electric fields. These mitigating circumstances mean that the actual slowing down times may be of limited value in evaluating the model. The scaling of trapping, with the variation of controlling parameters is

a second method of evaluation which can provide much more useful information. If the trapping of injected plasma scales with the magnetic field structure and parameters of the injected plasma, as predicted, then the underlying physical principles of the model can be presumed to be valid. Scaling will be the most important factor determining the success of the model.

B. Octupole Fields

Gun injected plasmas, trapped by multipole magnetic fields, have been used for experimental plasma physics for a some time[1-3]. This magnetic field configuration produces a stable, quiescent structure in which to study a plasma. Here, we are more concerned with the initial trapping of this plasma. A typical time evolution of density created by injection into an octupole field is shown in figure 5-1. This signal is a line-averaged density viewed along the midcylinder by an interferometer as depicted in figure 2-9. We are interested in the process that creates this increase in density. To get a value for trapped density as conditions are varied, the signal from the interferometer at a time 200 μsec after a trigger is sent to fire the gun is used. This was done to ensure a consistent measure. The time was chosen to be after the peak in the density, but before the density had dropped significantly. Also each data point consists of several data shots. This was done because of reproducibility problems. The error bars represent the standard deviation in the distribution of the data.

Figure 5-1. Time evolution of line-average density trapped in octupole field. I_h = 200 kA and B_t = 0.

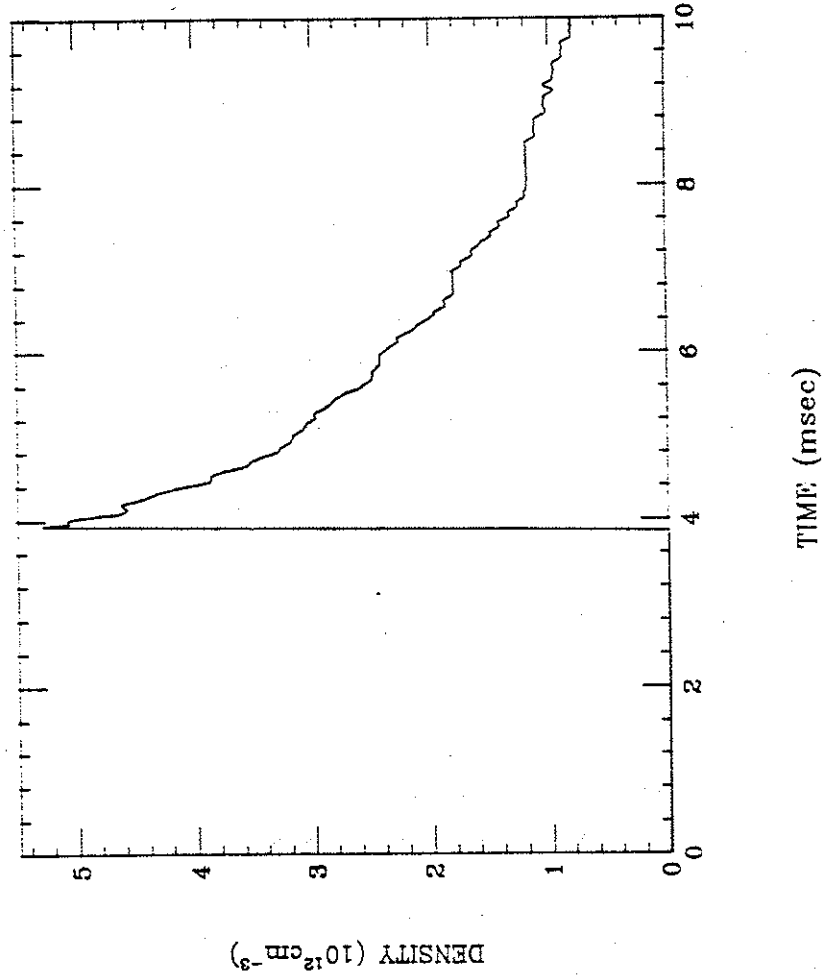

Figure 5-1

Figure 5-2 shows a graph of density trapped as the internal hoop current in Tokapole II was varied. Current in the hoops produces the poloidal field which traps the plasma. The poloidal field strength vs. position along the midplane is shown in figure 5-3, for an internal hoop current of 200 kA. There was no toroidal field present. The amount of density trapped increases with hoop current, but then saturates.

The experimental parameters can be used to calculate the slowing down distance for plasma moving in an octupole field, as predicted in the previous chapter. With equation 4-16 used as the slowing down time. a characteristic stopping distance would be

$$d_s = v_o \tau_s$$

The velocity, v_o, of the plasma in figure 5-2 was measured by time of flight to be 5 cm/μsec. With the slowing down time given by

$$\tau_s = \frac{n_b m L^2}{2\sigma_\perp A B^2} \qquad \text{with} \quad \sigma_\perp = \frac{n_b e^2 \nu_{ei}}{m_e(\nu_{ei}^2 + \omega_{ce}^2)}$$

as described in Chapter IV, we get an estimate for the predicted slowing down distance. For this experiment, at 200 kA of hoop current the magnetic field is 0.05 T. The injected plasma parameters were measured in Chapter III to be, $n_b \cong 10^{21}\ m^{-3}$, $L \cong 0.25$ m. Additional parameters of the plasma have to be

Figure 5-2. Trapped plasma versus poloidal field strength. $B_t = 0$.

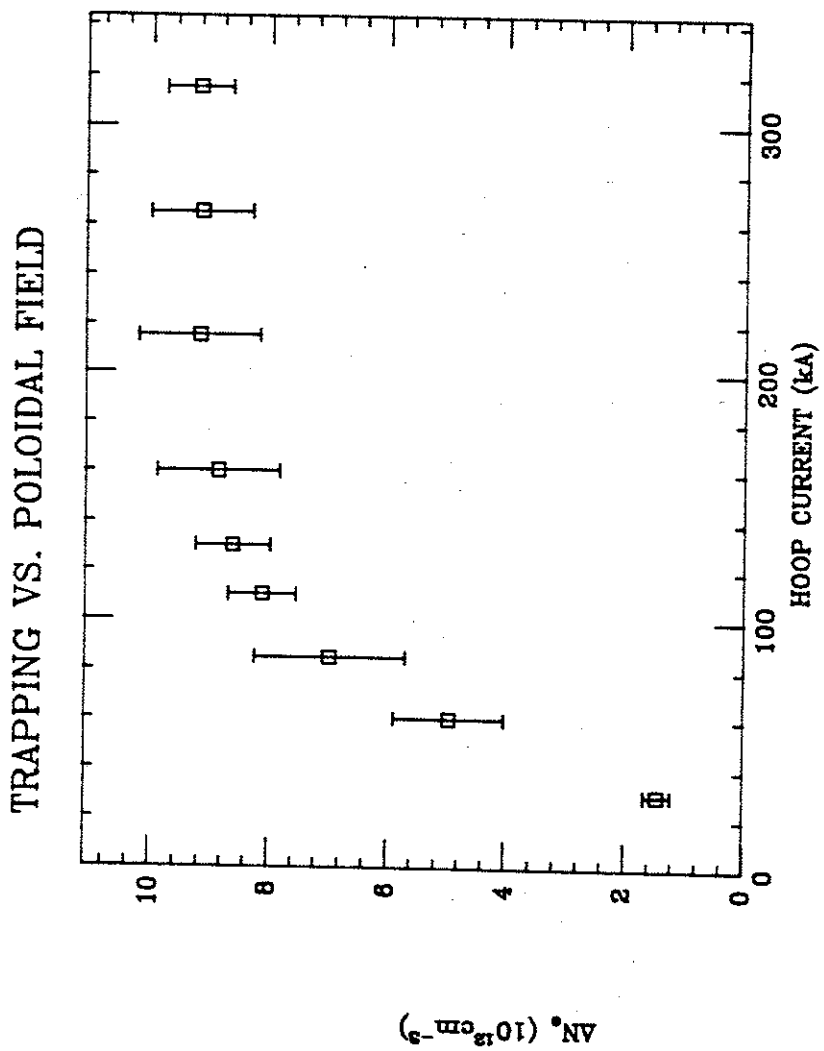

Figure 5-2

Figure 5-3. Poloidal field strength along horizontal midplane due to hoop current of 200 kA. $B_t = 0$.

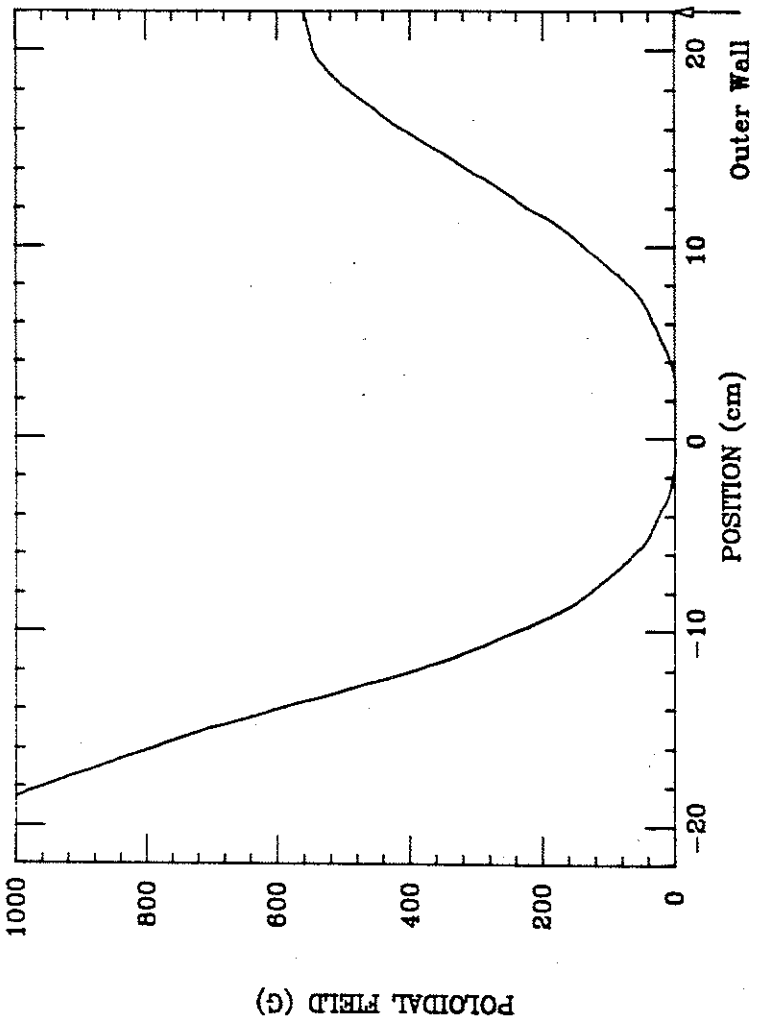

Figure 5-3

estimated. They are A ≅ 0.01 m^2, and T_e ≅ 1.0 eV. The beam density and temperature lead to

$$\nu_{ei} = 2\times10^{-6}\,\frac{n_b \ln\Lambda}{T_e^{3/2}}\ sec^{-1} \cong 2.45\times10^{10}\ sec^{-1}$$

which then leads to $\sigma_i \cong 1033\ (ohm\text{-}m)^{-1}$, and a slowing distance,

$$d_s \cong 9.6\ cm$$

The value of 200 kA was chosen by observation of figure 5-2. At hoop currents of greater than 200 kA there was little increase in the amount of plasma trapped. This value is a good point to observe if the predicted stopping distance is consistent with experimental observation. At a point where the process was just starting to saturate the predicted stopping distance should be on the order of the device size. The agreement obtained seems very good in light of the uncertainties that exist.

In calculating the conductivity, σ, several approximations were used. The value of the magnetic field varied along the direction of travel, with B = 0 at the center, therefore the conductivity was not constant. The value for B was obtained by viewing figure 5-3, which shows the magnetic field along the midplane calculated for a hoop current of 200 kA. Since most of the polarization current flows where $\frac{d^2B}{dx^2}$ is largest, the value B_o = 500 G was chosen. The density,

n_b, of the injected plasma, was assumed to be constant from the center to the edge where the depolarization current flows. It could have varied from this significantly. The conducting area, A, was also hard to estimate and could have varied by a factor of 5. Finally there was no measurement of the temperature, T_e, which is needed for the conductivity, $\sigma_\perp$. Because $\sigma_\perp$ is very dependent on T_e, this may have provided the greatest uncertainty. Temperatures of 1-10 eV are very common for this type of plasma discharge. 1 eV was chosen because it was reasonable, but also because it fit this and future data well. This free parameter, T_e, creates a large uncertainty in the predicted slowing distance, but the scaling arguments that follow should be unaffected. Finally, the density profile of the injected plasma was not known. A variation from the constant density profile of the model could affect the result somewhat. With these uncertainties, only limited conclusions should be drawn from the slowing distance. The data show that the model predicts a slowing force of the right order of magnitude to trap the injected plasma.

To ascertain if the model adequately represents the physical mechanisms involved, the scaling of equation 4-22 should be compared with the data.

$$\tau_s = \frac{(n_b^2 + kT_e^3 B^2)}{nB^2} \qquad (4\text{-}22)$$

The data in fig. 5-2 appears to follow the magnetic field scaling. The model predicts that at small magnetic field, B, the conductivity, $\sigma_\perp$, is dominated by collisions, with Spitzer conductivity resulting. This leads to

$$\tau_s \propto \frac{n}{B^2} \qquad \text{for } \omega_{ce} << \nu_{ei} \qquad (5\text{-}1)$$

When the magnetic field is increased, the gyro radius dominates the cross-field conductivity. The slowing down time is then predicted to go as

$$\tau_s \propto \frac{1}{n} \qquad \text{for } \omega_{ce} >> \nu_{ei} \qquad (5\text{-}2)$$

As the poloidal magnetic field was increased the amount of trapped density in (figure 5-2) also increased. This continued until the process saturated. The transition from equation 5-1 to 5-2 occurs in the region where $\nu_{ei} \approx \omega_{ce}$. For the plasma parameters listed previously this transition should occur at a magnetic field strength of ~1.0 kG. In figure 5-2 this transition, where trapping saturates, occurs at 100 kA of hoop current. From figure 5-3 it is observed that the middle 10-15 cm of the device had less than 150 gauss of magnetic field at 100 kA. This saturation of trapping took place at an earlier value than would be expected.

There is uncertainty in the value of ν_{ei}. The collision time, ν_{ei}, is very dependent on T_e, which could easily be different from 1 eV. This would affect where the transition occurs. But more importantly, the data observed, Δn_e, is not the same as the slowing time, τ_s. Though it is true that as τ_s decreases, Δn_e should increase, but the leveling off of Δn_e is not necessarily due to τ_s also leveling off. If τ_s is sufficiently short, the plasma will be stopped in a distance that is short compared to machine size. In this case all of the plasma is stopped and any further decrease in τ_s will not increase Δn_e. Once again viewing the trapping of figure 5-2, the saturation of trapping at about 150 kA of hoop current, was probably due to all of the plasma being trapped and not a saturation of τ_s. This would occur at a somewhat higher magnetic field strength. The trapping of figure 5-2 is probably a manifestation of the scaling in the low field regime, equation 5-1.

In order to observe how trapping varies with changes in the injected density, gun plasmas with different densities were injected into the same poloidal fields. For case I, in figure 5-4, the gun was filled to approximately 160 mtorr of hydrogen gas before initiation of the gun discharge. If all of the gas were ionized and trapped in the octupole field, the average density would be 3×10^{13} cm^{-3}. With 1×10^{13} cm^{-3} trapped at high fields, the data suggest that about 30% of the initial gas was ionized assuming the saturation in trapped density was due to all of the plasma being stopped. In case II the gun was filled to only 40 mtorr, so 1/4 of

Figure 5-4. Trapped density versus poloidal field. $B_t = 0$. Case I has gun filled to 160 mtorr of hydrogen gas. Case II, 40 mtorr.

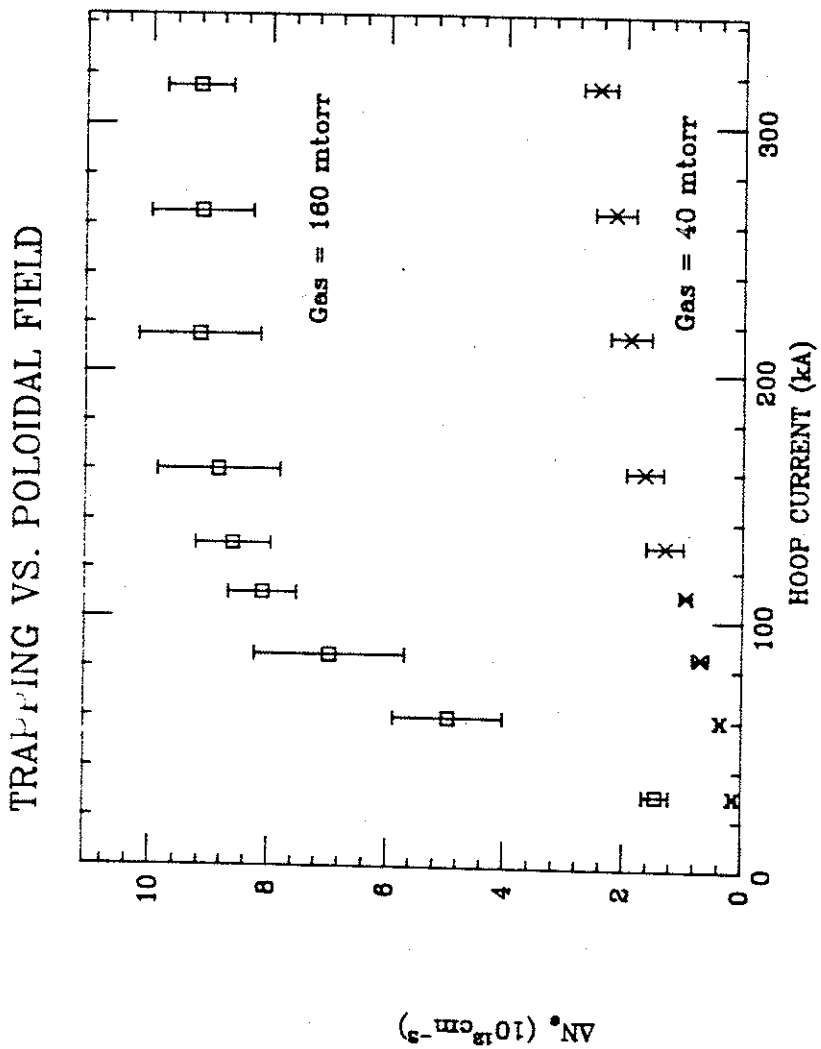

Figure 5-4

the density of case I should have been trapped. Case I did reach this level of 2-3 $\times 10^{12}$ cm^{-3}, but at a higher poloidal field strength. Apparently the less dense plasma was trapped less efficiently for a given poloidal field.

Examination of the slowing time in the low field regime (equation 5-1) and the data of figure 5-4 shows that a conflict exists. The model predicts that at low field strengths, $\omega_{ce} < \nu_{ei}$, the slowing time should go as $n_b B^{-2}$. The magnetic field dependence is seen in the data, but the beam density dependence observed is opposite of that predicted. To account for the data the cross-field conductivity must be different from what was assumed. In order for a more dense plasma to trap better, more depolarization current, per beam momentum, must flow. The conductivity must then increase with increasing density. The low-field Spitzer conductivity is apparently not accurate in describing this process.

An anomalous, high resistivity might account for the data. A lower conductivity with a different density dependence could reconcile discrepancies. The nature of this proposed resistivity is not understood and is open to speculation. One possibility is runaway electrons produced by large electric fields.[4] This conductivity scales as $n_b T_e^{-1/2}$ as opposed to $\sigma \propto T_e^{3/2}$ for Spitzer conductivity. This might account for the data. Large electric fields are needed, however, to produce the runaway electrons. For the experimental conditions the necessary electric field is 10^4-10^5 V/cm.[5] There are large fluctuating electric fields in the

plasma beam that could possibly create the runaway electrons. This mechanism is possible though not likely. Another possibility is turbulent resistivity.[6] This also has a conductivity proportional to n_b. These two possibilities are speculation and have not been investigated. Further work is needed to settle this issue.

Injection into octupoles is the only case where the low-field, $\omega_{ce} < \nu_{ei}$, condition occurs. The anomalous resistivity will be shown to not exist at higher fields when the conductivity is gyro-radius dominated. Thus, the uncertainty in conductivity at low field strengths, should not detract from the wider picture of injection into higher strength magnetic fields, such as the tokamak, which are yet to be examined.

For the case of injection of plasma into pure octupole fields, the theoretical model produces a slowing down time and distance which is consistent with experiment. The trapping scales with magnetic field as predicted. A discrepancy exists in scaling with beam density, n_b, however, at low magnetic fields. This conflict might be resolved by an anomalous resistivity.

C. Poloidal and Toroidal Fields

The modeling of plasmas injected into a combination of poloidal and toroidal fields, presented in the previous chapter, extends the theory of trapping to a wide range of magnetic field configurations, including that of a tokamak. To test this model, gun plasmas were fired into an octupole field with added toroidal field.

Figure 5-5 shows the results of injecting plasma into a background toroidal field of 1.5 kG, with different octupole fields added. The results appear similar to that for injection into a pure octupole field. As the poloidal field was increased more plasma was stopped until the process saturated at ~150 kA of hoop current. Additional poloidal field provided a shift in the angle of the magnetic field lines as the plasma crossed the device. More depolarization current was able flow and more plasma was stopped. These results are consistent with the model, at least in a qualitative sense.

Before a detailed comparison is made between the experimental results and theoretical predictions, figure 5-6 should be examined. This figure graphs the angle, α, that the magnetic field makes with the horizontal midplane, calculated for a case of $B_t = 1.5$ kG and $I_h = 200$ kA. The angle α is given by

$$\alpha = \tan^{-1}\left(\frac{B_p}{B_t}\right) \qquad (5\text{-}4)$$

Figure 5-5. Trapped density versus hoop current with added toroidal field. B_t = 1.5 kG. Gun filled to 160 mtorr.

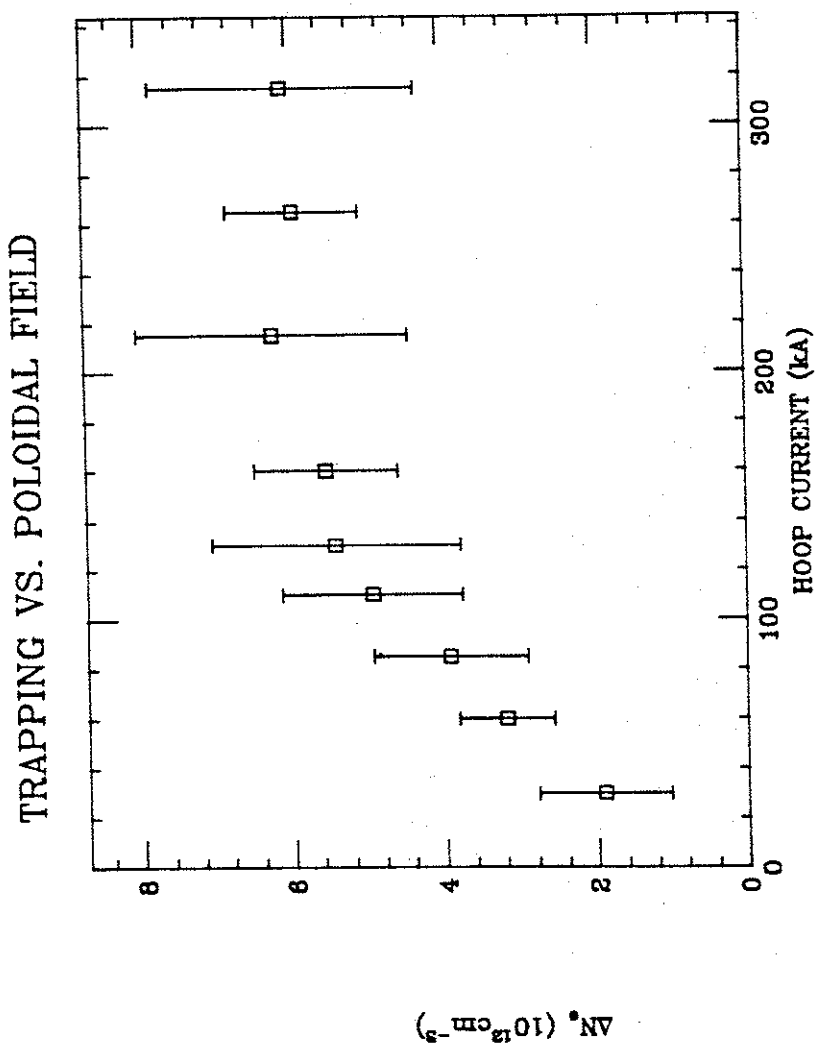

Figure 5-5

Figure 5-6a. The angle, α, that the magnetic field makes with the horizontal midplane versus position. Calculated for I_h = 200 kA, and B_t = 1.5 kG.

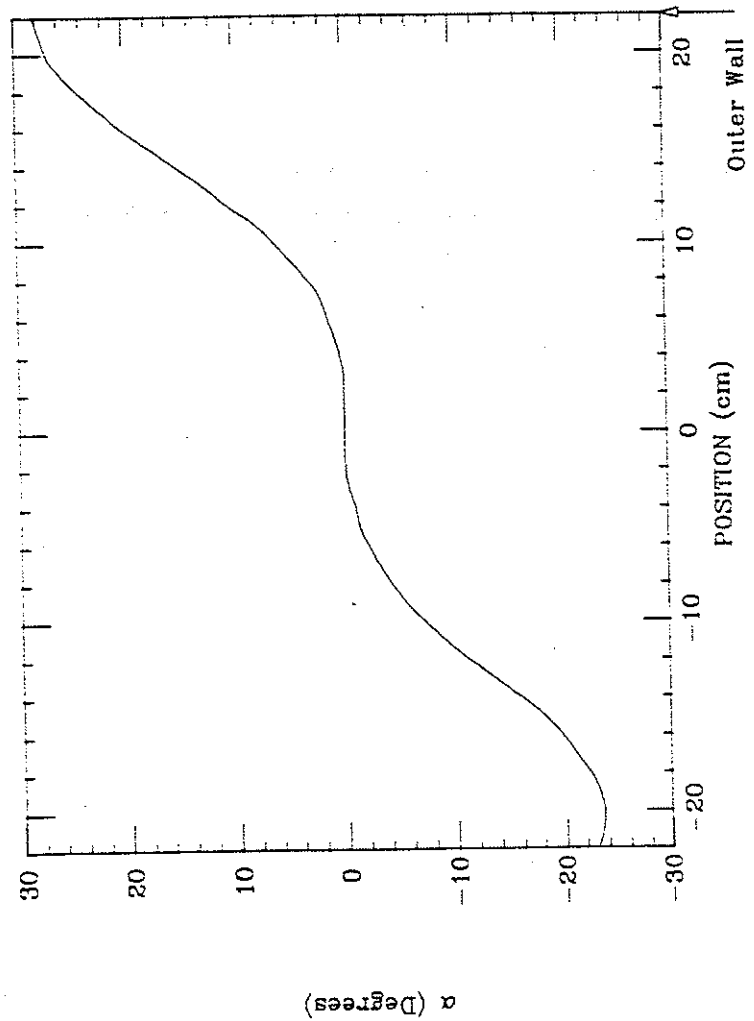

Figure 5-6a

Figure 5-6b. The magnetic field strength, $|B|$, versus position along the horizontal midplane. Calculated for I_h = 200 kA, and B_t = 1.5 kG.

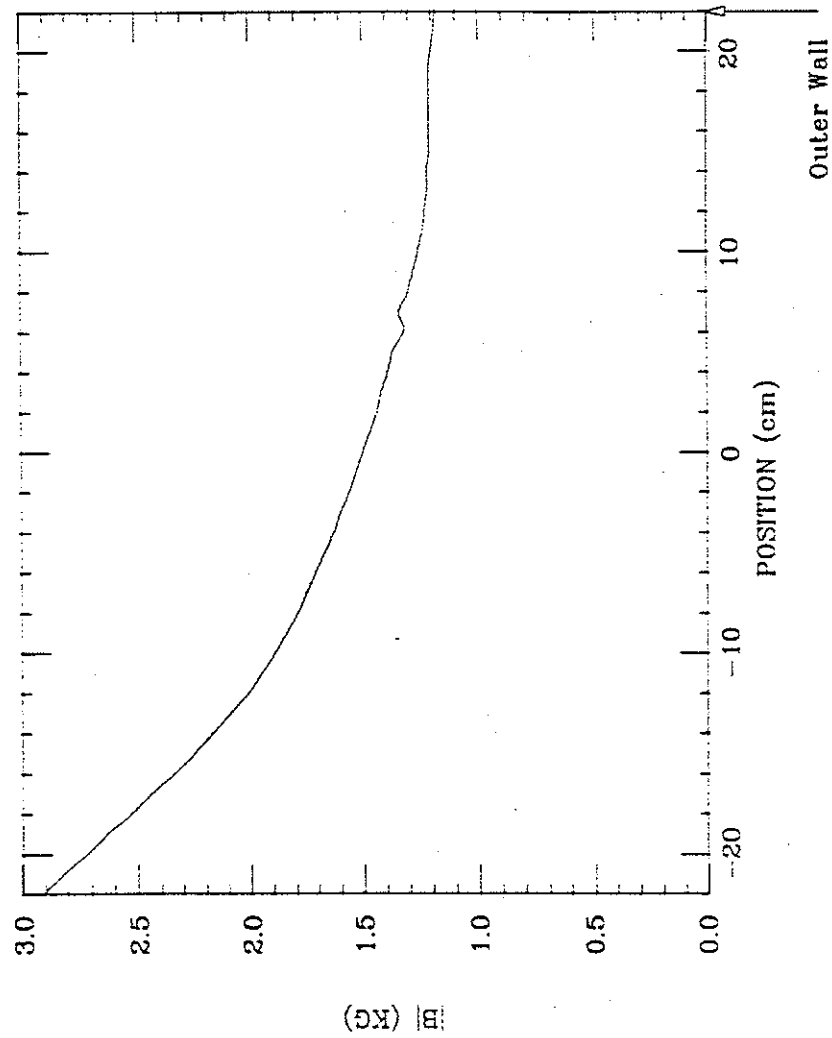

Figure 5-6b

Note, also, that the magnetic field strength is not constant. Comparison of figure 5-6 with the idealized fields of figure 4-6 shows how the experimental conditions and the idealized model differ.

The slowing down time of equation 4-40 can be evaluated to see how well it predicts the data of figure 5-5. With the use of figure 5-6, the parameters of injection can be estimated in a similar manner to that used for pure octupole fields. For a slowing time given by

$$\tau_s = \frac{L^2 m n_b}{4\alpha_o^2 B^2 a \ell \sigma} \qquad (4\text{-}40)$$

a reasonable choice for α_o from figure 5-6 is 0.3 radians, with $L \approx 30$ cm. The injected plasma parameters are the same as the previous octupole case. We have $n_b = 10^{21}\ m^{-3}$, $B \approx 0.15$ T, $a \approx 5$ cm, and $\ell \approx 5$ cm. The conductivity, σ, with $T_e = 1$ eV, is about 530 $(\text{ohm-m})^{-1}$. With $d_s = v_o \tau_s$, we get a stopping distance of

$$d_s \approx 16.7 \text{ cm}$$

This is similar to the size of the device. As in the previous octupole case the uncertainties are large. This result is meant to show that the model predicts a stopping force of the right order of magnitude to trap the plasma.

As hinted at earlier, the electron temperature was somewhat arbitrarily taken to be approximately 1 eV. It should be shown why this fits the data well. A comparison of figures 5-2 and 5-5 shows that trapping saturates at nearly equal values of poloidal field. At first it would seem that for equal values of poloidal field, the pure poloidal field case should provide the greatest stopping power. This is because it has complete field reversal. However at low temperatures, $\nu_{ei} >> \omega_{ce}$, the slowing down times become similar for both cases. Inspection of equations 4-40 and 4-20 reveal that for $\nu_{ei} >> \omega_{ce}$ the slowing down time is proportional to $\alpha_o^2 B^2$. In the pure poloidal case this quantity, $\alpha_o^2 B^2$ is approximately $\frac{\pi}{2} B_p^2$. For the toroidal field case, but still in the low field regime, if $B_t >> B_p$, then $\alpha_o^2 B^2 \approx B_p^2$. This shows that at low fields the stopping force is nearly constant for a given poloidal field strength no matter what the toroidal field is.

For the injected plasma used in this experiment, a temperature of 1 eV would mean the transition region, $\omega_{ce} \approx \nu_{ei}$, occurs at ~1 kG. The data of figure 5-5 occur just after this transition. One would then expect the slowing distances to still be somewhat similar for the two cases. The derived slowing distances are,

d_s, octupole = 9.6 cm

d_s, toroidal = 16.7 cm

at a value of 200 kA hoop current. It is not certain how well this

derived difference in slowing distances for the two cases should show up in actual data.

If an anomalous low field resistivity exists, as was conjectured earlier, it would serve to lower the conductivity of the pure poloidal case. As the magnetic field strengths are raised and the transition region is passed, the conductivity should become more classical. This would cause the slowing distance for the two cases to become similar.

If the electron temperature is 1 eV, then $\nu_{ei} = \omega_{ce}$ at 1 kG. If injection occurs at fields higher than 1 kG the expression for slowing time becomes

$$\tau_s \propto \frac{1}{n_b} \left(\frac{L}{\alpha_o}\right)^2 \qquad \text{for} \quad \omega_{ce} >> \nu_{ei} \qquad (5\text{-}4)$$

The time, τ_s is no longer dependent on the magnetic field strength, $|B|$, but just the density of the injected plasma, n_b, and the changing pitch of the magnetic field lines (α_o/L). The previously discussed regime should make a transition into this regime at ~1 kG. The following data should obey the scaling of this expression.

The scaling with density at high fields was examined in the same manner as in the previous section. Two different plasmas were injected into varying amplitudes of poloidal field added to a background toroidal field of 1.5 kG. The results are shown in figure 5-7. Case I was created by filling the gun to a pressure of

Figure 5-7. Trapped density versus poloidal field with added toroidal field. B_t = 1.5 kG. Case I has gun filled with gas to 160 mtorr. Case II, 40 mtorr.

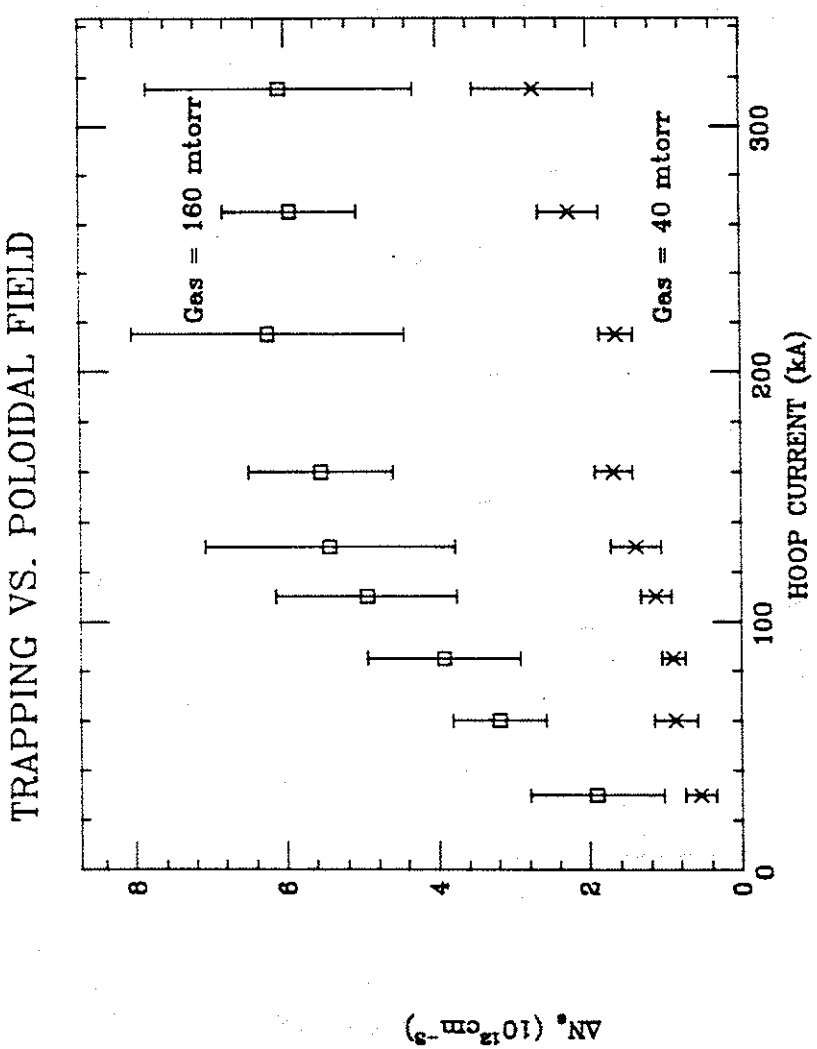

Figure 5-7

160 mtorr of hydrogen gas before firing. For case II the pressure was reduced by a factor of four to 40 mtorr. The results fit well with the model. For the dense plasma, as the poloidal field was increased, the slowing time became shorter, and an increasing amount of density was trapped. This occurred until all of the plasma was stopped.

Case II peaked at an average density of 3×10^{12} cm^{-3}, while case I peaked at 2-3 times this value. This in conjunction with the gas fill leads to the conclusion that the case I plasma was 2-3 times as dense as case II. The model would then predict that case II would have needed twice as much poloidal field to have the same stopping time as case I, if T_e were the same for both cases. If the less dense plasma were hotter, then it would need even more poloidal field to be stopped. The data appear to be consistent with this. Also note, that no anomalous resistivity is needed to explain this case. Apparently, for some unknown reason, in the high field regime the conductivity is more nearly classical.

The variation of the trapping of plasma with the changing pitch of field lines can be further investigated by varying the toroidal field for a given poloidal field. A decrease in the trapping was seen as toroidal field was added to a given poloidal field. This is shown in figure 5-8. The decrease in trapping was due to a decrease in α_o/L.

Figure 5-8. Trapped density versus toroidal field with added poloidal field. I_h = 150 kA.

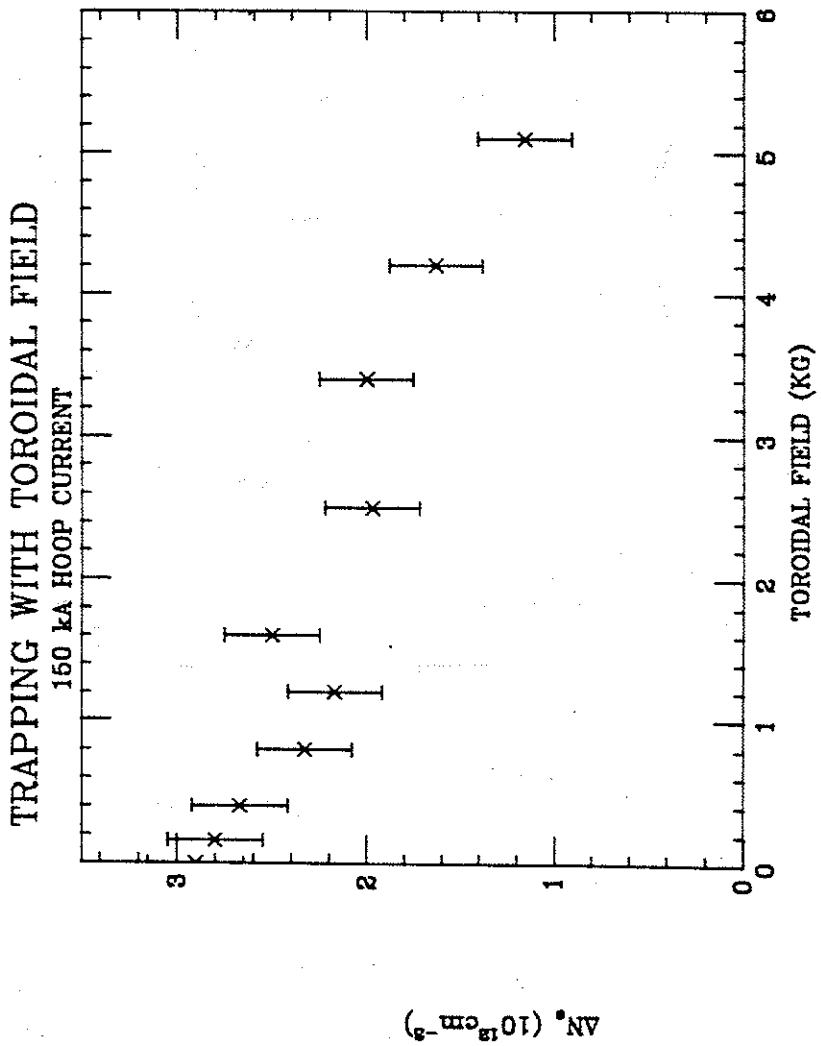

Figure 5-8

Figure 5-9. Trapped density versus poloidal field with added toroidal field. Case I B_t = 1.5 kG, Case II B_t = 3.0 kG. Gun filled to 160 mtorr.

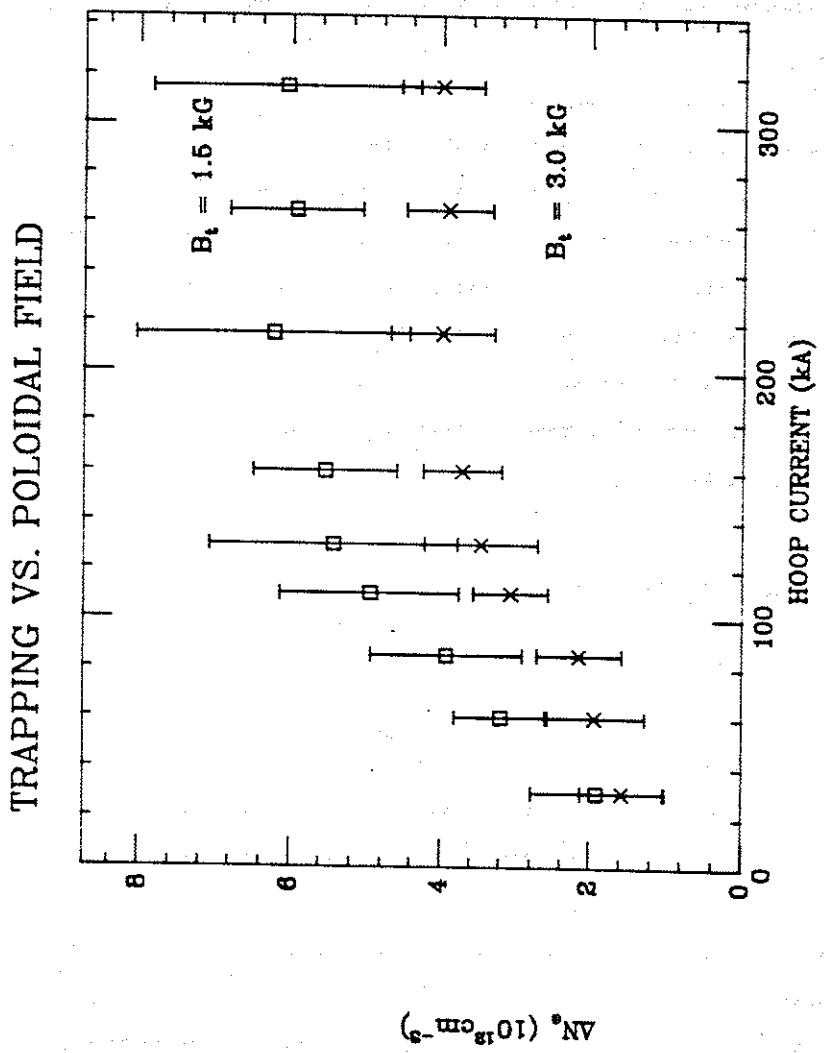

Figure 5-9

Another way of observing this can be seen in figure 5-9. Plasmas were injected into two different toroidal fields, 1.5 kG and 3.0 kG. Various amounts of poloidal field were added. With differences in the toroidal field of a factor of two, one would predict that twice as much poloidal field is needed for the high toroidal field case. to get equivalent trapping. In order to test this, the first five data points, for both cases, were fit in a least squares approximation to a straight line. The first five were taken to avoid the saturation that occurs at higher fields.

The incremental increase in trapping with added poloidal field was found to be

$$\frac{dn_e}{dI_h} = 3.5 \times 10^{10}\ kA^{-1}cm^{-3} \qquad \text{for } B_t = 1.5\ kG$$

$$= 1.9 \times 10^{10}\ kA^{-1}cm^{-3} \qquad \text{for } B_t = 3.0\ kG$$

The difference is well within the experimental error of being the factor of two predicted. Both cases started at a similar value at low poloidal fields. The trapping for the low toroidal field case then increased at a rate twice that for the high toroidal field case. The trapping of plasma then saturated as all the plasma was stopped.

One would expect the high toroidal field case to have continued increasing until it saturated at a value equal to that of the low field case. This did not happen. The high field case leveled off

at a value about 2/3 of the low field case. Some of the plasma that was trapped at low fields was not trapped at high fields. Since additional poloidal field did not increase the trapping, it is likely that the missing density was lost before entering the containment fields. The plasma had to cross some region of space filled with toroidal field before it was in a stable confinement region. As the moving plasma crosses magnetic field, the outer shell of the plasma that creates the polarization field is tied to the magnetic field lines. The act of crossing a magnetic field leaves some of the plasma behind. The outer edge of the plasma was stripped away before entering the device. The remaining plasma was then stopped according to the model that has been derived.

The trapping of a gun injected plasma was seen to be adequately described by the theoretical model derived in Chapter IV. If the collisionality of the injected plasma, ν_{ei}, is low compared to the electron cyclotron frequency, ω_{ce}, the scaling of trapping fits the model quite well. In this high field regime the slowing time of the injected plasma fit the scaling relation, $\tau_s = n_b^{-1}\alpha_o^{-2}$. At low field strength, $\omega_{ce} < \nu_{ei}$, the slowing time should have followed the relation, $\tau_s \propto n\alpha_o^{-2}B^2$. Only the density dependence in this case was not observed. Some anomalous resistivity was apparently present at low fields. The model was seen to fit the data well, with only a qualification in one parameter in one trapping regime.

References for Chapter V

[1]M. C. Zarnstorff and S. C. Prager, Phys. Fluids 29, 298 (1986)

[2]J. H. Halle, A. G. Kellman, R. S. Post, S. C. Prager, E. J. Strait, and M. C. Zarnstorff, Phy. Rev. Lett. 46, 1394 (1981)

[3]A. J. Cavallo, Phys. Fluids 19, 394 (1976)

[4]H. Dreicer, Phys. Rev. 115, 238 (1959)

[5]D. A. Brouchous, University of Wisconsin, PhD thesis (1980)

[6]B. B. Kadomtsev, Plasma Turbulence, Academic Press, N. Y., (1965)

CHAPTER VI

RESULTS FOR INJECTION INTO A TOKAMAK

A. Introduction

The goal of this thesis is to explain the process of gun-injection of plasma into a tokamak. The theoretical model derived to explain this process has been shown to adequately describe the trapping of gun plasmas by vacuum magnetic fields, i.e. no plasma present. If the trapping of plasma in a tokamak, as observed in Chapter III, is to be explained, then it should also fit within the model. Several experiments have been done over a variety of conditions in a Tokapole II discharge. The results should give a fairly accurate description of how well the process is understood.

A tokamak discharge adds two new parameters to the injection process. Added to the vacuum poloidal and toroidal fields, is a plasma throughout the device. This plasma is two orders of magnitude less dense and somewhat hotter than the gun-injected plasma. As shown in Chapter III, the tokamak plasma generally has a density of $\sim 5\times10^{12}$ cm^{-3} with a temperature of 50-100 eV. The second parameter is the plasma current localized around $x = 0$, or the magnetic axis of the device. This current can vary from 0 to 25 kA. The hoop current is ~200 kA at this point for comparison. Any changes one observes while injecting plasma into a tokamak as

opposed to vacuum magnetic fields, should be explainable in terms of one or both of these two parameters.

B. Experimental Results

Evaluation of trapping in the tokamak case is done in a similar manner to that for the vacuum field case. The efficiency of trapping under a given set of conditions is measured by the change in the line-averaged density in the device about 200 μsec after the gun is triggered. The difference is that the tokamak already has an existing density. This plasma in the region where more plasma is to be trapped means that there are several issues that should be considered.

The first concern is that of reproducibility. Because the interferometer could not track the density change at injection, the density after injection was measured by subtracting a late-time baseline, when the density was known to be zero. This means that the density prior to injection was unknown. This problem was solved by measuring the density of an identical discharge, but without gun refueling, just prior to the gun refueled case. The density prior to injection was then assumed to be that of the previous nonrefueled discharge. This, unfortunately, adds to the irreproducibility of measuring the trapped plasma.

A second concern is that some of the plasma existing in the tokamak discharge may be expelled from the device because of the injection process. This would lead to the observation of a reduced

trapping efficiency. This concern arises from the nature of the electric polarization field, which allows plasma to enter. Because the total injected charge is zero, Gauss's law states that in steady state, $\int \vec{E} \cdot d\vec{\ell} = 0$. This means that if there is a region where $\vec{E}\times\vec{B}$ points into the device, there must also be a region where $\vec{E}\times\vec{B}$ points out of the device. A perturbing electric field of this type would cause as much density flux in as out, if the particle density was constant everywhere. By concentrating high density in the region of inward transport, presumably a net increase in density will result.

It was not easy to separate plasma density and plasma current effects in Tokapole II. No means existed to create a reasonably dense plasma in Tokapole II, without plasma current or gun injection. However experiments were done on The Wisconsin Levitated Octupole to study injection into a pre-existing plasma[1]. A gun plasma was injected into another plasma which was created by electron cyclotron heating and contained by an octupole field with added toroidal field. Little effect was found due to the pre-existing plasma. This is fortunate, because the model does not take into account the presence of another plasma in the device. This result will be corroborated by data presented in the next section of this chapter, when other possible trapping mechanisms are examined.

To study the effect of plasma current on trapping, the data of figure 6-1 were taken. The data show that more density was trapped as the plasma current was increased. This looks very similar to the

Figure 6-1. Trapped density versus plasma current. B_t = 5.0 kG, I_h = 200 kA.

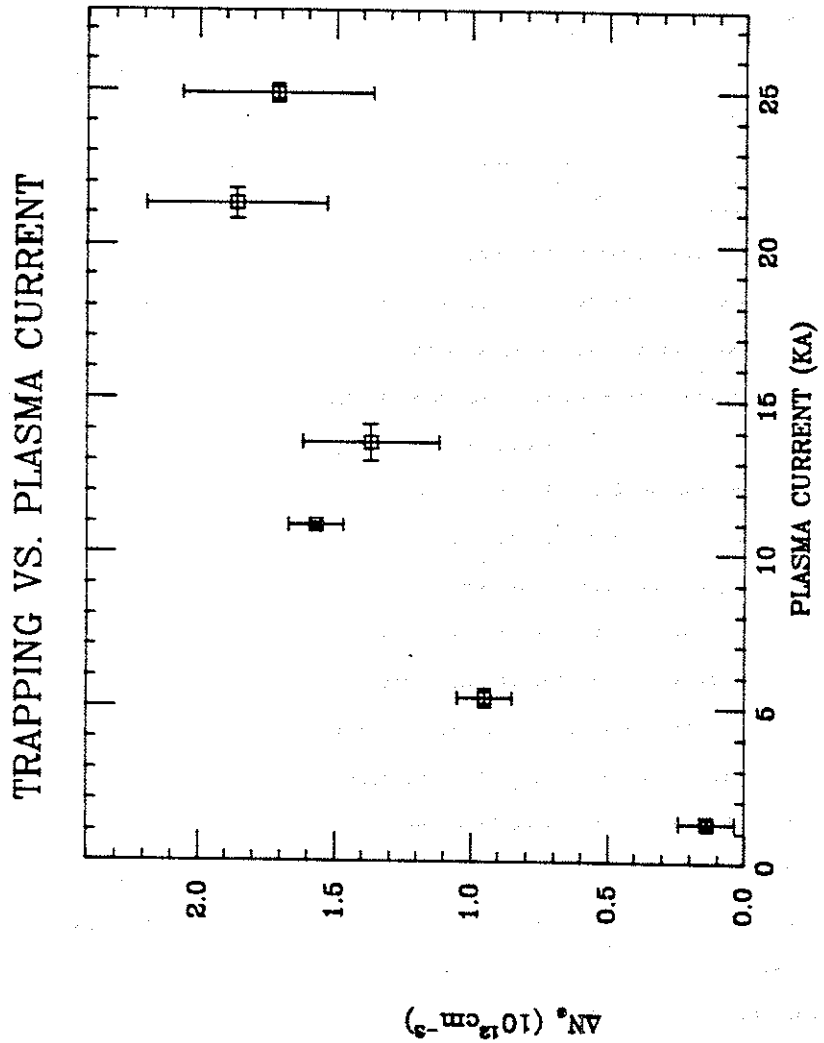

Figure 6-1

data of figure 5-5. This is reasonable since plasma current adds poloidal field, which is the strongest factor controlling trapping for vacuum fields.

The effect on the poloidal field due to the plasma current is shown in figure 6-2. The plasma current was assumed to be of constant density over the current channel. The resulting poloidal field was added to the known field for a given hoop current. A plot of the field pitch, α, is shown versus position for the case of a tokamak discharge and also for the case of the corresponding vacuum magnetic fields. For this calculation the tokamak discharge is that described in Chapter III. The plasma current was 25 kA, with a hoop current of 200 kA, and a toroidal field of 5.0 kG. Figure 6-2 shows that even though the plasma current is 1/8th of the hoop current, it considerably alters the pitch of the field lines. This is especially true at the center of the device.

To see if the data fit the model, one first observes that the slowing time, τ_s, goes as $(L/\alpha_o)^2$. The high value of $d\alpha/dx$ through the center of the device should help the trapping. Comparison of three cases can now be made. The first two are vacuum fields of B_t = 1.5 kG and B_t = 5.0 kG both with a hoop current of 200 kA. The last case is injection into a tokamak with B_t = 5.0 kG and I_h = 200 kA.

The low toroidal field vacuum case was examined in the previous chapter. A slowing distance of ~30 cm over the central 30 cm of the device was obtained. Experimental evidence showed that these

Figure 6-2. For Case I angle, α, the magnetic field makes with the horizontal midplane versus position, in a tokamak discharge. Plasma current assumed constant over current channel, x <10 cm. Calculated for I_p = 25 kA, B_t = 5.0 kG, I_h = 200 kA. Case II, same vacuum fields, no plasma current.

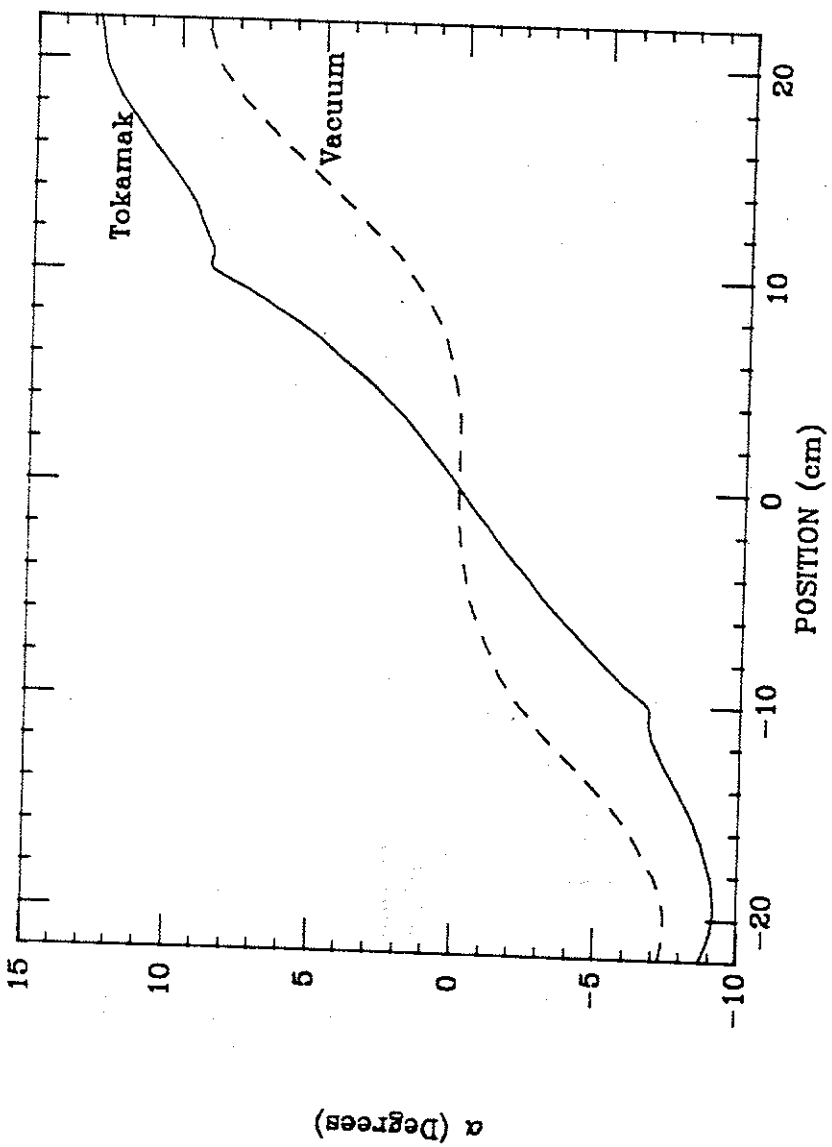

Figure 6-2

onditions adequately stopped the injected plasma. As the toroidal ield was raised to 5.0 kG, the trapped density dropped by a factor of 2-3, as observed in figure 5-8. The value of α_o/L was reduced rom 0.01 radians/cm to 0.003 radians/cm as the toroidal field was ncreased. An increase in B_t by some factor reduces α_o/L by approximately that same factor. Because the slowing distance was roportional to $(\alpha_o/L)^2$, the slowing distance was increased by a factor of 9 when the toroidal field was increased. The corresponding decrease in trapped plasma was observed in figure 5-8.

When plasma current was added to the vacuum fields, the value of $d\alpha/dx$ was increased, especially over the center of the device. α_o/L was raised to 0.006 radians/cm by the additional poloidal field. The slowing time was decreased by a factor of 4 over the corresponding vacuum field case. Figure 6-1 shows this, in that the trapped density increased as plasma current was added.

Another effect of the plasma current on trapping was seen in density profiles. The profiles of trapped density in Chapter III, figures 3-9 and 3-10, showed that most of the trapped density was deposited in the region of the central current channel. This occurs because $d\alpha/dx$ was greatest inside the separatrix where the plasma current was flowing. The plasma current concentrated the changing pitch in field lines into the center of the discharge where trapping was most beneficial.

Figure 6-3. Trapped density versus toroidal field for injection into a) tokamak discharge and b) the corresponding vacuum magnetic fields, I_h = 200 kA. The injected density is determined by firing gun into high strength pure octupole fields.

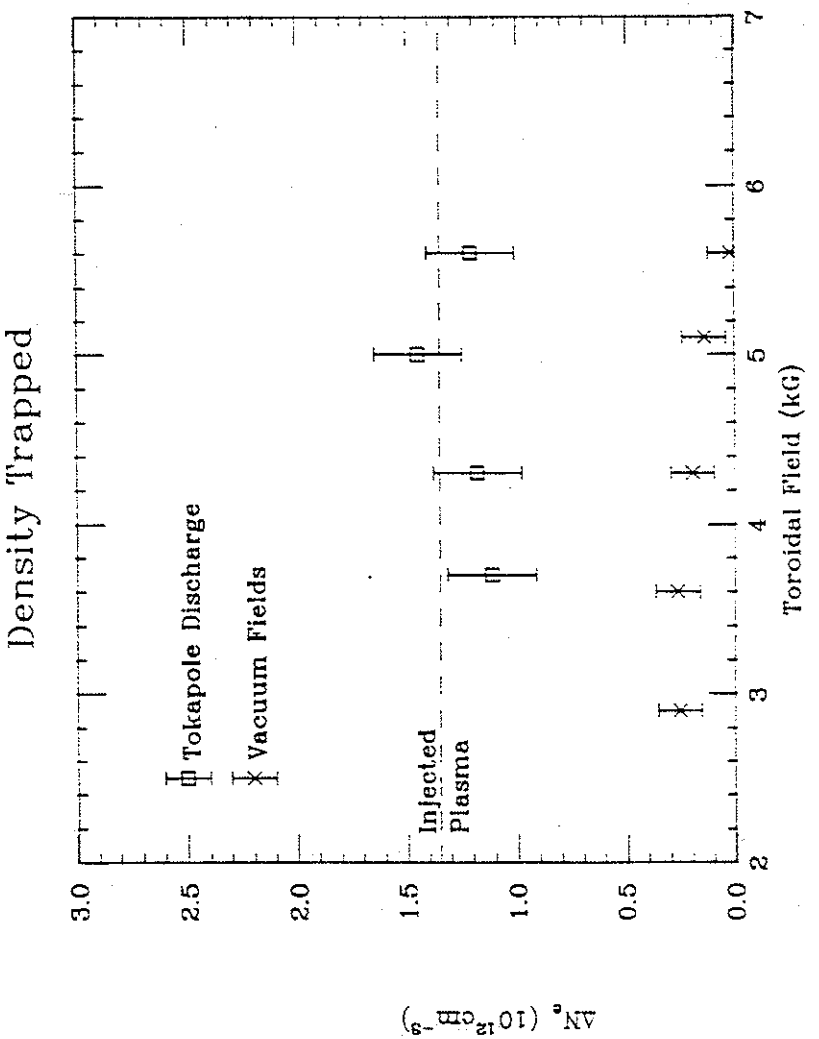

Figure 6-3

Trapping due to plasma current is also seen in the data of figure 6-3. The density trapped in a tokamak discharge is plotted for several values of toroidal field. Also plotted on this graph is the density resulting from injection of the same gun plasma into the corresponding vacuum magnetic fields of the tokamak discharge. The vacuum fields had the same hoop current and toroidal field as the tokamak discharge. They lacked only the plasma density and current. The addition of plasma current greatly enhanced the trapping. The injected density, also plotted on the graph, was arrived at by injecting the same gun plasma into a pure octupole field where the greatest trapping occurs.

The tokamak plasmas of figure 6-3 had different values of B_t, but the value of α_o/L remained fairly constant. The tokamak discharge preferred to operate at a constant ratio of B_t/B_p. The trapping remained constant as α_o/L did also, even though the toroidal field changed. This shows that the trapping was independent of magnetic field strength.

C. Other Possible Mechanisms

Support can be lent to the model if other possible mechanisms are shown to be inconsistent with the data. As seen in figure 6-3, the addition of plasma and plasma current markedly increases the trapping of an injected plasma. This increase is greater than might be expected due to an increase in α_o/L by only a factor of 2. If

other mechanisms are aiding trapping, they should be taken into account when designing refueling systems for a larger tokamak.

There are two mechanisms, that have been presented in the past as a possible way to stop an injected beam of plasma in a tokamak. The first of these is a collisional slowing down. It seems reasonable that the plasma in a tokamak could slow down a beam of injected plasma through collisions. This could be responsible for the increase in trapping.

If a beam of plasma is passing through a background of stationary plasma, the velocity of the moving beam will diffuse away as the stream's particles have collisions with the background plasma[1]. For a charged test particle, α, moving through a background of particles, β, the forward velocity of the test particle is given by,

$$v = v_o \exp\left\{-\frac{t}{\tau_s^{\alpha/\beta}}\right\} \tag{6-1}$$

where

$$\tau_s^{\alpha/\beta} = \frac{\tau_1^{\alpha/\beta}(E_\alpha)}{(1+\frac{m_\alpha}{m_\beta})\mu(\chi_\alpha)} \tag{6-2}$$

with

$$\tau_1^{\alpha/\beta} = \frac{m_\alpha^{1/2} E_\alpha^{3/2}}{\pi 2^{1/2} (e_\alpha e_\beta) \lambda n_\beta} \qquad (6\text{-}3)$$

where E_α, m_α, and e_α is the energy, mass, and charge respectively of the test particle α. n_β is the density of background particles. λ is the Coulomb logarithm. $\mu(\chi)$ is the Maxwell integral given by

$$\mu(\chi) = \frac{2}{\pi} \int_0^\chi e^{-\xi} \xi^{1/2} d\xi \qquad (6\text{-}4)$$

with the expression for χ being

$$\chi_\beta = \frac{m_e E_\alpha}{m_\alpha T_\beta} \qquad (6\text{-}5)$$

We are interested in the slowing times $\tau^{i/i}$ and $\tau^{i/e}$. The electrons in the moving beam carry negligible momentum and are basically dragged along by the ions. It is the ions' momentum that must be stopped. To calculate $\tau^{i/i}$ and $\tau^{i/e}$, the conditions stated previously can be used, $E_\alpha = 13$ eV, $n_\beta = 5\times10^{12}$ cm^{-3}, $T_e = 100$ eV, and $T_i = 30$ eV. With these conditions we get

$$\tau_s^{i/e} = 2.17 \times 10^{-2} \text{ sec}, \qquad \tau_s^{i/i} = 27.5 \times 10^{-6} \text{ sec}$$

The stream is obviously retarded mostly by the background of ions. With an initial velocity of 5×10^4 m/sec,

$$d_s = v_o \tau_s^{i/i} = 1.4 \text{ meters}$$

This distance is about four times the distance across the machine. Because of the uncertainties in density and temperature, collisional slowing can not yet be ruled out.

To further investigate this issue a gun plasma was injected into a tokamak discharge of various densities. The results are shown in figure 6-4. The density in Tokapole II was varied from 1×10^{12} cm^{-3} to 4×10^{12} cm^{-3}, with a constant plasma current, I_p, while being refueled by gun-injection. Over this range of density there was no discernible change in the amount of plasma trapped. This was true for three different gun plasmas. If collisional slowing was an important process less plasma should have been trapped in the less dense tokamak plasma. The data of figure 6-1 also support this conclusion. As the plasma current was increased, the temperature of the tokamak plasma also increased. A hotter background plasma should have been less effective than the colder plasma in stopping the plasma beam through Coulomb collisions. This is in contrast to the dramatic increase in trapping that occurred for the higher current tokamak discharges. These data support those of the previous refueling work carried out in octupoles.[1] A

Figure 6-4. Trapped density versus tokamak density, for three cases of gun injection. Gun power supply voltages of 10.0 kV, 12.5 kV, and 15.0 kV.

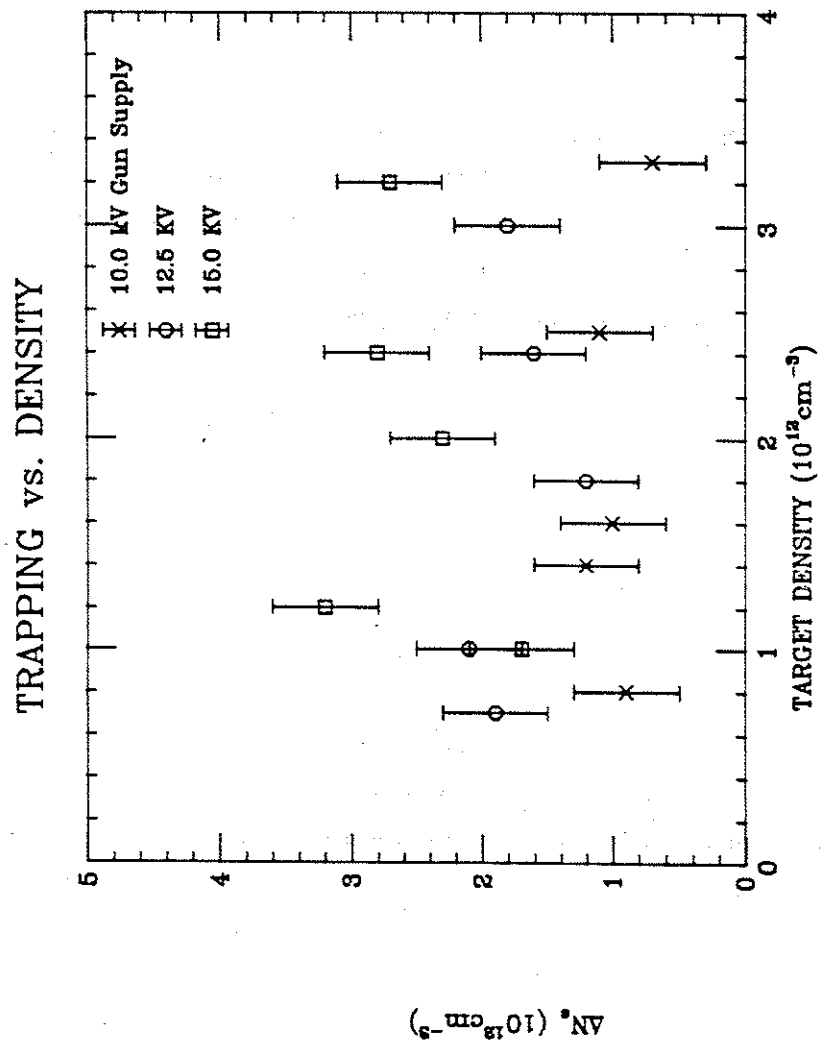

Figure 6-4

different mechanism must have been responsible for stopping the plasma stream.

A second possible mechanism for stopping a gun plasma in a tokamak was proposed by Ott and Manheimer[2]. They suggested that a plasma streaming through another pre-existing plasma could be susceptible to the Kelvin-Helmholtz instability. This instability would occur if the plasma beam velocity was less than the Alfvén speed of the plasma beam. With a wave number of $k = a^{-1}$ being assumed for effective mixing, the instability would have a spatial growth rate of

$$L_{KH} = \frac{a(\rho_s+\rho_p)}{(\rho_s\rho_p)^{1/2}} \qquad (6-6)$$

where a is the stream radius, and ρ_s and ρ_p are the plasma beam and tokamak plasma mass densities, respectively. For our experiment, the plasma beam was moving much slower than the Alfvén speed ($V_A = 3.4\times10^7$ cm/sec). This instability could have grown. The spatial growth length was too long, however, for effective mixing. With a beam radius of 5 cm and $\rho_s = 100\rho_p$, one spatial growth length was

$$L_{KH} = 50 \text{ cm}$$

or the whole width of the machine. This would be too long a

distance for the beam to be broken up and mixed with the background plasma. Our experimental evidence supports this. The trapping versus plasma current data of figure 6-1 indicates that plasma current was a strong controlling factor for trapping. If an instability of the Kelvin-Helmholtz type were responsible for trapping of the injected plasma, there should be little correlation between plasma current and trapping efficiency. This was not observed. Also, changes in the tokamak density should have affected this instability. A greater tokamak density would aid the instability. The data of figure 6-4 show that this was not the case.

In summary, the trapping of a gun injected plasma by a tokamak is seen to fit within the framework of the depolarization current model. The extension from the vacuum field to the tokamak discharge followed with the addition of plasma density and plasma current. The plasma density had little effect on the trapping. Plasma current added poloidal field which increased the trapping efficiency above the vacuum field case. This increase was more than might be expected, but the scaling still fit within the model. Other possible mechanisms to account for this increase were seen to be inconsistent with the data.

The various parameters which might affect trapping in a tokamak can be summed up as follows:

Poloidal Field aids trapping and is basically responsible for the mechanism involved. This field creates the polarization charge reversal which allows current to flow.

Toroidal Field decreases trapping by decreasing the charge reversal.

Plasma Density is not important at the temperatures and densities of these experiments.

Plasma Current increases trapping by increasing the poloidal field through the central current channel.

D. Extrapolation to a Reactor

The study of gun refueling was undertaken with the idea that this might be an attractive means of refueling a tokamak reactor. With a model that adequately explains the experimental observations, a useful exercise is to extrapolate from this experiment to a large reactor-size tokamak. With an accurate model, a prediction can now be made as to how this scheme might work.

At high magnetic fields, the slowing down time was shown to obey the relation

$$\tau_s \propto \frac{1}{n_b}\left(\frac{L}{\alpha_o}\right)^2 \qquad (5\text{-}4)$$

where n_b is the beam density. For most tokamaks the toroidal field

is much larger than the poloidal field. or $B_t > 5B_p$. This means that

$$\alpha_o \approx \frac{B_p}{B_t} \qquad \text{for } B_p << B_t$$

Also tokamaks run with a safety factor. q, greater than 2 in most cases, where q is given by

$$q = \frac{rB_t}{RB_p} \qquad (6\text{-}8)$$

where r and R are the minor and major radii of the plasma respectively. This leads to a slowing time of

$$\tau_s \propto \frac{(qR)^2}{n_b r} \qquad (6\text{-}9)$$

Because the larger machine has a longer distance over which to slow the plasma beam. a more appropriate figure of merit may be a dimensionless trapping efficiency given by the minor radius divided by the stopping distance. or

$$\kappa \equiv \frac{r}{v_o \tau_s} \qquad (6\text{-}10)$$

This leads to a trapping efficiency of

$$\kappa = \frac{Cn_b r}{v_o q^2 R^2} \qquad (6\text{-}11)$$

If we assume that the aspect ratio, r/R, does not vary much between tokamaks, then we have

$$\kappa = \frac{Cn_b}{v_o R}$$

where C is an experimentally determined constant. This means, if the gun parameters are held constant the trapping efficiency, κ scales inversely with the linear size of the device. This is fortunate in that little change is needed in designing a refueling system for a truly large device.

In scaling a gun refueling system up from a Tokapole size device to a reactor size device, it is desirable to keep the trapping efficiency, κ constant, to trap the plasma beam in the center of the device. TFTR is the largest operating tokamak in the U. S. and would work well for this exercise. The parameters for the device are as follows,

$R = 2.6$ m $\qquad r = 0.6$ m

$I_p = 1.4$ MA $\qquad n_e = 3 \times 10^{13}$ cm^{-3}

$B_t = 2.5$ T

Even though the total number of particles in TFTR is greater than in Tokapole II by a factor of a thousand, the linear size of the device is only five times greater. To keep κ constant when scaling a refueling system from Tokapole II to TFTR, a gun would need to increase its density by only a factor of five. This factor should be easy to achieve.

The flexibility to design a system for a larger device is readily available in Marshall guns. A gun of the same design as used on Tokapole II has been used to fill the Wisconsin Levitated Octupole with plasma. This device has 10 times the volume of Tokapole II and it was filled to similar densities. The factor of 10 in total number of particles was achieved by additional puffing of gas into the breach of the gun, and the addition of capacitors to the gun power supply. In fact, guns have routinely reported densities of 10^{17} cm^{-3}, with 10^{18} cm^{-3} also achievable[3]. The radius of the plasma beam is also expandable as is the pulse length and initial velocity of the gun discharge by at least a factor of 10. All of this can be done by a reconfiguration of the hardware.

A refueling system on TFTR might then consist of 3 guns that produce densities of 10^{16} cm^{-3}. The plasma beam could have a radius of 15 cm with a pulse length of 5 usec. The velocity of the plasma beam could easily be constructed to be 10 cm/usec. All three guns firing at once would raise the line-averaged density by 5×10^{13} cm^{-3}. This kind of density increase seems very feasible.

There is some concern that at this much larger scale some of the physics involved in trapping would change. As was seen in figure 5-8, the trapping at high toroidal field versus poloidal field leveled off at a lower value than for the low toroidal field case. One might need to take care that the gun plasma does not have to cross much strong magnetic field before entering the tokamak plasma. This might be done by either placing the gun close to the discharge or by use of a divertor type configuration.

The possibility also exists that other mechanisms may trap the gun plasma in a larger device. The previously described instability between the tokamak plasma and the plasma beam is one such possibility. Ultimately the real hope for trapping a dense gun plasma in a much larger tokamak rests upon the fact that gun plasmas can be varied over a wide range of parameters. The ability to vary densities, velocities, and temperatures over orders of magnitude increase the likelihood that efficient refueling can be obtained.

There are other issues a reactor-size, gun refueling system would have to address. One of these is cleanliness and impurity generation. In Chapter III it was shown that the level of impurity

radiation created by gun-injection did not rise significantly above the background. This does not mean that impurities were at a low enough level for a reactor. This is especially true of metal impurities which could be sputtered off the electrodes. Metal impurities can reach much higher ionization states and produce more radiation in a hot reactor and can thus be more harmful than light impurities. There is much to be done and learned about conditioning of surfaces and techniques to reduce impurity generation. It appears though that this task would not be too formidable.[4]

Another concern is of the disruption of magnetic surfaces by the plasma beam. The beam is a turbulent plasma containing embedded electric and magnetic fields. These fields could disrupt the flux surfaces allowing the outward transport of plasma and energy. Instabilities might also be set up which could disrupt the discharge. Since the duration of the beam is 10^{-5} to 10^{-6} of the confinement time, it is likely that the plasma will relax to a quiescent state before significant energy or particle loss takes place. For the refueling experiment on Tokapole II, as described in Chapter III, there was no observable loss of this type. It is hoped that the same will be true for a larger scale experiment.

Most other issues that might be of concern for gun-refueling should also be of concern for experiments that use pellet injectors. Once a dense plasma is deposited in the center of a tokamak discharge, the physics should be the same. For instance the

improved confinement times that occur during pellet refueling should also be observed if a gun is doing the refueling.

Finally, the last concern is cost effectiveness and reliability. Marshall guns are mechanically simple devices with very few moving parts. The electrical circuit that energizes the Marshall gun is also very simple. It consists of charged capacitors and a switching circuit to discharge them. This is all more simple and inexpensive than are pellet injectors. The Marshall gun looks like an attractive candidate for refueling a large tokamak.

E. Future Work

Work that yet needs to be done for gun refueling exists in two areas. The first involves basic physics of the trapping process. Through the use of probe techniques and spectroscopic measurements, further investigation of the depolarization currents needs to be carried out. Details of the cross field conductivity are especially needed. What is the conductivity and effective conducting area on the outside edge of the plasma beam? This question has been only partially answered by this work. The anomalous resistivity for trapping in a pure octupole field is a process that is not well understood. Also, a nonuniform density profile for the plasma beam has an unknown effect on the trapping process.

These are not easy questions to answer. The plasma to be measured is very dense, turbulent, and not extremely reproducible. It is destructive to probes, and these probes tend to arc in the

presence of such plasmas. The turbulence makes it difficult to get reliable measurements and profiles. Very careful techniques will be needed to complete this work. Spectroscopic measurements may be of help in doing this since nothing physical need exist in the plasma to interact with it.

The second area of work requires a larger tokamak. Now that injection into Tokapole II has been shown to be successful, this refueling technique should be tried on a larger device. Issues relevant to a reactor could then be addressed. Whether other mechanisms become involved at higher densities and fields could be investigated. Questions of turbulence and impurities could be answered. Most important though, a gun refueling experiment on a large tokamak would give a much better assessment of the feasibility and reasonableness of using this technique to refuel a large tokamak reactor.

References for Chapter VI

[1]E. J. Strait and J. C. Sprott, Nuclear Fusion 18, 1595 (1978)

[2]B. A. Trubnikov, Reviews of Plasma Physics, Vol. 1, Consultants Bureau, New York, p.105 (1965)

[3]E. Ott and W. M. Manheimer, Nuclear Fusion 17, 1057 (1977)

[4]J. Marshall, Proc. High Beta Workshop, Los Alamos, New Mexico July 28-August 1, 470 (1975)

[5]D. A. Ehst, Argonne Report ANL/FPP/TM-140 (1980)

CHAPTER VII

SUMMARY AND CONCLUSIONS

Efficient refueling has become an important issue as tokamaks have become larger. Gun-injection is a possible means of refueling and has been investigated in this thesis. It offers the advantage of delivering dense plasma to the center of a discharge, while using inexpensive and simple hardware.

A plasma beam traveling 5×10^4 m/sec. with a density of 1×10^{15} cm^{-3} was injected into a Tokapole II discharge. Gun-injection raised the line-averaged density by $\sim 2 \times 10^{12}$ cm^{-3} or about 50%. A density profile measured with an interferometer and a Langmuir probe, indicated that most of the injected plasma was trapped in the central current channel of the discharge. No significant increase in energy confinement time, τ_E, was observed. Also, the background impurity radiation did not increase significantly due to gun injection.

A slowing time, τ_s, was derived for the slowing of a plasma beam in a pure poloidal field. A change in direction of the magnetic field lines as the beam crosses the magnetic axis results in a reversal of the polarization charge which allows the plasma to cross the magnetic field. This charge reversal creates an electric field in the direction of travel along the outside edge of the

plasma beam. Currents which flow due to the electric field, create $\vec{J} \times \vec{B}$ forces in the plasma beam which slows it down. The more general case of toroidal field added to the poloidal field was examined. A slowing time, τ_s, was derived due to the same slowing mechanism. The slowing time was found to follow the relation, $\tau_s = \frac{1}{n_b} \left(\frac{L}{\alpha_o}\right)^2$, where n_b is the beam density, L is the scale length of the device and where $\alpha_o = \tan^{-1}(B_p/B_t)$ at the device boundaries.

An experimental investigation of injecting plasma into octupole fields was carried out. For conditions in which significant plasma was trapped, the model predicted a slowing time of the right order of magnitude to stop the injected plasma. At low poloidal field strengths, $\omega_{ce} < \nu_{ei}$, the trapping followed the derived magnetic field scaling. The beam density dependence, however, was different from the observed experimental dependence. For a more dense plasma to trap better more current must flow. This requires the conductivity to increase with increasing density. This should not be the case at low field. An unspecified anomalous resistivity might account for the data.

Injection of plasma into octupole and toroidal fields fit the derived slowing relation well. The derived magnetic field dependence was observed in the data. The trapped density was seen to be a strong function of the changing pitch of the magnetic field lines. The expected density dependence was also observed. The more dense plasma beam was seen to be trapped more easily.

Investigation of trapping injected plasma in a tokamak was carried out. The results were explained in terms of adding plasma density and current to the vacuum field case. There was little effect on trapping due to plasma density at the densities and temperatures of of this experiment. The increase in trapping with increased plasma current was explained in terms of added poloidal field to the central current channel. The model adequately described trapping of plasma injected into a tokamak.

An extrapolation of this refueling system to one appropriate for a reactor-size tokamak was carried out. The efficiency of a given system was found to scale inversely with the linear size of the device. The flexibility available in Marshall guns should allow for the adaptation of gun refueling systems from small to truly large tokamaks. A possible system for refueling the TFTR device was described.

Further work is necessary to fully understand the trapping process. The depolarization currents and the factors that control them are not well understood. Low field conductivity is an example of where discrepancies occur. Also, a large tokamak is needed to investigate the feasibility of refueling a reactor with a Marshall gun.